



Norwegian University of  
Science and Technology

# Concepts for Large Scale Hydrogen Liquefaction Plants

**Jørgen Eckroll**

Master of Energy and Environmental Engineering

Submission date: June 2017

Supervisor: Petter Nekså, EPT

Co-supervisor: David Berstad, SINTEF  
Øivind Wilhelmsen, SINTEF/EPT

Norwegian University of Science and Technology  
Department of Energy and Process Engineering



# Concepts for large scale hydrogen liquefaction plants

**Jørgen Eckroll**

Master of Science in Mechanical Engineering

Submission date: June 2017

Supervisor: Adj. Prof. Petter Nekså

Co-supervisors: Msc. Techn. David Berstad, SINTEF Energy Research

Adj. Prof. Dr. Øivind Wilhelmsen, SINTEF Energy Research

Norwegian University of Science and Technology  
Department of Energy and Process Engineering  
Trondheim



Norwegian University of  
Science and Technology



EPT-M-2017-18

**MASTER THESIS**

for

**Student Jørgen Eckroll**

Spring 2017

**Concepts for large scale hydrogen liquefaction plants***Konsepter for storskala hydrogen flytendegjøringsanlegg***Background and objective**

Hydrogen has the potential to become a central energy carrier in the likely carbon-constrained energy systems of the future. The European Commission and the International Energy Agency point at utilisation of hydrogen as an energy carrier as an absolute prerequisite for reaching global greenhouse gas reduction targets. Hydrogen use will be of key importance with respect to decarbonisation of the transport sector, power generation and several other industries. Norwegian strategic documents also point to hydrogen as an important contributor to curbing greenhouse gas emissions, and for valorisation of Norwegian energy resources.

On the supply side, Norway is a net exporter of energy and therefore a potential supplier of hydrogen to domestic, regional and global markets in the future. Norway's surplus is currently dominated by fossil energy, and this will be the case for a long time still. However, the importance of renewable power for Norwegian energy export is expected to be enhanced in the long term as the installed capacity is extended.

The Hyper project (ENERGIX programme, funded by the Research Council of Norway) started mid-2016 and runs through 2019. The main objective of the project is to generate fundamental knowledge required for planning, construction and operation of a pilot and thereafter a commercial plant in Norway for large-scale hydrogen production, liquefaction and export.

Liquefaction of hydrogen is an energy demanding process. Improvements in this part of the value chain is therefore very important in the context of increased use of hydrogen as an energy commodity.

The aim of this Master thesis work is to develop the modeling basis for hydrogen liquefaction plants, with emphasis on the pre-cooling part, and utilize this modelling framework to improve the efficiency of large-scale liquefaction plants.

**The following tasks are to be considered:**

1. Literature survey related to process concepts for hydrogen liquefaction.
2. Further develop a model in Hysys for a full liquefaction plant, with precooling and a low temperature cycle using He-Ne or H<sub>2</sub>-Ne mixture as refrigerant
3. The precooling plant utilizing mixed component refrigerant should be optimized and benchmarked with a nitrogen cycle plant
4. Evaluate utilization of simple chillers for improving efficiency by precooling and subcooling at the upper temperature level
5. Perform loss analysis with the main focus on the precooling part of the liquefaction plant

-- ” --

Within 14 days of receiving the written text on the master thesis, the candidate shall submit a research plan for his project to the department.

When the thesis is evaluated, emphasis is put on processing of the results, and that they are presented in tabular and/or graphic form in a clear manner, and that they are analyzed carefully.

The thesis should be formulated as a research report with summary both in English and Norwegian, conclusion, literature references, table of contents etc. During the preparation of the text, the candidate should make an effort to produce a well-structured and easily readable report. In order to ease the evaluation of the thesis, it is important that the cross-references are correct. In the making of the report, strong emphasis should be placed on both a thorough discussion of the results and an orderly presentation.

The candidate is requested to initiate and keep close contact with his/her academic supervisor(s) throughout the working period. The candidate must follow the rules and regulations of NTNU as well as passive directions given by the Department of Energy and Process Engineering.

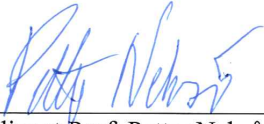
Risk assessment of the candidate's work shall be carried out according to the department's procedures. The risk assessment must be documented and included as part of the final report. Events related to the candidate's work adversely affecting the health, safety or security, must be documented and included as part of the final report. If the documentation on risk assessment represents a large number of pages, the full version is to be submitted electronically to the supervisor and an excerpt is included in the report.

Pursuant to “Regulations concerning the supplementary provisions to the technology study program/Master of Science” at NTNU §20, the Department reserves the permission to utilize all the results and data for teaching and research purposes as well as in future publications.

The final report is to be submitted digitally in DAIM. An executive summary of the thesis including title, student's name, supervisor's name, year, department name, and NTNU's logo and name, shall be submitted to the department as a separate pdf file. Based on an agreement with the supervisor, the final report and other material and documents may be given to the supervisor in digital format.

- Work to be done in lab (Water power lab, Fluids engineering lab, Thermal engineering lab)
- Field work

Department of Energy and Process Engineering, 15. January 2017



---

Adjunct Prof. Petter Nekså  
Academic Supervisor

Research Advisors/ Co-supervisors:

David Berstad, SINTEF Energy Research

Øivind Wilhelmsen, SINTEF Energy Research





# Abstract

The main objective of this thesis is to perform a technical-exergetic analysis of a large-scale hydrogen liquefaction system. The system boundary of the technical analysis is isolated to the precooling part of the overall process, which gives potential for extensive Case Study Analysis and benchmark possibilities of present conventional systems.

From a hydrogen precooling point of view, the predictions for long- and mid-term development options for a large-scale liquefaction scenario (50-200 tpd), tends towards Mixed Refrigerant and Nitrogen Cycles, both in combination of simple, high-efficiency chillers in the upper temperature region.

Four different Case Study Models has been simulated in Aspen HYSYS, optimized and re-modified with emphasis on the net exergy destruction within the entire process model, the overall exergy efficiency defined by the system boundary and specific energy consumption of the isolated system. The two baseline models has been adapted from the Liquefied Natural Gas (LNG) industry, where the utilization rate of Mixed Refrigerants has a high level of experience. The two precooling processes are the Single Mixed Refrigerant (PRICO) process and the Cascade Mixed Refrigerant process.

The precooling systems are simulated both in combination with and without integration of R290-Chillers (propane) and with additional cooling of a generic helium stream as cryogenic working fluid. Recent concepts of complete liquefaction systems, propose to perform heat integration of the cryogenic fluid into the precooling process, in favour of heat transfer minimization. Hence, a process with integrated cryogenic working fluids creates a better framework model, easier to adapt into a bigger system for future work.

Each of the Case Study models were optimized by employment of simulation iterations  $i$ , where the best performing simulation from each Case Study Model was benchmarked with a conventional Liquid Nitrogen Precooling process.

With an average hydrogen feed of 150 tonnes/day, the CMR precooling process with implemented chillers and integrated liquid expanders, proves to be the most energy- and exergy efficient process, with an exergy efficiency calculated to above 45,0% and a corresponding specific energy consumption of 1,974 kWh/kg<sub>H2</sub>, required to cool both the hydrogen feed stream and helium working fluid down to a temperature of 130 K. Reassignment to higher isentropic efficiencies for expanders and compressors were tested for each Case Study model, resulting in an exergy efficiency above 50% for the equivalent CMR+ process.



# Sammendrag

Hovedformålet med denne avhandlingen er å utføre en teknisk-eksergetisk analyse av et storskala hydrogen-flytendegjøringssystem. Systemgrensen til den tekniske analysen er isolert til forkjølingsdelen av den overordnede prosessen, noe som gir potensial for omfattende casestudie analyser, samt større sammenlikningsgrunnlag med dagens konvensjonelle systemer.

Med hensyn til forkjølingsprosesser for hydrogen, peker langsiktige prognoser for ulike utviklingsalternativer for et storskala produksjonsscenario (50-200 tpd), mot utnyttelse av henholdsvis blandende hydrokarboner og nitrogen som kjølemedium. Disse systemene ansees integrert både med og uten utnyttelse av simple, kjølerenheter i øvre temperatursjikt, for å redusere total varmeoverførings effekt i varmevekslerene

Fire forskjellige case-studiemodeller har blitt simulert i Aspen HYSYS, optimalisert og re-modifisert med vekt på reduksjon netto eksergitap i hele prosessmodellen, maksimering av den totale eksergi virkningsgraden, i så henseende definert av en gitt systemgrense, samt reduksjon av spesifikt energiforbruk av det isolerte systemet. To referansemodeller er tilpassede prosesser fra LNG-industrien, hvor utnyttelsesgraden av blandede kjølemidler er vesentlig høy. De to forkjølingsprosessene er MR PRICO (Single Mixed Refrigerant) og Kaskade MR prosessen (Cascade Mixed Refrigerant).

Forkjølesystemene simuleres både i kombinasjon med og uten integrasjon av R290-kjølere (propan) samt integrasjon av en generisk strøm av det kryogene arbeidsmedium som anvendes i et lavere temperaturintervall. Nylige konsepter av komplette flytendegjøringssystemer, foreslår å utføre varmeintegrasjon av kryogenvæsken i forkjølingsprosessen, til fordel for minimal varmeoverføring. Derfor resulterer en slik prosess med integrerte kryogen arbeidsfluider en bedre rammemodell, lettere å tilpasse et større system for fremtidig arbeid.

Med en gjennomsnittlig hydrogeninnmating på 150 tonn / dag og en forkjølingstemperatur på 130 K, viser CMR+ prosessen med implementerte tilleggskjølere og integrerte væske-ekspandere, den mest energi- og eksergi-effektive prosessen, med en eksergivirkningsgrad beregnet til over 45,0% og et tilsvarende spesifikt energiforbruk på 1,974 kWh / kgH<sub>2</sub>. Økning av isentropisk virkningsgrad for væske-ekspandere og kompressorer ble testet for hver casestudie-modell, som resulterte i en økt eksergivirkningsgrad på over 50% for tilsvarende CMR + prosess.



# Preface

This masters thesis was carried out at the Department of Energy and Process Engineering at the Norwegian University of Science and Technology (NTNU) from mid January to mid June 2017. My supervisors were Professor II Petter Nekså (NTNU and SINTEF Energy Research), David Berstad (SINTEF Energy Research) and Øivind Wilhelmsen (SINTEF Energy Research).

In dialogue with the supervisors it was decided to omit point 2) of the task description in order to limit the overall workload.

I would like to thank my supervisors David Berstad, Øivind Wilhelmsen and Professor Petter Nekså, for the time they spent providing me with their valuable experience and insights, especially associated with the simulation models and problem solving in Aspen HYSYS.

Trondheim, June 16, 2017

A handwritten signature in black ink, reading "Jørgen Eckroll". The signature is written in a cursive style with a large, prominent 'J' and 'E'.

Jørgen Eckroll



# Contents

<b>Abstract</b>	<b>ii</b>
<b>Sammendrag</b>	<b>iv</b>
<b>Preface</b>	<b>vi</b>
<b>List of Figures</b>	<b>xi</b>
<b>List of Tables</b>	<b>xiv</b>
<b>1 Introduction</b>	<b>1</b>
1.1 Background and motivation . . . . .	1
1.1.1 The SINTEF HYPER Project and Norwegian Hydrogen Infrastructure . . . . .	2
1.2 Thesis structure . . . . .	4
<b>2 Theory</b>	<b>5</b>
2.1 Hydrogen Liquefaction Chain . . . . .	5
2.2 Target parameters in liquefaction plants . . . . .	7
2.2.1 Key performance indicators in process components . . . . .	7
2.2.2 Exergy and minimum energy requirement . . . . .	9
2.3 Precooling principles . . . . .	14
2.3.1 Precooling technology in existing hydrogen liquefaction plants	15
2.3.2 Mixed refrigerant process concepts from the LNG industry relevant for hydrogen precooling . . . . .	16
2.3.3 Nitrogen expansion concepts for hydrogen precooling . . . . .	22
2.3.4 Implementation of simple chillers in upper temperature level as partial precooling . . . . .	22
2.4 Ortho-para conversion . . . . .	22
2.4.1 Example plant: <i>Linde, Ingolstadt</i> - Adiabatic/isothermal batch conversion beds . . . . .	24

2.4.2	Example plant: <i>Linde, Leuna</i> - Continuous conversion catalyst-packed heat exchangers . . . . .	25
2.5	Principles and theory of cryogenic cooling . . . . .	26
2.5.1	Hydrogen Claude concepts . . . . .	26
2.5.2	Reversed Brayton concepts using both single and binary mixtures as working fluid . . . . .	28
2.6	Literature survey on conceptual hydrogen liquefaction plants . . . . .	30
2.6.1	New concepts for hydrogen precooling . . . . .	30
2.6.2	New concepts of cryogenic cooling and liquefaction of hydrogen . . . . .	34
2.6.3	Key findings from literature; cryogenic- and precooling concepts . . . . .	40
<b>3</b>	<b>Case Study Process Models</b>	<b>45</b>
3.1	Case study models . . . . .	45
3.1.1	Case 1: SMR PRICO precooling . . . . .	45
3.1.2	Case 2: SMR PRICO+ precooling . . . . .	46
3.1.3	Case 3: CMR precooling . . . . .	47
3.1.4	Case 4: CMR+ precooling . . . . .	48
3.1.5	Benchmark Case 6: Conventional liquid nitrogen precooling process . . . . .	48
<b>4</b>	<b>Technical Methodology</b>	<b>53</b>
4.1	Modelling the case study systems . . . . .	54
4.1.1	Design of simple refrigerators in case 2 and 4 . . . . .	54
4.1.2	HYSYS simulation of continuous ortho-para conversion . . . . .	59
4.1.3	Baseline Design of the Case Study Models . . . . .	62
4.1.4	Definintion of system boundaries when evaluating exergy parameters . . . . .	64
4.2	Optimization Approach . . . . .	66
<b>5</b>	<b>Technical Results and Discussion</b>	<b>69</b>
5.1	Results and discussion: SMR PRICO precooling . . . . .	70
5.1.1	Mixed Refrigerant Optimization Procedure . . . . .	70
5.1.2	Key Performance Indicators in the Case Study I process . . . . .	73
5.1.3	Analysis of exergy losses and efficiency . . . . .	75
5.2	Results and discussion: SMR PRICO+ precooling . . . . .	81
5.2.1	Mixed Refrigerant Optimization Procedure . . . . .	81
5.2.2	Key Performance Indicators in the Case Study Process . . . . .	86
5.2.3	Analysis of exergy losses and efficiency . . . . .	88
5.3	Case 3: CMR precooling . . . . .	95
5.3.1	Mixed Refrigerant Optimization Procedure . . . . .	95



5.3.2	Key Performance Parameters of process components . . . . .	99
5.3.3	Analysis of exergy losses and efficiency . . . . .	101
5.4	Case 4: CMR+ precooling . . . . .	108
5.4.1	Mixed Refrigerant optimization procedure . . . . .	108
5.4.2	Key Performance Parameters of process components . . . . .	112
5.4.3	Analysis of exergy losses and efficiency . . . . .	116
5.5	Benchmark comparison: Liquid Nitrogen Precooling (LIN-PC) . . . . .	122
5.5.1	Evaluating exergy- destruction and efficiency of Case Study V	123
5.5.2	Final comparison . . . . .	124
<b>6</b>	<b>Conclusion</b>	<b>127</b>
<b>7</b>	<b>Proposal for further work</b>	<b>129</b>
7.1	Further work proposals within process design and simulation . . . . .	129
	<b>Bibliography</b>	<b>131</b>
	<b>Appendices</b>	<b>136</b>
<b>A</b>	<b>Technical design parameters</b>	<b>137</b>
A.1	Case Study I and II . . . . .	138
A.2	Case Study III and IV . . . . .	139
<b>B</b>	<b>Exergy analysis and equations of Case Study I, SMR PRICO</b>	<b>141</b>
B.1	SMR PRICO . . . . .	141
<b>C</b>	<b>Case Study Process Flow Diagrams, HYSYS</b>	<b>145</b>
C.1	Case Study I: SMR PRICO . . . . .	147
C.2	Case Study II: SMR PRICO+ . . . . .	150
C.3	CMR . . . . .	153
C.4	LIN-PC . . . . .	156

# List of Figures

1.1	The SINTEF HYPER project illustration [2] . . . . .	3
2.1	Generic Process Flow Diagram (PFD) of the hydrogen liquefaction chain, obtained from Walnum et al. in [50] . . . . .	6
2.2	Exergy content of the different molecular forms of hydrogen assuming 300 K surrounding temperature at 1 bara . . . . .	10
2.3	Specific power consumption as function of exergy efficiency, $\varepsilon_x$ . . . . .	13
2.4	Specific heat capacity for equilibrium hydrogen at 20 and 80 bar . . . . .	15
2.5	Simple temperature profile for precooling using liquid nitrogen. Figure generated in Aspen <sup>®</sup> HYSYS . . . . .	16
2.6	The single Kleemenko cycle . . . . .	17
2.7	The single PRICO process cycle . . . . .	18
2.8	The Dual/Cascade MR process cycle . . . . .	19
2.9	A simplified PFD of the Linde MFC <sup>®</sup> process for liquefaction of natural gas at the Statoil Snøhvit facility. Some details are missing for simplicity but can be found in [3] . . . . .	20
2.10	The LIMUM 1 <sup>®</sup> process cycle . . . . .	21
2.11	Comparison of para-hydrogen composition at temperature, $T$ with three different references from literature . . . . .	23
2.12	PFD of different concepts of integration of ortho-para conversion . . . . .	25
2.13	The theoretical basis of the <i>Claude liquefaction cycle</i> . . . . .	27
2.14	The Claude cycle integrated separately from the hydrogen feed stream . . . . .	28
2.15	The reversed Brayton cycle integrated with the hydrogen feed stream . . . . .	29
2.16	Original IDEALHY-model with MR precooling, by Berstad et al. [43] . . . . .	32
2.17	Nitrogen expansion precooling, proposed by Quack et al. [42] . . . . .	33
2.20	A simplified PFD indicating difference between the original and modified Linde Leuna process . . . . .	38

2.21	Specific energy consumption of conceptual hydrogen liquefaction plants from literature . . . . .	40
2.18	Concept A by Cardella et al.: MR LIMUM (two-HX-stage) pre-cooling, by Cardella et al. [13]. . . . .	42
2.19	Concept B: MR single LIMUM precooling, by Cardella et al. [13] .	43
3.1	Simulation case model one: PRICO SMR . . . . .	46
3.2	Simulation case model two: PRICO SMR+ . . . . .	47
3.3	Simulation case model three: Hydrogen CMR precooling . . . . .	49
3.4	Compression train of lower temperature MR cycle. The pump increase the minor fraction of liquid to the same pressure level as the compressors . . . . .	50
3.5	Simulation case model no. 4: Hydrogen CMR+ precooling . . . . .	51
4.1	Single R290 refrigeration circuit, as a partial precooling process . .	56
4.2	HYSYS Steady state model of propane (R290) refrigerator . . . . .	56
4.3	Pressure-enthalpy diagram for R290, with indicated isotherms . . .	58
4.4	Caption . . . . .	60
4.5	Test experiment to quantify the enthalpy- and cooling duty difference of the two hydrogen forms used in the HYSYS simulation environment . . . . .	61
4.6	System boundary benchmark for each MR Precooling Case Study Model . . . . .	64
4.7	System boundary benchmark for LIN Precooling Case Study Model	66
5.1	Test run generated in HYSYS to quantify pressure- and mass flow values with the given heat exchanger constraints . . . . .	71
5.2	Optimization of the composite curves within the main heat exchanger (HX-1), Case Study I . . . . .	72
5.3	Compressor power impact at variable pressure and mass flow in the MR cycle with a given MR composition, Case Study I . . . . .	75
5.4	Overall exergy balance of Case Study I. The stacked bars indicates that the overall exergy input and destruction within the system (LHS, Eq. 4.4), equals total power input (RHS, Eq. 4.4) into the system, for each iteration . . . . .	76
5.5	Comparison of composite curves with throttling valves and isentropic expanders . . . . .	80
5.6	Optimization of cooling curves within heat exchanger HX-1 . . . . .	83
5.6	Optimization of temperature match in MR cycle, Case Study II . .	85
5.7	Power input for each iteration in case II . . . . .	87
5.8	Exergy input plus exergy destruction within the process, Case Study II . . . . .	88

5.9	Comparison of composite curves with throttling valves and isentropic expanders . . . . .	94
5.10	Optimization of temperature match in MR cycle, Case Study III . . . . .	99
5.12	Exergy input plus exergy destruction within the process of the three best solution proposals in Case Study III . . . . .	101
5.11	Net power consumption within the process of the three best solution proposals in Case Study III . . . . .	102
5.13	Draft of alternative process design to Case Study III . . . . .	107
5.14	Optimization of temperature match in MR cycle <i>a</i> and <i>b</i> , with composite curves as benchmark, Case Study IV . . . . .	112
5.15	Heat transfer duty, $Q$ and $UA$ for each iteration solution, Case Study IV . . . . .	113
5.16	Net- power consumption and irreversibilities with its respective distribution component-wise . . . . .	116
5.17	Composite curves (T-Q-Diagram) of liquid nitrogen precooling heat exchanger . . . . .	122
5.18	Component-wise distribution of exergy destruction, best performance iteration . . . . .	125
5.19	Specific energy consumption, $w_{net}$ , Case Study I-IV . . . . .	126
5.20	Exergy efficiency, $\varepsilon_x$ , Case Study I-IV . . . . .	126
C.1	SMR PRICO model, with isenthalpic throttling . . . . .	147
C.2	SMR PRICO model, with isentropic expansion . . . . .	148
C.3	SMR PRICO+ model, with isenthalpic throttling . . . . .	150
C.4	SMR PRICO model+, with isentropic expansion . . . . .	151
C.5	CMR precooling model, with isenthalpic expansion . . . . .	153
C.6	Alternative CMR precooling model design, with isenthalpic expansion . . . . .	154
C.7	Simple model of Liquid Nitrogen Precooling . . . . .	156

# List of Tables

2.1	Key findings from conceptual precooling processes . . . . .	41
2.2	Key findings from conceptual cryogenic liquefaction processes . . .	41
4.1	Chiller cooling requirements in Case study 1 and 2: PRICO/- PRICO+ precooling . . . . .	55
4.2	Chiller cooling requirements in Case study 3 and 4: CMR/CMR+ precooling . . . . .	55
4.3	Design parameters generated by CoolPack, Refrigeration Utilities .	57
4.4	Approximation of adiabatic temperature increase, final design para- meters . . . . .	60
4.5	Caption . . . . .	67
5.1	Final results of optimization parameters, Case Study I . . . . .	70
5.2	Heat exchanger performance indicators, $i_0$ - $i_6$ , Case Study I . . . .	74
5.3	Performance indicators of Mixed Refrigerant compressor train, Case Study I . . . . .	74
5.4	Main resulting exergy parameters in the Case Study I process . . .	76
5.5	Exergy destruction in process components, $i_4$ and $i_5$ , Case Study I	77
5.6	Results from integration of expander, LP = 4 bar, Case Study I . .	78
5.7	Results from integration of expander, LP-4 = 4,75 bar and LP-5 = 4,8 bar, Case Study I . . . . .	78
5.8	Final exergy efficiency of Case Study I, PRICO SMR precooling, with integrated turbo liquid expanders . . . . .	79
5.9	Final results of optimization parameters, Case Study II . . . . .	82
5.10	Heat exchanger performance indicators, Case Study II. . . . .	86
5.11	Performance indicators of Mixed Refrigerant compressor train, Case Study II . . . . .	86
5.12	R290-Chiller performance, Case Study II . . . . .	88
5.13	Main resulting exergy parameters in the Case Study II process . .	89
5.14	Exergy destruction of the original process design; $i_1$ , $i_9$ and $i_{11}$ . .	90

5.15 Exergy destruction with integrated expander, operating at equal pressure ratio . . . . .	91
5.16 Exergy destruction with integrated expander, operating at $\Delta T_{min}$ -adjusted pressure ratio . . . . .	92
5.17 Final exergy efficiency and power requirement of Case Study II, PRICO SMR precooling . . . . .	93
5.18 Summary of the final result of the MR optimization procedure . . . . .	96
5.19 Compressor- suction and discharge parameters of MR cycle <i>a</i> and <i>b</i> . . . . .	96
5.20 Key Performance Indicators of HX-1 and HX-2, Case Study III . . . . .	100
5.21 Key Performance Indicators of compressors in MR cycle <i>a</i> and <i>b</i> . . . . .	101
5.22 Main resulting exergy parameters in the Case Study III process . . . . .	103
5.23 Exergy destruction of the original process design; <i>i</i> <sub>1</sub> , <i>i</i> <sub>8</sub> and <i>i</i> <sub>9</sub> , Case Study III . . . . .	103
5.24 Main results, expander integration with constant pressure ratio, Case Study III . . . . .	104
5.25 Main results, expander integration with $\Delta T_{min}$ -adjusted pressure ratio, Case Study III . . . . .	105
5.26 Net compressor power and irreversibility, for $\eta_c = \eta_e = 85\%$ , Case Study III . . . . .	106
5.27 Final exergy efficiency and power requirement of Case Study III, Cascade Mixed Refrigerant (CMR) precooling . . . . .	107
5.28 Summary of the final result of the MR optimization procedure, Case Study IV . . . . .	109
5.29 Compressor- suction and discharge parameters of MR cycle <i>a</i> and <i>b</i> , Case Study IV . . . . .	109
5.30 Key Performance Indicators of HX-1 and HX-2, Case Study IV . . . . .	114
5.31 Key Performance Indicators of compressors in MR cycle <i>a</i> and <i>b</i> , Case Study IV . . . . .	114
5.32 R290 chiller performance in <i>i</i> <sub>4</sub> <sup>*</sup> , Case Study IV . . . . .	115
5.33 R290 chiller performance in <i>i</i> <sub>8</sub> , Case Study IV . . . . .	115
5.34 Main results from best iteration solutions original design in Case Study IV . . . . .	117
5.35 Distribution of irreversibilities in best iteration solutions, Case Study IV . . . . .	118
5.36 Main results, expander integration with constant pressure ratio, Case Study IV . . . . .	119
5.37 Main results, expander integration with $\Delta T_{min}$ -adjusted pressure ratio, Case Study IV . . . . .	120
5.38 Net compressor power and irreversibility, for $\eta_c = \eta_e = 85\%$ . <i>i</i> <sub>4</sub> <sup>*</sup> <i>b</i> ' . . . . .	120
5.39 Final exergy efficiency and spec. power requirement of Case Study IV, Cascade Mixed Refrigerant+ (CMR+) precooling . . . . .	121

5.40	Final exergy balance of the LIN-Precooling Case Study V. . . . .	123
A.1	Initial parameters applied to Case Study I and II . . . . .	138
A.2	Initial parameters applied to Case Study III and IV . . . . .	139
B.1	Calculated irreversibilities for Case Study I, SMR PRICO . . . . .	144

# Chapter 1

## Introduction

In Paris, December 2015, consensus among 195 nations was fulfilled with commitment of reaching the two degrees global warming target, and reduce the global greenhouse emissions per capita with 8% in 2025 and 9% by 2030 [38, 1]. The growth of demand forecast for a green and clean energy carrier, points in direction of hydrogen, as an energy commodity for decarbonization of the next-generation transport sector, as well as to the power generation industry.

### 1.1 Background and motivation

Production of green and clean hydrogen in a foreseeable carbon-restrained future will indisputably require a level of emission-free applications, as the utilization may be of significant priority in reaching the COP21 targets. Portability achievement of renewable energy resources will be of great importance in the future, as the worldwide energy demand are expected to increase proportionally to arising living standards. Efficient hydrogen storage technology may be one solution to the prior, by initiating a large-scale liquefaction value chain.

Hydrogen is abundant in fossil resources, hence 96% of the worldwide production is based on Reforming Processes related to coal, natural gas and oil [26]. Production from water electrolysis represents the remaining 4%. As described by Kramer et al.[24], for a large-scale hydrogen production scenario to fulfill the criteria as "clean" or green hydrogen, Carbon Capture and Storage (CCS) must be applied to the value chain, on accord to the well-to-wheel evaluation.



Hydrogen from a gravimetric point of view, conceals large amounts of energy. In order to store and transport the extensive energy amount, hydrogen gas density must be increased significantly to compete with other energy storage alternatives, such as state-of-the-art batteries. The two methods of high-density storage of hydrogen is by liquefaction or compression. A comparison of optional hydrogen states for transportation states, provided by Berstad et al. in [9]: "...shows that LH2 at 0.1 MPa (1 bar) contains about four times the energy per volume unit than does CGH2 at 25MPa (250 bar) and almost three times as much than for 35 MPa (350 bar)..".

Today, energy efficient hydrogen liquefaction technology exists to a limited extent. Still, nations worldwide express their commitment through upcoming research projects. In Japan, the green technology transition is emerging as a result of the gradual termination of the national nuclear program. At the World Hydrogen Energy Conference 2016 in Spain, Toyota presented their expectation on the growing market of hydrogen fuelled cars of more than 30,000 units per year on a global scale, and 1000 units per month on a national scale within 2020 [35]. In California, Royal Dutch Shell Plc, through a partnership with Toyota Motor Corp, will build 7 hydrogen fueling stations, where several motor companies such as Honda Motor Co., Hyundai Motor Co. and Daimler AG., are intending to be selling fuel cell vehicle during the end of the year [11]. In UK, earlier this year, Shell opened the first vehicle refuelling station in addition to propose plans for at least two further stations later in 2017 [20], as a part of the European hydrogen project HyFIVE [21].

### 1.1.1 The SINTEF HYPER Project and Norwegian Hydrogen Infrastructure

With emphasis on the hydrogen initiative in Japan, the SINTEF (The Foundation for Scientific and Industrial Research in Norway) project HYPER [2], propose a large-scale production scenario of liquid hydrogen, with energy resources based on Norwegian renewable power surplus, mainly from wind- and hydro-power, and natural gas reserves. With a plant capacity expected somewhere between 150-500 tons per day (tpd), the liquid product are to be exported in large tankers to Japan, representing approximately 820 MW on an energy point of view and around 7 TWh on an annual basis [45].

Experiences from liquefaction technology in Norway is already developed within the Liquefied Natural Gas (LNG) industry, and with an LNG carrier fleet capacity of 13,000 tons per day [22], a high experience framework basis exists for creation of a new value chain. The hydrogen infrastructure in Norway, is on the other

hand limited. Still, companies within the refrigeration and food industry, such as TINE ASA and ASKO Norway, are expressing their interests in hydrogen fueled vehicles for bulk transport purposes [46, 4, 19]. Simultaneously, the Scandinavian Hydrogen- Fueling Station and Production Company, NEL ASA, are experiencing a milestone in the company, as a big co-operation agreement was signed with H2V Product in France, in June 2017, with intentions of building hydrogen production facilities of above 700 MW [16].

The hydrogen liquefaction process requires considerable amounts of energy on a large-scale level, and within the scope of the HYPER project, this thesis work will investigate the potential of implementing the existing natural gas liquefaction technology into a hydrogen pre-cooling cycle, with emphasis on Mixed Refrigerant Technology. Efficient pre-cooling systems has proven to be a benchmark within complex liquefaction cycles, in order to achieve the energy efficiency required to realize such future projects.

Therefore, a comprehensive exergy evaluation will in addition to the process simulations be performed for each Case Study model which is buildt up in the simulation software, Aspen HYSYS. In order to do so, many parameters needs to be handled simultaneously. Aspen HYSYS provides possibilities of real-time spreadsheet calculations which makes the calculation steps more automated. As a final validation of the proposed Case Study processes, each will be benchmarked with a Liquid Nitrogen Precooling (LIN-PC) process

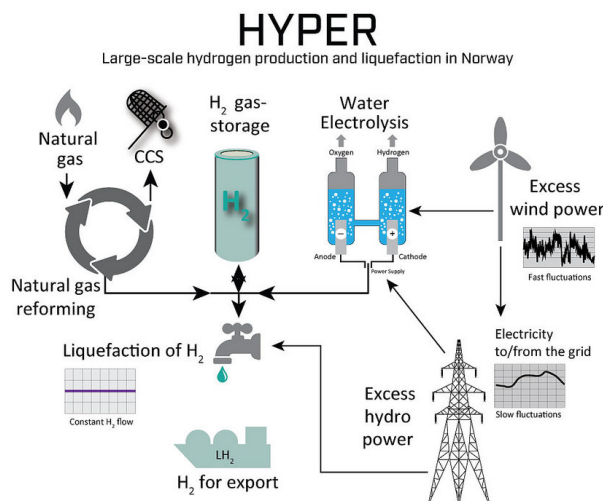


**Figure 1.1:** The SINTEF HYPER project illustration [2]

## 1.2 Thesis structure

The overall structure of the thesis is presented below:

- **Chapter 2: Theory - Target parameters:** The introductory part of the thesis will elaborate on the target parameters of interest within liquefaction processes, such as Key Performance Indicators (KPI) of process equipment and energy efficiency, with emphasis on exergy- destruction analysis and efficiency maximization. To get a deeper understanding of the upcoming analysis work.
- **Chapter 2: Theory - Review of hydrogen liquefaction concepts:** A literature review is presented, with major focus on new and theoretical concepts for both precooling and cryogenic cooling of hydrogen. KPI's relevant for comparison and benchmarks are extracted and will be summarized at the end of this section.
- **Chapter 3: Case Study Process Models:** Four Case Study process models are presented, as they are subject for simulation, optimization, and further re-modification in the analysis chapter.
- **Chapter 4: Technical Methodology:** A technical methodology is presented, with emphasis on the process design of each Case Study process. Property data of different hydrogen forms are validated and compared with different reference sources. System boundaries for each Case Study process is defined, with emphasis on the upcoming exergy loss analysis. A brief description of the optimization procedure will also be explained in this chapter.
- **Chapter 5: Technical Results and Discussion:** The main results from each Case Study are presented, analyzed and discussed with emphasis on: i) the process component KPI's and ii) the final resulting exergy losses and efficiencies. A final benchmark with a conventional process is presented as the last discussion of this thesis.
- **Chapter 6 and 7: Conclusion and further work proposals:** The last part of the thesis consist of the conclusion, which presents the best results from the analysis chapter and puts the work into a bigger perspective, when proposing recommendations for further work.

# Chapter 2

## Theory

This chapter will elaborate on theoretical and state-of-the art aspects related to hydrogen liquefaction. The beginning of the chapter will discuss on the basics of the hydrogen value chain, from well to tank storage, followed up on a brief overview of the most essential KPI's that comprises efficient liquefaction processes.

An extensive literature survey follows, with a major focus on both existing and conceptual processes of complete hydrogen liquefaction systems, as well as alternative process concepts in favour of precooling processes. As an example, industries with higher degree of establishment, such as the Liquefaction of Natural Gas (LNG) industry and nitrogen liquefaction systems in Air Separation Units (ASU), may be an interesting benchmark while considering the Technological Readiness Level (TRL) of new process concepts.

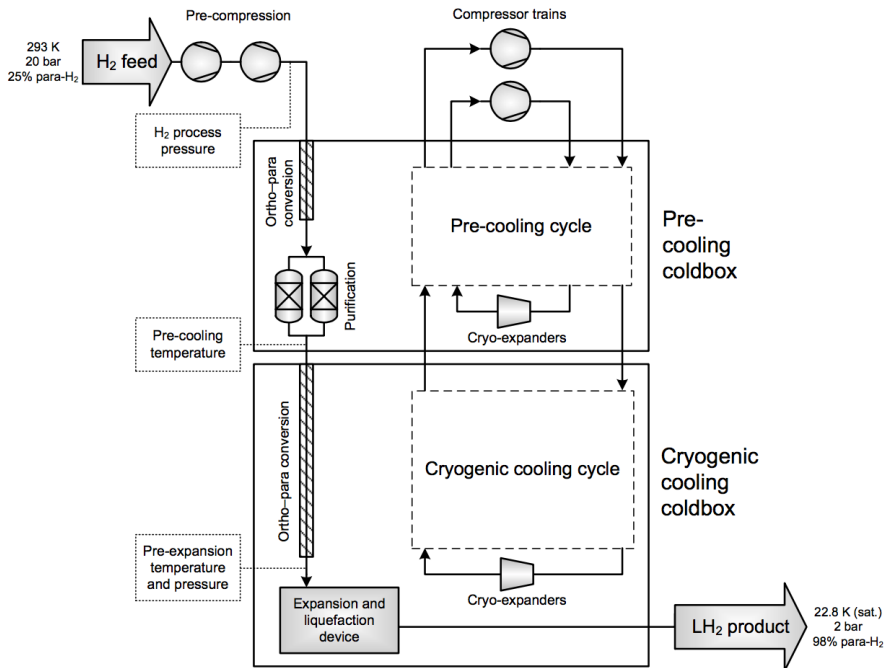
### 2.1 Hydrogen Liquefaction Chain

Figure 2.1 shows the most fundamental parts of the hydrogen liquefaction chain, with evident system boundaries defined. The first block of the liquefaction system involves the production and purification unit, which is not indicated in Figure 2.1.

The most common technologies for hydrogen production is Steam Methane Reforming (SMR), Water Electrolysis (WE) and Coal Gasification (CG) [7]. On the other hand, coal is not part of the energy mix in Norway, hence the main production source, also defined within the scope of the HYPER project [2], are the two

former. Apart from the above mentioned processes, there are many methods still at the research and development stage, in particular based on biomass. These are described more in detail in Ball and Wietschel in [7].

The SMR process generates a synthesis gas from Natural Gas (NG) in two different reactors, where hydrogen is extracted. This concept can be modified into many different designs, and were also covered in a detailed simulation and optimization work in the master thesis of Åtland and Jakobsen [53] in spring 2016. In addition to hydrogen, there are great amounts of  $\text{CO}_2$  in the synthesis gas. Therefore arguments in favour of SMR as the hydrogen production unit were made on the condition that Carbon Capture and Storage (CCS) was successfully integrated into the process, providing a pure, carbon lean hydrogen product. The final step of the conventional production unit is the Pressure Swing Adsorption (PSA), which removes impurities from the product down to a very low ppm-level. Hence, typical feed pressure is given by the PSA-unit at 20 bar.



**Figure 2.1:** Generic Process Flow Diagram (PFD) of the hydrogen liquefaction chain, obtained from Walnum et al. in [50]

The major system-module of interest in this thesis work is the first block, which comprises the precooling system. Typical precooling temperatures varies from 130 down to 80 K, dependent on the choice of precooling cycle and refrigerant. It can also be seen that working fluids from the Cryogenic cooling cycle are integrated into the precooling-module and compressed at ambient temperature. This approach has been investigated, and will be further elaborated in Chapter 3 and 4.

Within the precooling system, conversion of ortho-to-para hydrogen is initiated, in addition to a final purification system, which will be further explained later in this section.

The cryogenic cooling coldbox-module is out of scope of this thesis analytic work and simulations. Instead, new and theoretical concepts for different cryogenic cooling cycles from literature will be investigated in the literature survey, later in this chapter, searching for parameters which makes heat integration with the precooling system feasible.

## 2.2 Target parameters in liquefaction plants

The main target parameters for a gas liquefaction plant can be divided in two groups; Key Performance Indicators (KPI), of each component that comprises a liquefaction plant. The major components of interest are gas compressors, cryogenic heat exchangers, throttling valves and liquid/cryogenic expanders. The second group is the efficiency parameters, which for low-temperature systems is the Exergy Efficiency, ( $\varepsilon_x$ ) and the Specific Energy Consumption (SEC) of either the overall process, or a part of the process, such as Precooling (PC), Cryogenic Cooling (CC/Liquefaction) or Subcooling (SC).

### 2.2.1 Key performance indicators in process components

The minimum energy requirement is found by analysing the exergy balance throughout the process and inside its main components, such as heat exchangers and compressors. In an extensive optimization model proposed by Aspelund et al. [6] the heat exchanger for a simple LNG process was analysed with emphasis on key parameters such as the Minimum Internal Temperature Approach (MITA or  $\Delta T_{min}$ ), the size and overall heat transfer coefficient parameter  $U$  and  $A$ , and the driving forces represented as the logarithmic mean temperature difference (LMTD).

The relation between  $UA$  and  $LMTD$  and the heat transfer duty,  $Q$  is defined by Incropera in [23] as

$$Q = UA \cdot (LMTD) \quad (2.1)$$

where  $UA$  is a function of the overall heat transfer coefficient.  $U$  is also determined by fluid specific thermophysical parameters, such as the heat conduction and convection, which is described in further detail by Incropera [23].  $U$  then represents a common measure of the total driving force in the heat transfer mechanism.  $LMTD$  is defined by [23] as

$$LMTD = \frac{\Delta T_A - \Delta T_B}{\ln(\Delta T_A / \Delta T_B)} \quad (2.2)$$

where  $A$  and  $B$  represents each end of the heat exchanger where the streams enter or exit on either hot or cold side. Note that Eq.2.2 only is valid with two different channels.

In the simulation environment of the software used in this thesis, Aspen HYSYS, the calculation of the  $LMTD$  and  $UA$  parameter for a multi-channel heat exchanger are broken into intervals [29]. An energy balance is applied along this interval and summed to calculate the overall exchanger  $UA$  and  $LMTD$ , hence represented as an average "weighted" temperature difference instead of the logarithmic approach. The parameter obtained, and analyzed in the simulations will be given as  $WMTD$  (Weighted Mean Temperature Difference). The method used for the simulation and optimization for liquefaction of hydrogen, in this thesis emphasized on the precooling process, will be described further in Chapter 4.

Further in [6], the visualization of the heat transfer,  $Q$ , along the temperature range was represented by the hot and cold composite curves of the streams, indicating at which temperature level the exergy losses were most intensive. Hence, a given  $\Delta T_{min}$  at a low temperature will generate higher exergy losses than at a higher temperature, as illustrated by Figure 2.2. A correlation between the composite curves and compressor work was also proven by the optimization model. Compressors may be connected in series, defined as multi-stage setup, to confine the high level of discharge temperatures generated at a given pressure. Determination of the intermediate pressure level is defined by Øverli [39] as

$$\Delta p_n = (p_1 p_2)^{1/n} \quad (2.3)$$

where  $n$  is the number of compressors in series.

### 2.2.2 Exergy and minimum energy requirement

In liquefaction processes, the required amount of useful energy (which from a thermodynamical point of view is known as the required exergy), to cool a process stream one degree below ambient temperature,  $T_0$ , is always larger than the necessary exergy or heat to warm the same process one degree above  $T_0$  [30]. This can also be shown in Figure 2.2, where hydrogen exergy content with respect to a surrounding temperature of 300 K and a pressure of 1 bar is plotted<sup>1</sup>. Neglecting kinetic and potential energy changes, the specific exergy of any stream with respect to the ambient conditions at  $T_0$  is then given as

$$\dot{e}_x = (h - h_0) - T_0(s - s_0) = E_x/\dot{m} \quad (2.4)$$

where  $h$  is the specific enthalpy,  $s$  the specific entropy, with  $h_0 = h(T_0, p_0)$  and  $s_0 = s(T_0, p_0)$ .

With emphasis on the low temperatures required to liquefy hydrogen, the most essential key performance parameter of the process is the equivalent energy required energy to liquefy one unit [kWh/kg<sub>H2</sub>] of hydrogen. This target parameter has also been analyzed to a great extent in recent proposed papers on a period of 20 years, which is found in [41, 10, 9, 47, 14, 8]

Below, the generalized exergy balance equations for each component,  $k$ , in the liquefaction process are listed together with its respective efficiency. These equations will be used for analysis of the irreversibilities,  $\dot{I}_{k,j}$  in Chapter 5, to quantify which of the processes in the case studies that require the lowest specific power consumption and generate minimum amounts of losses.

#### 2.2.2.1 Exergy balance in heat exchangers

For a multi-channel heat exchanger with a number,  $s$  of inlet/outlet streams, the exergy balance, which describe the destroyed exergy known as the irreversibility,  $\dot{I}$ , in the subsystem is

$$\begin{aligned} \dot{I}_{hx,j} &= (\dot{E}_{in} - \dot{E}_{out})_{hx,j} \\ &= \left[ (\dot{m}e)_1 + \dots + (\dot{m}e)_s \right]_{in,j} \\ &\quad - \left[ (\dot{m}e)_1 + \dots + (\dot{m}e)_s \right]_{out,j} \end{aligned} \quad (2.5)$$

---

<sup>1</sup>Data values obtained from NIST Refprop



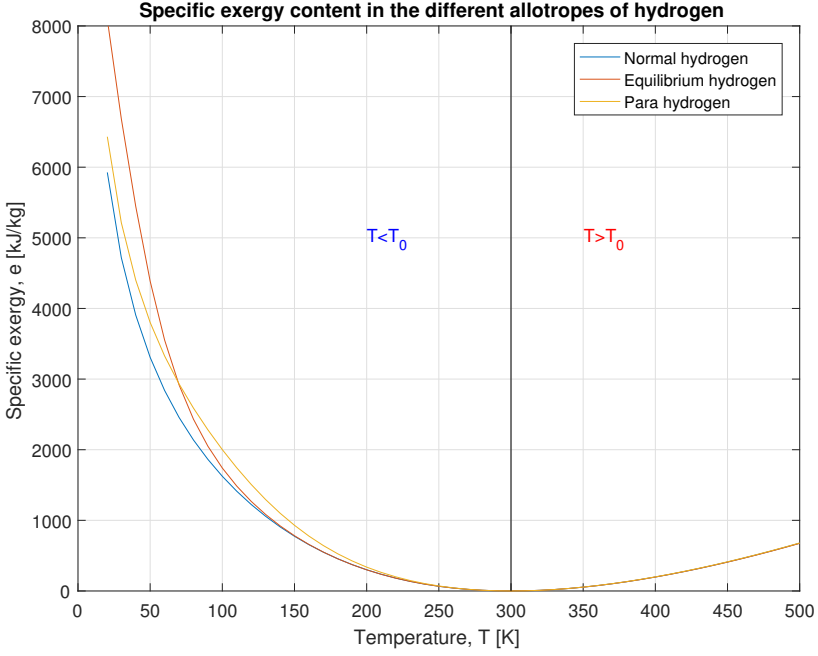


**Figure 2.2:** Exergy content of the different molecular forms of hydrogen assuming 300 K surrounding temperature at 1 bara

where  $e$  and  $m$  is the specific exergy and mass flow respectively for stream  $s$ , in heat exchanger  $j$ .

The exergy efficiency of the subsystem simply becomes the total outgoing balance over the total incoming balance

$$\begin{aligned}
 (\varepsilon_{hx,j})_1 &= \frac{\dot{E}_{out}}{\dot{E}_{in}} \\
 &= \frac{\left[ (\dot{m}e)_1 + \dots + (\dot{m}e)_s \right]_{in,j}}{\left[ (\dot{m}e)_1 + \dots + (\dot{m}e)_s \right]_{out,j}}
 \end{aligned} \tag{2.6}$$

Another definition of the heat exchanger exergy efficiency is given by Wark [51],

which is given as the ratio of the increase in the cold,  $c$ , fluid exergy to the decrease in the hot,  $h$ , fluid exergy. The efficiency then becomes

$$\begin{aligned} (\varepsilon_{hx,j})_2 &= \frac{\dot{I}_{cold}}{\dot{I}_{hot}} \\ &= \frac{\sum (\dot{m}e)_{out,c} - \sum (\dot{m}e)_{in,c}}{\dot{I}_{hot}} \end{aligned} \quad (2.7)$$

where,

$$\dot{I}_{hot} = ((\dot{m}e)_{in,h} - (\dot{m}e)_{out,h})_1 + \dots + ((\dot{m}e)_{in,h} - (\dot{m}e)_{out,h})_s$$

### 2.2.2.2 Exergy balance in compressors

The exergy balance for a given compressor,  $j$ , with inlet- and outlet conditions from an arbitrary stream,  $s$ , in the system is given as the exergy difference between the inlet and outlet streams plus the input power,  $\dot{W}_{cpr,j}$  of compressor  $j$ .

$$\begin{aligned} \dot{I}_{cpr,j} &= \dot{E}_{in} - \dot{E}_{out} \\ &= (\dot{m}e)_{s,in} + \dot{W}_{cpr,j} - (\dot{m}e)_{s,out} \end{aligned} \quad (2.8)$$

The exergy efficiency of any compressor is given as the ratio between the minimum work,  $W_{min,j}$ , of compressor  $j$ , and the actual work given above

$$\varepsilon_{cpr,j} = \frac{\dot{W}_{min,j}}{\dot{W}_{cpr,j}} \quad (2.9)$$

where  $\dot{W}_{min,j} = \sum (\dot{m}e)_{s,out} - \sum (\dot{m}e)_{s,in}$ .

### 2.2.2.3 Exergy balance in expansion- valves and turbines

The exergy balance for stream,  $s$ , through an expansion valve,  $j$ , is given as

$$\dot{I}_{vlv,j} = \dot{E}_{in} - \dot{E}_{out} = \sum (\dot{m}e)_{s,in} - \sum (\dot{m}e)_{s,out} \quad (2.10)$$

If the expansion is done by an energy recovery expansion turbine, the irreversibility is also given by the power generated,  $\dot{W}_{trb,j}$ , by the turbine

$$\dot{I}_{trb,j} = \dot{I}_{vlv,j} - \dot{W}_{trb,j} \quad (2.11)$$

The exergy efficiency of a valve is simply the ratio of the total exergy output to the total exergy input

$$\varepsilon_{vlv,j} = \frac{\sum (\dot{m}e)_{s,out}}{\sum (\dot{m}e)_{s,in}} \quad (2.12)$$

while the efficiency using a turbine will be higher, because the exergy destroyed decreases proportional as the turbine develops work. The exergy efficiency of the turbine is therefore

$$\varepsilon_{trb,j} = \frac{\dot{W}_{trb,j}}{\sum (\dot{m}e)_{s,in} - \sum (\dot{m}e)_{s,out}} \quad (2.13)$$

#### 2.2.2.4 Exergy balance in mixers with streams of different mole-fractions, pressures and temperatures

It is assumed that every component within a simplified liquefaction process, as in this particular case, generates zero chemical exergy, with the exception when a stream mixer component is integrated. If two streams with different mole fractions of the mixture components, together with different pressure and temperature, chemical exergy contributes to generation of irreversibilities in addition to the thermo-mechanical irreversibility. For an arbitrary mixer unit, with  $n$  streams at inlet and  $m$  streams at outlet, the chemical exergy destruction,  $\dot{I}_{mix}^{ch}$  becomes

$$\begin{aligned} \dot{I}_{mix}^{ch} &= \bar{R}T_0 \left[ \sum_{in} \dot{N}_i (x_i \ln x_i) - \sum_{out} \dot{N}_i (x_i \ln x_i) \right] \\ \dot{I}_{mix}^{ch} &= \bar{R}T_0 \left[ \dot{N}_{i,tot} \cdot \sum_{in} (x_i^2 \ln x_i) - \dot{N}_{i,tot} \cdot \sum_{out} (x_i^2 \ln x_i) \right] \end{aligned} \quad (2.14)$$

where  $\dot{N}_i = x_i \cdot \dot{N}_{tot,i}$ .  $\bar{R} = 8,314[\text{kJ}/\text{kmoleK}]$  is the universal gas constant. The overall exergy destruction of the mixer is defined as  $\dot{I}_{mix} = \dot{I}_{mix}^{ch} + \dot{I}_{mix}^{tm}$ , where  $\dot{I}_{mix}^{tm}$  is the thermo-mechanical exergy destruction defined by

$$\dot{I}_{mix}^{tm} = \sum_{in} \dot{E}_i - \sum_{out} \dot{E}_i \quad (2.15)$$

## 2.2.2.5 Summary - Overall exergy efficiency of a cycle

The total balance of irreversibilities in the cycle is the sum of every irreversibility,  $\dot{I}_{k,j}$ , generated within each type of process component,  $k$ , number  $j$ , as explained above. Adding all of the expressions for the irreversibilities in terms of Equations (2.5), (2.8), (2.10) and (2.11) the overall exergetic efficiency is defined as

$$\varepsilon_{tot} = \frac{\dot{E}_{out} - \dot{E}_{in}}{\dot{W}_{actual}} = \frac{\dot{W}_{actual} - \dot{I}_{tot}}{\dot{W}_{actual}} = \frac{e_{product} - e_{feed}}{w_{actual}} \quad (2.16)$$

Note that the numerator of Eq. (2.16) is equal to the minimum specific power to liquefy 1 kg of hydrogen,  $w_{min}$ . Assuming both liquid saturated product and gaseous feed stream leaves and enters the system at atmospheric pressure, the actual liquefaction power can be visualized as a function of the overall exergy efficiency (see Figure 2.4), as

$$w_{actual} = \frac{w_{min}}{\varepsilon_{tot}} = \frac{e_{product} - e_{feed}}{\varepsilon_{tot}}$$

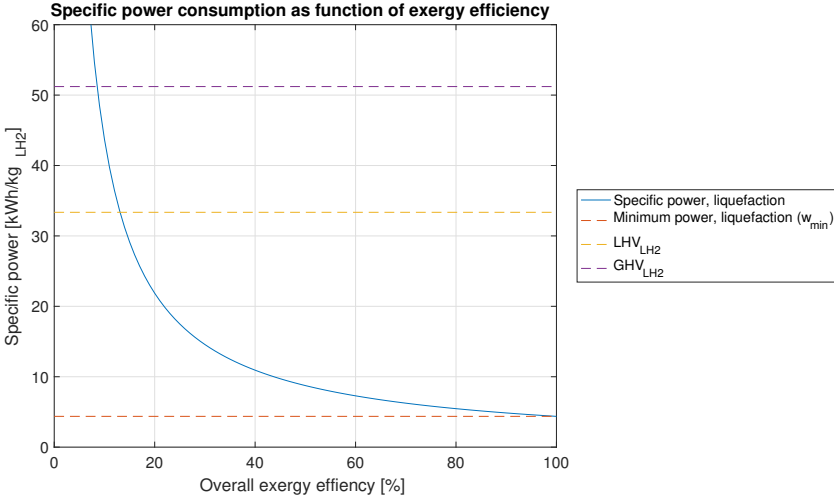


**Figure 2.3:** Specific power consumption as function of exergy efficiency,  $\varepsilon_x$

The Lower Heating Value (LHV) of liquid hydrogen is indicated by the dashed line in the middle, while the the minimum power requirement of liquefying 1 kg

is indicated by the lower dashed line. Hence, the interval in between determines the valid range of power consumption as a function of the exergy efficiency. A comparison study between gaseous and liquid hydrogen as transportation options, proposed by Wolf [52], concluded that the specific liquefaction power should be equal or lower than 30% of hydrogen LHV. It can be observed, by inspection of Figure 2.4, that an exergy efficiency of 40% or higher must be achieved to meet the LHV criteria.

## 2.3 Precooling principles

Development of an exergy efficient precooling process is critical for the overall minimum power consumption. As described in [50] a conventional Liquid Nitrogen (LIN) process is used for hydrogen precooling in every existing liquefaction plants at present time.

The drawback of this concept is that the minimum energy requirement for producing the LIN is two times the minimum energy for precooling of the hydrogen down to 80 K. Nevertheless, many liquefaction plants are located close to an air separation unit (ASU), where LIN is a byproduct available "for free", in terms of exergy losses. Analysis in favor of minimization of exergy losses still concludes that other applications, where the precooling media can be recycled back to the system, must be considered for future large-scale systems.

In order to realize such concepts, the precooling target temperature concerning the analysis work in this thesis, is set to 130 K.

Hydrogen pre-compression must also be considered. One of the main reasons is that the heat capacity,  $c_p$ , in the cryogenic temperature region (<130 K) is highly variable, hence difficulties related to the temperature match inside the heat exchangers occurs. If the pressure of the feed stream is increased (pre-compression), the slope of  $c_p$ , becomes less steep, hence it is easier to control the variable cooling demand. See Figure 2.4.

As the precooling temperature range is down to 130 K, Figure 2.4 also indicates that  $c_p$  for normal hydrogen is more or less constant.

Case studies are presented in chapter 5, where it will be crucial if the system boundary is defined with or without pre-compression with emphasis on the minimum energy requirement, or exergy.

In the following sections, different solutions and concepts for precooling processes will be discussed.

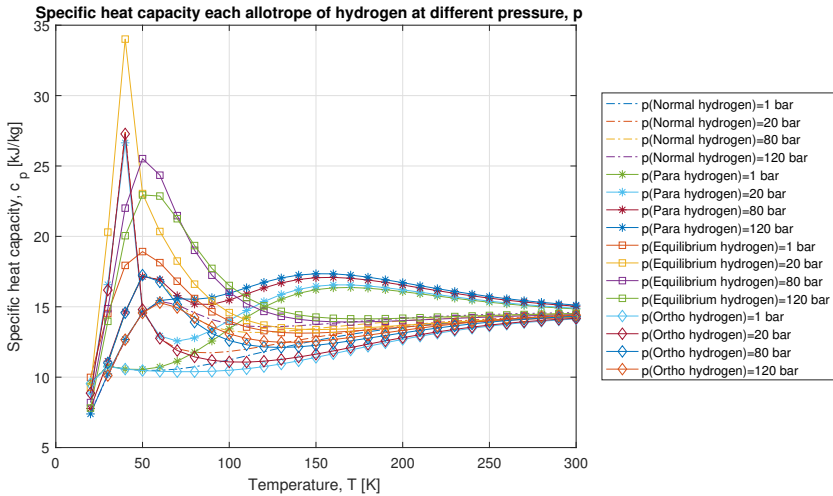


**Figure 2.4:** Specific heat capacity for equilibrium hydrogen at 20 and 80 bar

### 2.3.1 Precooling technology in existing hydrogen liquefaction plants

#### 2.3.1.1 Liquid nitrogen (LIN) precooling concepts

Liquid nitrogen is the only precooling medium used in the hydrogen liquefaction plants in operation today [50]. As a precooling agent it is superior due to its temperature range to below 80 K. Nevertheless, Figure 2.5 shows great temperature gaps between the hot and cold composite curve, which generates a great portion of exergy losses.

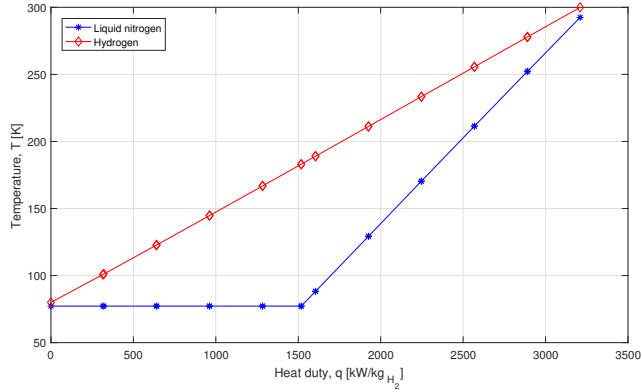


**Figure 2.5:** Simple temperature profile for precooling using liquid nitrogen. Figure generated in Aspen<sup>®</sup> HYSYS

The concept of adaption of LIN into a precooling cycle for hydrogen liquefaction gives an exergy penalty associated with generation of liquid nitrogen. When analyzing the overall exergy efficiency of a liquefaction system, this penalty has to be taken into account in the overall balance.

### 2.3.2 Mixed refrigerant process concepts from the LNG industry relevant for hydrogen precooling

Mixed Refrigerant (MR) as working fluids in liquefaction processes is a mature technology concept within the LNG industry [49]. In a hydrogen liquefaction scenario, this technology can be suitable within a precooling concept, mainly because the temperature targets are more or less equal ( $T(\text{LNG})=113\text{ K}$  and  $T(\text{Hydrogen precooling})=130\text{-}110\text{ K}$ ), and adaption of existing technology is easier to accomplish.

A typical MR composition suitable in this context, should consist of the least volatile hydrocarbons, ranging from methane (C1) to buthane (C4), first of all to avoid freeze-out of the heavy components. In order to reach below the C1 boiling point, a major mole fraction of nitrogen is commonly used. The product stream is cooled due to evaporation of the MR stream in one or several heat exchangers by releasing the latent heat of vaporization [40].

In the upcoming sections, several MR processes are described and analyzed. In contrast to single component refrigerant, which gives a constant temperature

phase change (see Figure 2.5), the MR concept achieves a gliding temperature during vaporization and condensation. This phenomena is one of the major advantages within this MR concept, and allows a better temperature match between the fluids when adjusting the composition. To find a suitable MR process for hydrogen precooling, arguments in favor of an optimal temperature match in the heat exchangers will be decisive, despite that the cooling curve of pure hydrogen is more or less constant in the given temperature interval.

### 2.3.2.1 Kleemenko Cycle

The Kleemenko cycle was the first proposed mixed refrigerant process for liquefaction of natural gas, by the Russian engineer Aleksandr Petrovich Klimentko in 1959 [49]. The Kleemenko principle is clever, simply because the phase separation in the ambient temperature region allows for additional control to avoid freeze out of the heaviest components in the mixture. E.g. if the MR composition contains heavier hydrocarbons such as buthane ( $C_4$ ), pentane ( $C_5$ ) etc. and the required cooling temperature is below it's freezing points, it is possible to integrate several separators in between the heat exchanger stages to neglect those components.

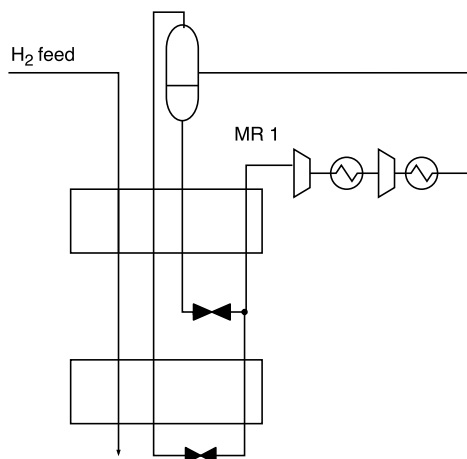


**Figure 2.6:** The single Kleemenko cycle

One of the common thread of the mixed refrigerant processes are the benefit of working at relative low-pressure (LP) levels compared to single fluid refrigerants, which minimizes the power input of the compressors. On the other hand, to achieve the required duty with variable pressure, lower pressure levels result in



higher mass flow because of reduced density of the mixture compared with higher pressure. Therefore, many trade-offs needs to be evaluated.

### 2.3.2.2 The PRICO process

In today's LNG industry, the PRICO process is one of the simplest systems, using only one refrigeration cycle [30]. The main constituents in this single cycle is a mixture of the lightest hydrocarbons including a major fraction of gaseous nitrogen. In order to fit this technology into a hydrogen liquefaction process, there are a number of degrees of freedom defining the optimization potential of the process. This is mainly the duty that describes the cooling power down to the preferred temperature level plus the composition of the working fluid. Since PRICO can be used for LNG production (close to 113 K) [30] it is reasonable to assume that a single refrigeration cycle can obtain a precooling effect down to 130-110 K.

Still, a major drawback of this cycle and its simplicity is the limited degrees of freedom in the process design. Because of the volatility of the heaviest components in the working fluid, temperatures below or down to 80 K can cause freeze out in the system [50]. Therefore, more recent precooling systems proposes a temperature at a higher level, e.g. in the IDEALHY project [8] a precooling temperature of 130 K using an alternative MR approach is used.

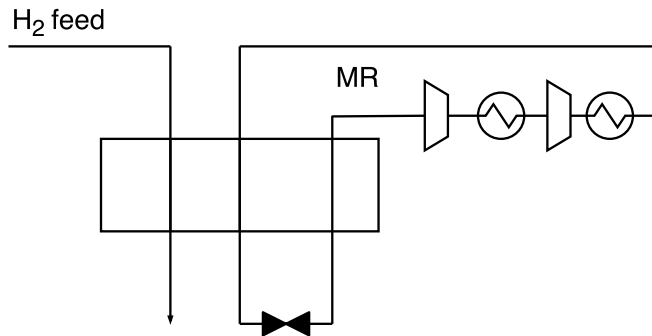


**Figure 2.7:** The single PRICO process cycle

### 2.3.2.3 Dual/Cascade Mixed Refrigerant cycles (MFC Snøhvit)

The PRICO process can be modified and extended by use of the cascade concept. The process flow diagram indicated in Figure 2.8 shows the basic principle of the

cascade; two separate Single Mixed Refrigerant (SMR) cycles are connected where the first heat exchanger pre-cools the second cycle, reaching for a temperature level of 120-80 K according to the first proposal given by [50]. Similar as the single PRICO process both the pressure levels and the working fluid composition of each cooling cycle should be adjusted with emphasis on the given cooling target temperature. If there are volatile components such as *i*-butane and heavier gases, freeze-out will occur at temperatures close to 90-80 K.

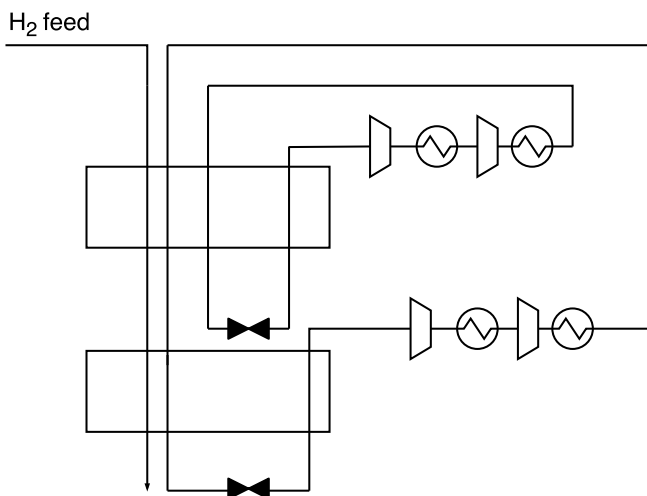


**Figure 2.8:** The Dual/Cascade MR process cycle

An important feature of the MR cascade process is that it is possible to control the volatility of the working fluid in each cooling circuits, and thence design a perfect heat overlap between those. The LNG plant from Conocco Phillips, described in Pettersen et al. [18], is a three-circuit cascade with pure fluids, such as propane, ethylene and methane with temperature levels down to target in the respective order. In this cycle condensation of ethylene is not possible without precooling with boiling propane. The same principle yields for the lower temperature level with methane. By changing the working fluid to an MR stream, this process is easier to control by adjusting the MR composition, hence the properties of each stream.

An example of the CMR process is the Statoil Snøhvit LNG facility in northern Norway, which utilizes the concepts of MR cascade design in the process. This by using three different and separate MR cycles which gives minimum compressor shaft power requirement as indicated in [3]. The simplified PFD of the Linde

Mixed Fluid Cascade (MFC) process is shown in Figure 2.8. With emphasis on the excellent performance with the three optimized cycles in this facility, a study of utilizing a similar approach for hydrogen precooling will be very interesting.

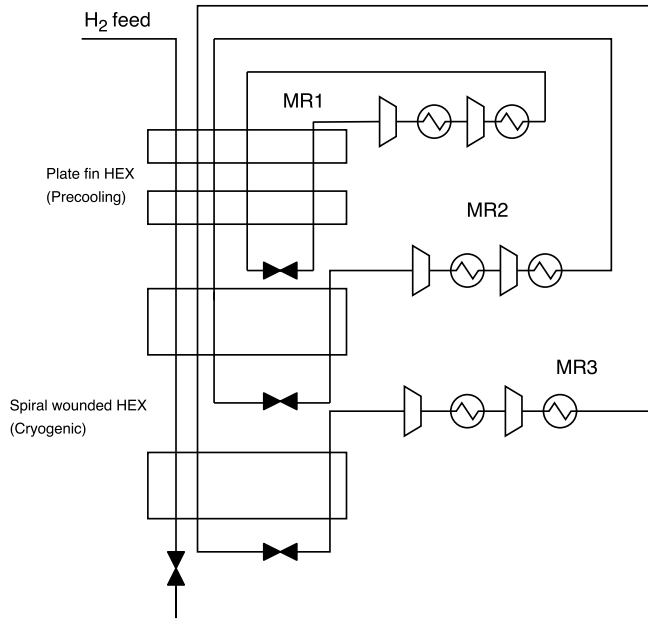


**Figure 2.9:** A simplified PFD of the Linde MFC<sup>®</sup> process for liquefaction of natural gas at the Statoil Snøhvit facility. Some details are missing for simplicity but can be found in [3]

#### 2.3.2.4 The LIMUM process

The Line-Multi-stage Mixed Refrigerant Process (LIMUM) is licensed by the Linde Group and can be designed with two different modifications. The first modification is the LIMUM 1 [3], which is indicated in Figure 2.10. The process consists of one plate-fin heat exchanger with a two-stage single MR compression cycle. In between the compression stages an intermediate pressure stream is extracted in a separator, where the flash gas is further compressed while heavier liquids are transferred to a mixing point at the exchanger inlet. The same principles apply to the LIMUM 3 process, [3] but with a more complex design. Due to the spiral wounded heat exchanger (SWHE), a multichannel flow arrangement allows for precooling, liquefaction and sub-cooling inside the same heat exchanger. This

process is obtained by using three expansion steps, either with Joule-Thompson valves or expanders in each temperature level. More information of the LIMUM 3 process can be found in the specifications given in [3].

With emphasis on the precooling of hydrogen, the LIMUM 3 process will probably be to complex and expensive, compared to the LIMUM 1. As an example, in [40] this process concept is reported to obtain a production capacity of 0,5 to 2,5 megatons per annum (MTPA). This corresponds to a theoretical cooling duty,  $\dot{Q}_{LNG}$ , given by

$$\dot{Q}_i = \dot{m}_i (c_p)_i \cdot \Delta T = \dot{m} (h_1 - h_2)$$

which results in a cooling duty in the range from 6.65 – 32.8 MW, assuming cooling from 300 K ambient down to 113 K, assuming constant specific heat capacity in this interval.

In comparison, a hydrogen precooling system with a much lower capacity, ranging from 150-500 tpd ( $\approx 0.05$ -0.2 MTPA), will require a theoretical cooling duty,  $Q_{H_2,precooling}$ , in the range from 4.72 – 15.75 MW, with a specific heat capacity,  $(c_p)_i(T_i)$  given by the temperatures from 300 K ambient down to 130 K as precooling target temperature.

The example proves, even if the variables are not quite accurate, that a high capacity process must be chosen for hydrogen precooling, because the specific cooling duty is many times larger than for natural gas.

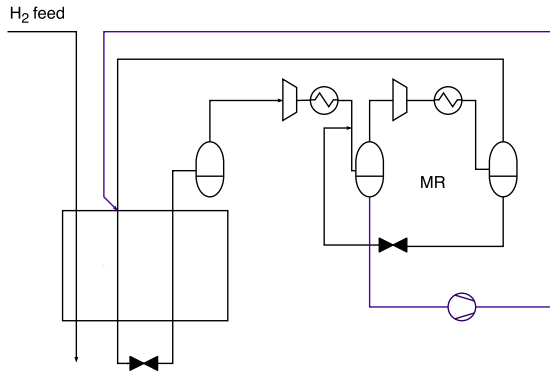


**Figure 2.10:** The LIMUM 1<sup>®</sup> process cycle

### 2.3.3 Nitrogen expansion concepts for hydrogen precooling

If a nitrogen process is to be integrated, the temperature approach in Figure 2.5 needs to be improved. One way to adjust the temperature approach, as described in [50], is to generate a greater portion of gaseous nitrogen instead of liquid. The flat line at 80 K will therefore be shortened and the curves become more parallel.

This phenomena could be further utilized by a reversed Brayton expansion cycle with multiple stream splits. The slope  $dT/dq$  is a function of the mass flow, so by designing a cascade-like process with the correct temperature values at different pressures, it is possible to generate a step-wise cooling curve with minimal gaps in between the curves. An example of this technique can be found in Aspenlund et al.[5], where a nitrogen expander process is utilized in an LNG plant.

### 2.3.4 Implementation of simple chillers in upper temperature level as partial precooling

In order to reduce the heat load and pressure drop in the coldbox-insulated (cryogenic) heat exchangers, simple chillers or refrigerators are suggested implemented as a partial precooling method after compression and aftercooling of the working fluid [43]. In the IDEALHY project the chillers cools the working fluid down to 279 K (6 °C), before it enters the coldbox. Case studies concerning the simulation models of this thesis will include this concept for comparison.

Refrigerators operating with conventional fluids such as ammonia (R717), propane (R290) or R134a were suggested. An evaporator temperature approach of  $\Delta T = 5K$  was recommended for the evaporators, assuming that a  $COP$  of 5-7 could be achieved.

A proposal for a chiller system will be presented in the next chapter, as a part of the different case studies for simulation

## 2.4 Ortho-para conversion

Another important aspect of the hydrogen liquefaction process, is the two isomers of hydrogen, known as ortho and para hydrogen. Ortho- and parahydrogen are defined by the nuclear spin orientation of the hydrogen molecule, where ortho-hydrogen is oriented in parallel and para-hydrogen antiparallel. At ambient conditions the equilibrium distribution is 75% as ortho-hydrogen and 25% as para-hydrogen. As the temperature of hydrogen decrease below the ambient

reference state, the composition tends towards increasing of para-hydrogen until a maximum of 100% is reached at 0 K, independent of pressure [33], see Figure 2.11.

Figure 2.11 shows the ortho-para distribution with varying temperature,  $T$ . The data are based on a property table given by co-supervisor David Berstad (source: for the time being unknown), quite similar to those found in [28, 32] and compared to an estimated polynomial formula provided by Meagher [33]. Figure ?? shows that the deviations are approximately negligible, which means that the polynomial is valid.

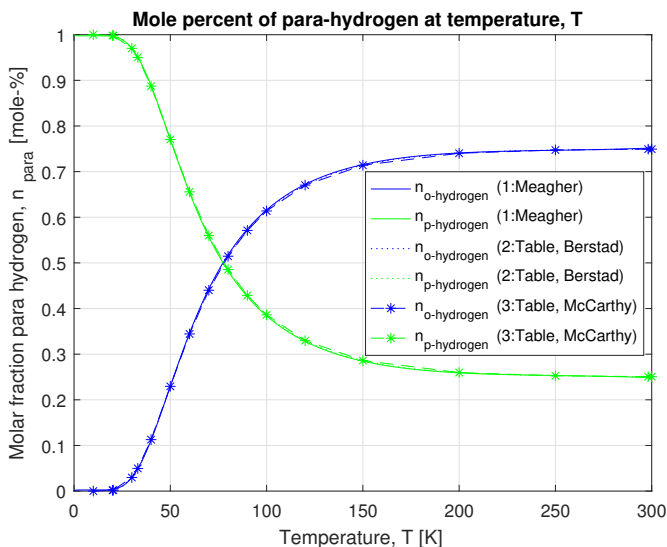


**Figure 2.11:** Comparison of para-hydrogen composition at temperature,  $T$  with three different references from literature

Ortho to para conversion is an exothermic and relatively slow process, hence a fraction of heat will naturally be released during storage at the liquid state<sup>2</sup>. During storage over longer time intervals, which is the case for a large-scale scenario, a large amount of the liquid product would potentially evaporate as a result of the prior phenomena. E.g. an experiment reported by Larsen et al. [27] in 1948, verified that about 18% of the liquid hydrogen product evaporated inside the Dewar vessel within one day, due to the self-conversion phenomenon.

<sup>2</sup>The half-life of the reaction is 4.87 d for pure normal-hydrogen, where the exothermic heat of conversion from normal to equilibrium is about 523 kJ/kg [17]

To solve this complication, a catalyst is always integrated into the liquefaction plant, to simply accelerate the conversion into the respective equilibrium composition at the hydrogen liquid state. In conceptual and existing plants there are two major technologies for ortho-para conversion, which are

1. **Continuous conversion catalyst-packed heat exchangers**
2. **Adiabatic batch conversion beds**

The technological development of ortho-para conversion can be illustrated with emphasis on the two existing liquefaction plants in Germany, operated by Linde in Ingolstadt and Leuna.

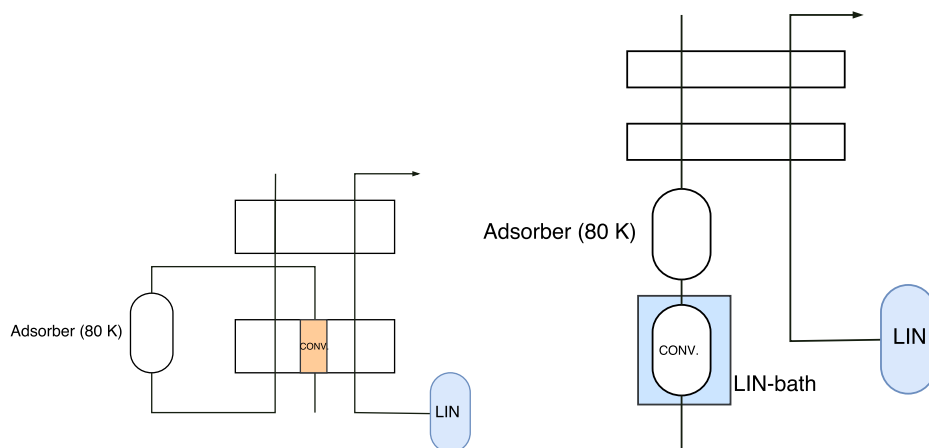
#### 2.4.1 Example plant: *Linde, Ingolstadt* - Adiabatic/isothermal batch conversion beds

Here, conversion is taking place inside multiple catalyst-filled adsorption beds at different temperature levels. Thermodynamically the conversion process is assumed either *isothermal* or *adiabatic*. Isothermal conversion is accomplished by a catalyst bed in a bath of boiling refrigerant, typically liquid nitrogen, to keep the temperature constant. In adiabatic conversion, there is no heat exchange with the surroundings, which leads to a temperature increase of the stream.

At the Ingolstadt plant, both concepts are utilized. One isothermal LIN bath reactor in the upper temperature region and one LH2 bath in the lower temperature region. In between there are two adiabatic reactors, and together a para-concentration of  $\geq 95\%$  is achieved in the final product [12]. In order to reach the necessary purity level of the hydrogen product, an adsorber bed at LIN temperature is integrated, leaving a  $N_2$  and  $CH_4$  content of less than 1ppm<sup>3</sup>.

---

<sup>3</sup>The nitrogen and methane content is only present when steam methane reforming (SMR) is assumed as hydrogen production source



(a) *Continuous conversion* concept from the Linde Leuna plant (b) *Batch conversion* concept from the Linde Ingolstadt plant

**Figure 2.12:** PFD of different concepts of integration of ortho-para conversion

### 2.4.2 Example plant: *Linde, Leuna* - Continuous conversion catalyst-packed heat exchangers

In the Leuna process, which is almost identical to the Ingolstadt process design, the catalysts are filled inside the channels of each heat exchanger as an approximation to continuous conversion, instead of the batch-wise principle.

Similar as in Ingolstadt, the feed stream needs an additional purification unit to meet the requisite purity level. At both Leuna and later the IDEALHY project (both according to the "standard Linde Kryotechnik method"[17]), the conversion was initially suggested implemented from ambient- to target temperature. However, since catalysts will be absorbing impurities and are complicated to refill, the purification unit needs to be implemented before the first conversion step. To reach the requisite purification level, temperatures at 80 K is as mentioned necessary. Unlike the Ingolstadt plant, this temperature is reached in the precooling heat exchangers instead of a LIN-bath.



## 2.5 Principles and theory of cryogenic cooling

In the cryogenic temperature range (defined at the boiling point for air at 77 K) of the hydrogen liquefaction process, there are basically two dominating concepts which are the most efficient, which are

1. **Reversed Brayton process**
2. **Hydrogen Claude process**

The two processes is described more in detail by Ohlig et al. [37], in a paper from 2013, focusing on the major challenges concerning the evolution of hydrogen liquefaction process efficiency, which states:

Hydrogen liquefaction for small scale plants with a maximum capacity of 3 tpd is accomplished with a Brayton refrigeration cycle using Helium as refrigerant. . . For larger plants, a hydrogen Claude cycle is used, characterized by higher investment but lower operating costs. However, liquefaction plants meeting the potentially high demand in the clean energy sector will need further optimization with regard to energy efficiency and hence operating costs

The production capacity target of this thesis is pushed to a great extent, compared to the maximum capacity of a pure Reversed Brayton processes described above. Therefore, as earlier mentioned in the precooling section, large-scale cryogenic processes are based on the combination of the Claude cycle as the main process and the Reversed Brayton cycle with helium and other light gases as working fluid as supplement. Hence the upcoming survey will yet again prove this and describe the different process concepts in the lower temperature range in detail.

### 2.5.1 Hydrogen Claude concepts

The theoretical basis of the Claude cycle began with the original *Linde-Hampson liquefaction cycle*, invented by Carl von Linde and William Hampson in 1895 demonstrating one of the first air separation experiments [49]. This simple ideal process involves an isothermal compression of the gas at ambient temperature. The HP gas is further cooled isobaric in a heat exchanger by its own cold return stream, where the temperature decrease is caused by the final JT throttling to a desired pressure level, see Figure 2.13a. After the throttling, a fraction (preferably high) of the gas is condensed and extracted in a phase separator. The Linde-Hampson process is shown in Figure 2.13a below.

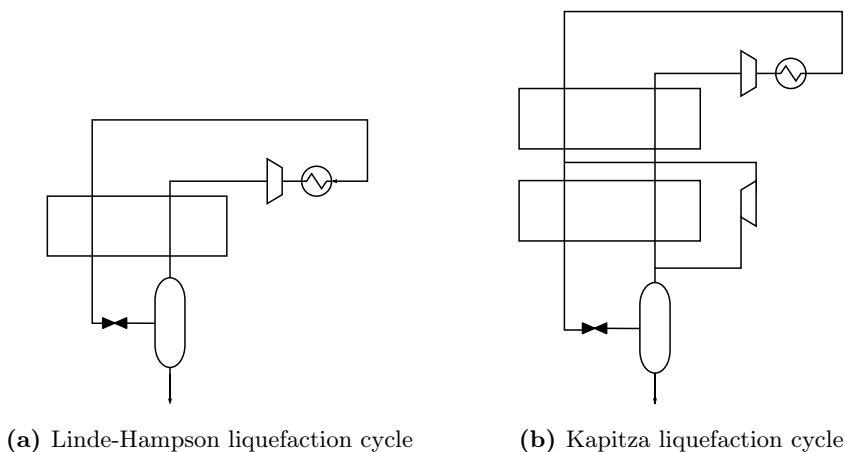


**Figure 2.13:** The theoretical basis of the *Claude liquefaction cycle*

Taking exergy efficiency into account, such a process will generate a lot of irreversibility's due to large temperature approaches in the heat exchanger [49]. With emphasis of hydrogen this is especially important, because of the great variation of its specific heat,  $c_p(T)$ , at low temperature and different pressure levels, as seen in Figure 2.2. How is it possible to generate a more tight temperature approach at the lower temperature range? E.g. the mass flow of the LP cold stream has to be much greater than the HP stream. This is accomplished in the *Kapitza liquefaction cycle*, where a large fraction of the HP stream is diverted through an expander, undergoes a great temperature drop and is redirected into a second heat exchanger to cool down the HP stream even further.

If another heat exchanger is added to the Kapitza cycle, it is equivalent to the *Claude liquefaction cycle*. In general, as described by [49], the duty of the third heat exchanger will be considerably smaller than the second, because of the cooling generated by the expander, hence it is recommended removed. However, proposed design from recent literature concepts proves that there are a huge number of ways to modify the Claude cycle into a much more efficient process than the Kapitza cycle.

As an example, Figure 2.14 shows a principle PFD of how the Claude cycle can be integrated into more complex systems; the feed stream is separated from the main refrigeration cycle<sup>4</sup>, in this case referred to as the *low temperature cycle*. Both

<sup>4</sup>The theoretical definition is opposite, where the feed stream works both as a refrigerant and product, solved by integrating a flash/separator after the last throttling. The product is extracted at the bottom while the flash gas is recycled on the cold return path, similar as

the feed- and refrigeration stream can be integrated in a precooling cycle before it enters the main liquefaction cycle. Integration of the ortho-para conversion must be in the proper temperature interval, as described in section 2.4

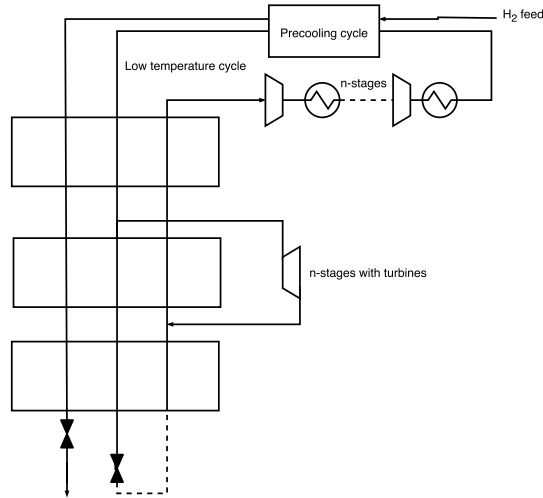


**Figure 2.14:** The Claude cycle integrated separately from the hydrogen feed stream

## 2.5.2 Reversed Brayton concepts using both single and binary mixtures as working fluid

The reversed Brayton process is the simplest turbine gas liquefaction process, usually working at high pressure levels [49, 34]. Similar as the Linde-Hampson cycle, the HP stream is precooled in the heat exchanger before it is expanded to an even lower temperature (see Figure 2.15). The LP return stream is then providing the cooling to the particular feed gas.

In LNG plants both nitrogen and mixtures with e.g. methane (C1) have been used. In hydrogen liquefaction, solutions with use of helium, hydrogen and neon are the major concept, because of the low temperature boiling points required without complications such as freeze-out. With current technology, liquefaction cycles operated by a reversed Brayton alone can achieve capacities up to 3 tpd, while a single hydrogen Claude cycle can operate at a capacity level from 2-15 tpd

---

described in Figure 2.13

[37]. The authors also predicts the short and medium term future development of the hydrogen liquefaction cycle, where hydrogen Claude is the major process, with capacities ranging from 15-200 tpd. Here both nitrogen expansion- (rev. Brayton) and MR precooling cycles will replace the LIN concept, due to the exergy penalties explained earlier.

Figure 2.15 illustrates (similar as the Claude in Figure 2.14) how the rev. Brayton can be integrated into a complex system design. The Figure is only generalized, which means that the number of stages of compression, heat exchangers and expansion stages can be modified by stream splitting into other heat exchangers and so on (see Figure 2.14 as an example).

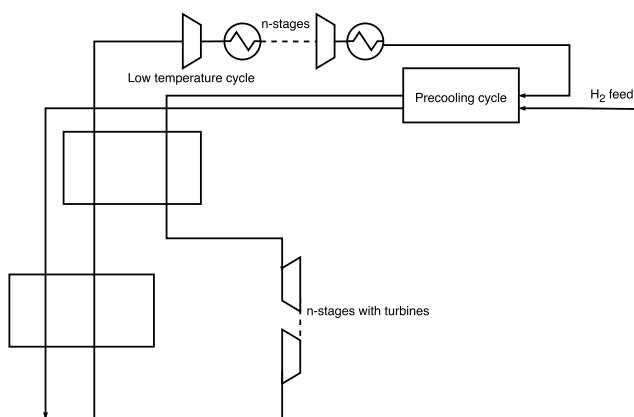


**Figure 2.15:** The reversed Brayton cycle integrated with the hydrogen feed stream

### 2.5.2.1 Complications due to choice of refrigerants

Another aspect of the reversed Brayton concept for hydrogen liquefaction, is the synergy between choice of the refrigerant and choice of compression equipment in a large-scale scenario. Integration of turbo compressors is not possible with neither pure hydrogen nor helium, unless a great number of compression stages is integrated, as shown by both Quack [41] and Valenti et al.[47] in their conceptual plant studies. Therefore recent conceptual plants such as the IDEALHY project [43] propose to use a binary mixture of helium and neon, to increase the molecular weight,  $M_i$  of the mixture in order to achieve turbo compression. Cardella et al. [14, 13] suggest to utilize hydrogen mixed with neon, because of lower CAPEX and OPEX due to the higher availability of hydrogen on site compared to helium and due to superior heat transfer properties.

## 2.6 Literature survey on conceptual hydrogen liquefaction plants

This section will discuss on different hydrogen liquefaction process concepts found in literature, both with emphasis on precooling systems and cryogenic cooling systems, evaluated separately.

### 2.6.1 New concepts for hydrogen precooling

Many of the different MR concepts described above are mainly utilized into a LNG process. During the last 15 years, many hydrogen liquefaction plant proposals using MR as a pre-coolant have been posted in literature, hence with utilization of the discussed LNG process concepts. The paper "Report on Technology Overview and Barriers to Energy- and Cost-Efficient Large Scale Hydrogen Liquefaction"[17] provided from the IDEALHY project webpage, presents several key performance indicators relevant for benchmarking the upcoming MR process proposed by the writer of this thesis. Hence some of the following parameters presented are provided from this paper instead of the originals, due to lack of accessibility.

#### 2.6.1.1 *WE-NET: Japan (1997-2004)*

The WE-NET Japan project has proposed four different plant proposals using LIN down to 80 K as precooling [17]. All the three concepts from 1997 and the one from 2004 has a production capacity of 300 tpd. Since the LIN process is based on the batch principle; basically a shell-and-tube heat exchanger, where the LIN embrace the inner tubes within the shell, it operates at a LP of 1.6 bar. In the latter paper there was also documented an energy penalty due to production of LIN. In the concepts of 1997 there was an overall nitrogen consumption energy penalty of  $0.5 \text{ kwh/Nm}^3_{LIN} + 0.14 \text{ kwh/Nm}^3_{GN_2} = 0.64 \text{ kwh/Nm}^3_{N_2}$  using LIN as precooling, while in the 2004 concept the total nitrogen penalty was  $0.637 \text{ kwh/Nm}^3_{N_2}$ . I.e. not the greatest improvement.

#### 2.6.1.2 *Conceptual liquefier by Quack (2001)*

The conceptual plant proposed by Quack [41] in 2001 utilize a pure propane (C3) three-stage compression cycle as precoolant down to a temperature of 220 K only. Further cooling down to 77 K is performed by a reversed Brayton cycle using a

binary mixture of helium and neon as working fluid. The overall process capacity is assumed about 170 tpd, working at a pressure of 13.3 bar in the precooling propane cycle [10]<sup>5</sup>

### 2.6.1.3 Conceptual liquefier (SINTEF) by Berstad et al. (2010)

The conceptual plant proposed by Berstad et al. at SINTEF Energy Research in 2010, is an adaption of the plant design by Quack explained above, and is one of the first recent plant concepts using the Kleemenko auto-cascade principle with a very complex MR composition<sup>6</sup>. The overall plant capacity is assumed 1 kg/s which corresponds to  $\approx 87$  tpd. As explained earlier the Kleemenko principle allows for precooling temperatures below the LIN temperature range due to the heavy component separation at each heat exchanger outlet, hence the precooling temperature ranges down to 75 K.

The conceptual plant was in addition simulated using both i) turbo expansion and ii) JT valve expansion resulting in a difference of the power input in the MR compressors of  $P_i - P_{ii} = 7.383 - 6.269 MW \approx 1.1 MW$  and an overall heat exchanger duty difference of  $16.849 - 19.341 \approx -2.492$ . The increased heat exchanger duty in the last case emphasize that a greater portion of liquid exits the expander and gives an increased heat transfer coefficient in the precooling heat exchanger.

### 2.6.1.4 The IDEALHY-project (2012-2013)

Integrated Design for Efficient Advanced Liquefaction of Hydrogen, IDEALHY is a finished collaboration project between industry partners and research organizations aiming for a high efficient process concept for liquefaction of hydrogen with a production rate of 50 tpd.

The process design is very complex, due to integration of both a closed MR precooling cycle together with a low-temperature working fluid cycle being precooled in the upper temperature region. Recent process design such as the IDEALHY integrated precooling concept will most likely prove to be the most efficient way of developing future plants.

Below, the original precooling concept is presented, followed up by a modification proposal done by [42] where a nitrogen expansion precooling model is integrated. The two precooling models is shown in Figure 2.16 and 2.17

<sup>5</sup>Data retrieved from reference case used in the plant proposal by Berstad et al.

<sup>6</sup>Hydrocarbons  $C_i$ : for  $i = [1, \dots, 5]$ ,  $N_2$ , Ne, Ethylene and R12 (Refrigerant)

**Original model: MR precooling** In the original precooling model, the MR stream is compressed in a two-stage compressor train to a pressure level of 26.6 bar with a pressure ratio of 9.5 [44], before the high-pressure (HP) stream is totally condensed inside HX-101, and evaporated as a low-pressure stream providing precooling at 130 K, both for the hydrogen stream and the two channel Nelium Brayton cycle.

The chiller unit is integrated in combination with the compressor aftercooler as a vertical shell-and-tube exchanger, stacked directly above each other [44]. At the chiller outlet, fractions of MR liquids are transferred into HX-101 (cold box) by a pump, while the vapour stream flows independently.

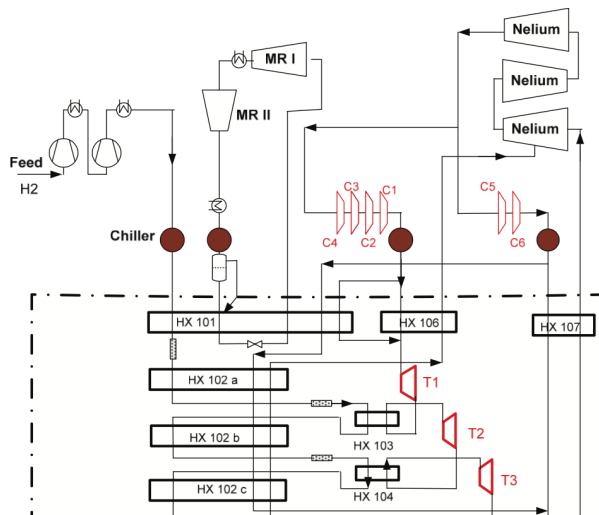


**Figure 2.16:** Original IDEALHY-model with MR precooling, by Berstad et al. [43]

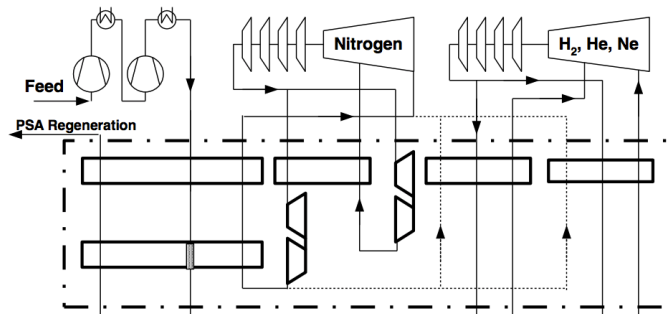


**Figure 2.17:** Nitrogen expansion precooling, proposed by Quack et al. [42]

**Modified model IDEALHY TUD 5: Nitrogen expansion precooling** In the proposal by Quack et al. [42] the MR precooling cycle is replaced by a nitrogen expander cycle (Brayton), which cools the hydrogen stream to a temperature of approx. 90 K. The new design allows a fraction of the coldest nitrogen stream for precooling of the the low-temperature Brayton noble gas mixture cycle. Data concerning the preferred pressure values was unfortunately not found during the literature review.

#### 2.6.1.5 *The Linde Leuna liquefier and the modified proposal by Ohlig et al.*

The precooling concept in the actual Linde Leuna plant is using conventional closed LIN cycle down to 80 K. However some simple modifications proposed by Ohlig et al. makes the overall process performance much more efficient; the LIN concept is replaced by a nitrogen expansion process, where the two-phase nitrogen is separated after expansion and guided through two heat exchangers. This is in general a recycle unit, which has a documented energy saving potential of 10% according to [37]. It is further suggested that LNG evaporation at import terminals could play an important role of obtaining so-called free precooling in the foreseeable future.

#### 2.6.1.6 *Cardella et al. (2016-2017)*

The hydrogen liquefaction plant proposal by Cardella et al. [13] is the most recent concept, with an exergy efficiency outperforming all of the last mentioned concepts and a specific energy consumption of 6.0 kWh/kg<sub>H<sub>2</sub></sub> in the range of 100



tpd liquefaction capacity. The process concept is using the IDEALHY-project and the modified Linde Leuna concept as the major benchmark criteria.

The precooling techniques in the two concepts are quite similar, however with some minor differences defined by concept A and B, which is presented below, and can also be shown in Figure 2.18 and 2.19

**Concept A: HP hydrogen Claude cycle** The precooling part of the first concept is an optimized MR cycle with a precooling temperature range from 110-90 K. The precooling process is a two-stage LIMUM cycle explained earlier in this chapter, with a four component MR working fluid consisting of hydrocarbons and nitrogen, to avoid complicated systems.

A HP hydrogen Claude cycle is working in the temperature range from ambient down to the cryogenic target. By integrating the hydrogen streams into the precooling heat exchangers, additional cooling of the feed stream is obtained due to the superior heat transfer properties of hydrogen. Together with an efficient precooling of the cold cycle, the concept is therefore quite similar as in the IDEALHY concept.

**Concept B: Dual hydrogen-neon cascade cycle** Concept B utilize the same precooling process as concept A, however by only one MR heat exchanger and one less stream due to the mixing point after the last HP separator at the HX01 inlet, as seen in Figure 2.19.

Together with a HP hydrogen stream, a mixture of neon and hydrogen is working from the ambient to the cryogenic temperature range, creating a similar additional precooling effect as in concept A.

## 2.6.2 New concepts of cryogenic cooling and liquefaction of hydrogen

Below, the most interesting low-temperature process concepts are presented, with focus on the specific energy consumption per kilogram of hydrogen [kWh/kg<sub>LH<sub>2</sub></sub>], pressure levels in the expanders and compressors, temperature levels in the Claude- and Brayton cycles and the overall exergy efficiency of the process, where Table 2.1 provides the final summary.

2.6.2.1 *WE-NET: Japan (1997-2004):*

The Japanese WE-NET project conducted four different proposals of hydrogen liquefaction concepts through the period of 1997 to 2004, with the respective precooling methods explained earlier in this section.

The three proposals from 1997 with emphasis on the low-temperature process included: *i) A hydrogen Claude cycle, ii) A helium reversed Brayton cycle and iii) A neon reversed Brayton cycle.* In 2004 a *iv) modified hydrogen Claude process* was proposed, as a modification of the old design.

Design i) and iv) are according to literature [17] quite similar, with the exception of one extra expansion turbine in the lower temperature in i). The iv) design neglected this unit due to operational and maintenance considerations resulting in a specific energy consumption of

$$w_{iv} = 8.7 \text{ [kWh/kg]}$$

$$w_i = 8.5 \text{ [kWh/kg]}$$

Both ii) and iii) are designed with a production capacity of 300 tpd. The helium process is a single compression/expansion Brayton, while the neon processes are a dual compression/expansion Brayton design. Figures can be found in appendix ???. The estimated specific energy consumption of the two concepts, provided by [17, 31] are

$$w_{ii} = 8.69 \text{ [kWh/kg]}$$

$$w_{iii} = 8.59 \text{ [kWh/kg]}$$

2.6.2.2 *Conceptual liquefier by Quack (2001)*

The design of the low-temperature cycle by Quack [41] comprises a 16-stage helium compression Brayton cycle, with a neon content of 20% to obtain a molecular weight that allows for HP compression with turbo machinery. The feed hydrogen is also compressed in five stages to 64 bar with inter-cooling, to minimize power consumption and to account for the proper heat capacity correction at HP (Figure 2.4).

The helium-20 is precooled in the last heat exchanger in the propane cycle as explained earlier, together with the main process a *specific energy consumption*

of

$$w_v = 7 \text{ [kWh/kg]}$$

is obtained, with a liquid hydrogen production capacity of 170 tdp. The literature survey conducted in the IDEALHY project [17] recommends the concept results as a benchmark for any future plant proposals with emphasis on the superior exergy efficiency,  $\varepsilon_x$  and specific energy consumption,  $w_i$ .

### 2.6.2.3 *Conceptual liquefier by Valenti et al.(2008)*

The proposed liquefier by Valenti et al. [47] use a four-stage Brayton cycle that provides cooling to the whole temperature range from 300 to 20 K with helium as working fluid. With a production rate of 860 tpd of liquefied hydrogen, the specific energy consumption of the process is documented to

$$w_{vi} = 5.04 \text{ [kWh/kg]}$$

Turbo machinery is in similarity to the Quack proposal also assumed here, with integrating an inter-cooled 15-stage compression train with an average pressure ratio of 1.2-1.3 between each stage [17]. An interesting aspect of this concept is the final expansion; instead of a flash gas recycle unit, the cold feed stream is expanded directly from the dense two-phase region, into the sub-cooled region, assuming an isentropic expander efficiency of 85% [17].

### 2.6.2.4 *Conceptual liquefier (SINTEF) by Berstad et al. (2010)*

The most interesting part of the SINTEF concept is the modified precooling approach already explained in the previous section, while the low-temperature is a direct derivation of the Quack concept with helium-20 as working fluid in the cryogenic temperature area. The resulting energy consumption was estimated to

$$w_{vii} = 6.2 - 6.5 \text{ [kWh/kg]}$$

with an exergy efficiency of 44.5-46.6% respectively [17].

### 2.6.2.5 *The IDEALHY-project; (2012)*

The complexity of the low-temperature IDEALHY concept is extensive, with several adaptations from both Quack and the latter SINTEF proposals. With a

liquefaction capacity of 50 tpd, the main cooling is produced by a 6-stage compression helium 25<sup>7</sup> Brayton cycle with pressures between 2.4 bar at the suction side to 60 bar at discharge side. The same number of turbines are working in a temperature area ranging from 131.9 to 26.3 K [44] to feed the heat exchangers with cold intermediate pressures (IP) and LP return streams. The overall specific energy consumption of the process is estimated to

$$w_{viii} = 6.4 \text{ [kWh/kg]}$$

Excluding the MR precooling cycle there are 14 heat exchangers that constitute the whole process, which makes the system much more cost intensive, relative to the high energy efficiency of the process. These results can be found in the CAPEX and OPEX study of several liquefier concepts, proposed by Cardella et al. [13]

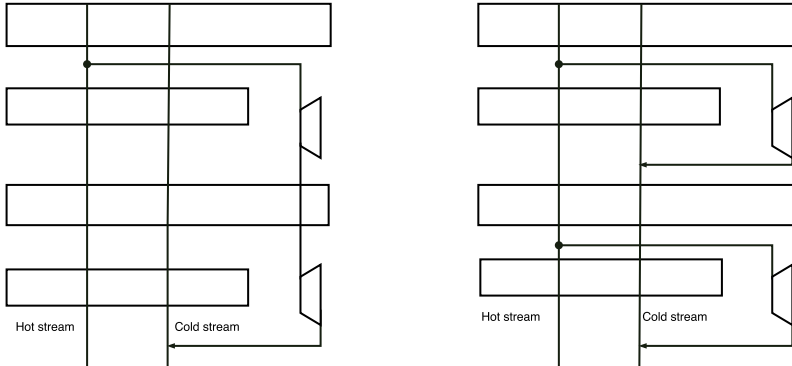
#### 2.6.2.6 The Linde Leuna plant (2007/2013)

**The original Linde Leuna process and plant (2007)** The actual state-of-the-art plant at the Leuna industrial complex in Germany, operated by Linde, has a liquefaction capacity of 5.7 [37] tpd, where the main cooling process is a hydrogen Claude cycle separated from the main feed stream. The hydrogen feed stream is entering the liquefaction process at a pressure of 20 bar, given by the PSA unit in the neighbor hydrogen production plant. The expander bypass is connected in series through the intermediate heat exchanger, see Figure 2.20, which gives two different temperature levels in the same expander bypass stream. The three expanders operates between 20 to 5.2 bar, with state-of-the-art oil bearing turbines with rotational speeds above 100,000 rpm (see [36] for more info on oil/gas-bearing technologies). The minimum energy requirement is documented in [17] to

$$w_{ix} = 11.9 \text{ [kWh/kg]}$$

---

<sup>7</sup>25% neon + 75% helium

(a) **Expanders in series:***The original Linde Leuna design [37, 25]*(b) **Expanders in parallel:***The modified Linde Leuna design by [37]*

**Figure 2.20:** A simplified PFD indicating difference between the original and modified Linde Leuna process

**Modified Leuna process, Ohlig et al. (2013)** In the paper "The Latest Developments and Outlooks for Hydrogen Liquefaction Technology" proposed by Ohlig et al. [37] in 2013, a modified design of the original Leuna process is put through. Simple improvements of the original Leuna process, such as LIN precooling replacement with a nitrogen expander cycle, using both liquid and gaseous nitrogen with phase separators, and implementation of simple chillers in the upper temperature region of the Claude cycle, is outlined as energy friendly adjustments. In addition, the Claude expanders are connected in parallel instead of series, as shown in Figure 2.20. The changes are reported to give a energy reduction on a large-scale level with 25%, which gives an approximated specific energy consumption of

$$w_x = 7.4 - 7.5 \text{ [kWh/kg]}$$

Although the specific power consumption is higher than many of the other concepts above, this design is proving an acceptable trade-off between energy efficiency and CAPEX and OPEX considerations.

#### 2.6.2.7 Cardella et al. (2016/2017)

The conceptual study by Cardella et al. [13, 14] is a continuation of the Leuna modification concept, with Linde Kryotechnik as one of the main contributor. There are two major concepts discussed in this article, where the corresponding

precooling concepts were described in Section . The common thread of the two concepts, with emphasis on the low-temperature process is that helium is fully replaced by hydrogen as a refrigerant. Compared to helium and neon, hydrogen has superior heat transfer properties and is cheaper on site, as proven in [43, 13].

Both concept A and B are simulated with various hydrogen feed pressure of 1) 25 bar (typically given by production plant, as mentioned before) and 2) variable adjustment between 25-80 bar (pre-compression with reciprocal hydrogen compressors):

**Low-temperature concept A: HP hydrogen Claude** Concept A, is quite similar to the modified Leuna process, except that LIN is replaced by MR in the precooling region and two additional expanders are integrated in the HP Claude cycle. Here, the major differences from the original/modified Leuna process, are the higher pressure ratio design in the compressors and expanders. The optimized model is performed with hydrogen reciprocating compressors integrated, assuming that turbo-machinery may be installed on a medium term future. The specific energy consumption was estimated both with emphasis on the energy- and cost optimization ( $EO$ ,  $CO$ ) respectively

$$\begin{aligned} w(EO, 25 - 80bar)_{xi} &= 5.9 \text{ [kWh/kg]} \\ w(EO, 25bar)_{xi} &= 6.0 \text{ [kWh/kg]} \\ w(CO, 25bar)_{xi} &= 6.2 \text{ [kWh/kg]} \end{aligned}$$

**Low-temperature concept B: Dual cascade hydrogen/neon mixture** The second concept involves two separate low-temperature cycles, operating at different temperature levels, hence both compressors are working at ambient temperature levels. Between precooling- and final liquefaction boiling point temperature, an innovative reversed Brayton cycle using a binary mixture of hydrogen and neon as refrigerant is integrated, instead of the discussed helium solution. This stream is also pre-cooled by the MR cycle. The final liquefaction cooling power is provided by a hydrogen Claude cycle. Multi-stage compression, similar as mentioned in [41, 44], is achievable with 6-8 stages, while a fewer number of expander stages is needed to obtain the same energy recovery as in A [14]. The specific energy is calculated with the same assumptions as in concept A:

$$\begin{aligned} w(eo, 25 - 80bar)_{xii} &= 6.0 \text{ [kWh/kg]} \\ w(eo, 25bar)_{xii} &= 6.3 \text{ [kWh/kg]} \\ w(co, 25bar)_{xii} &= 6.6 \text{ [kWh/kg]} \end{aligned}$$

In addition, a cost analysis is implemented into the model. Assuming an electricity price of 0.05 EUR/kWh, the specific liquefaction cost is estimated to

### 2.6.3 Key findings from literature; cryogenic- and precooling concepts

Hydrogen liquefaction concepts from the two last decades have been covered so far in this literature survey, showing that the most recent precooling methods are gradually moving away from the "old-fashioned" LIN precooling process. Binary light gas mixtures such as helium and neon, hydrogen and neon or another combination of these, combined with mixed refrigerant concepts are being used for precooling of the feed stream to a temperature ranging from 130-90 K. The pressure levels depends on the working fluid being used. As seen in the previous chapters, MR precooling can easier be operated at lower pressure levels than e.g. the helium refrigerant, but a trade-off between the high or low level of pressure has to be weighted against other parameters such as the magnitude of desired density or mass flow in the cycles. In table 2.1 the most important key performance indicators of the above mentioned processes are summarized.

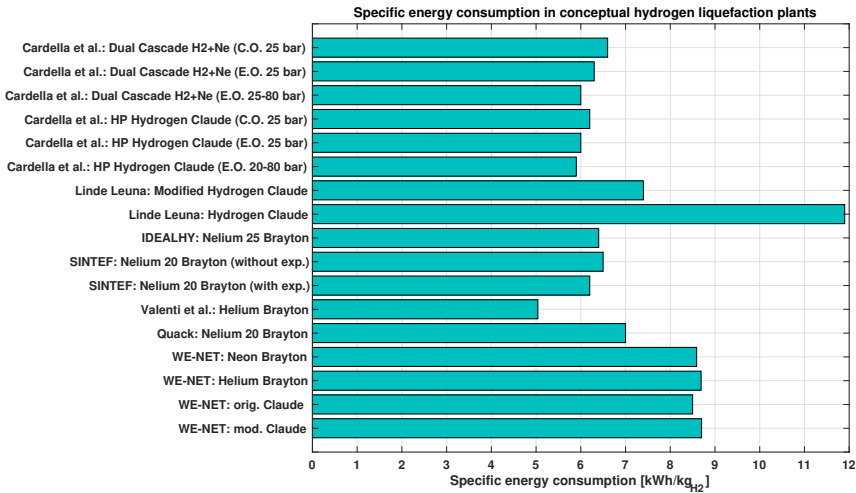


**Figure 2.21:** Specific energy consumption of conceptual hydrogen liquefaction plants from literature

## 2.6. LITERATURE SURVEY ON CONCEPTUAL HYDROGEN LIQUEFACTION PLANTS 41

	1 <sup>a</sup>	2 <sup>b</sup>	3 <sup>c</sup>	4 <sup>d</sup>	5 <sup>e</sup>
Precooling method	LIN	C3 (SR)	MR	MR+NEL-PC	MR+NEL-PC <sup>g</sup>
Target temperature [K]	80	220	75	130	110-90
High pressure level [bar]	1,6	13,3	14,9	26,6	N/A
Low pressure [bar]	1,6	1	1,2	2,8	N/A
Refrigerant mass flow [kg/s]	N/A	5,3	29,37-31,75	6,3	N/A
$\Delta T_{min}$ criteria [K]	N/A	2,12	2,0-10,4	N/A	0,5-25
WMTD [K]	N/A	N/A	3,4-20,1	N/A	N/A
Compressor stages [-] N/A	N/A	3	3	2	2
Compressor efficiency <sup>f</sup> [%]	N/A	N/A	85	80	76-85

*a*: Ohira et al. (WE-NET:1997-2004)

*b*: Quack (TU Dresden: 2001)

*c*: Berstad et al. (SINTEF: 2010)

*d*: Essler et al. (IDEALHY: 2012)

*e*: Cardella et al. (Linde: 2017)

*f*: Isentropic,  $\eta_{c,is} = \eta_c$

*g*: Including H<sub>2</sub>+Ne-mixture as an alternative refrigerant

**Table 2.1:** Key findings from conceptual precooling processes

Concept number:	1 <sup>a</sup>	2 <sup>b</sup>	3 <sup>c</sup>	4 <sup>d</sup>	5 <sup>e</sup>
Cryogenic refrigerant	H <sub>2</sub> , Ne, He	NEL-20	NEL-20	NEL-25	H <sub>2</sub> ,H <sub>2</sub> +Ne
Specific Energy Consumption [kWh/kg]	8,5-8,7	7	6,2-6,5	6,4	5,9-6,2
High pressure level [bar]	N/A	64	73	60	N/A
Low pressure [bar]	N/A	2,7	2,4	2,4	N/A
Exergy efficiency	45,1-46	56,8	45-48	N/A	33-43
Compressor stages [-]	N/A	8	15	6	6-8
Compressor efficiency <sup>f</sup> [%]	N/A	85	80-85	79-81	
Concept number:	6 <sup>g</sup>	7 <sup>h</sup>			
Cryogenic refrigerant	Helium Br.	Hydrogen Cl.			
Specific Energy Consumption [kWh/kg]	5,04	11,9			
High pressure level [bar]	40	N/A			
Low pressure [bar]	1,56-7,73	N/A			
Exergy efficiency	48,3	23,6			
Compressor stages [-]	15	N/A			
Compressor efficiency <sup>f</sup> [%]	92,96,7	85			

*a*: Ohira et al. (WE-NET:1997-2004)

*b*: Quack (TU Dresden: 2001)

*c*: Berstad et al. (SINTEF: 2010)

*d*: Essler et al. (IDEALHY: 2012)

*e*: Cardella et al. (Linde: 2017)

*f*: Isentropic,  $\eta_{c,is} = \eta_c$

*g*: Valenti et al. (Politecnico di Milano: 2008)

*h*: Decker et al. (Linde Leuna: 2007-2010)

**Table 2.2:** Key findings from conceptual cryogenic liquefaction processes



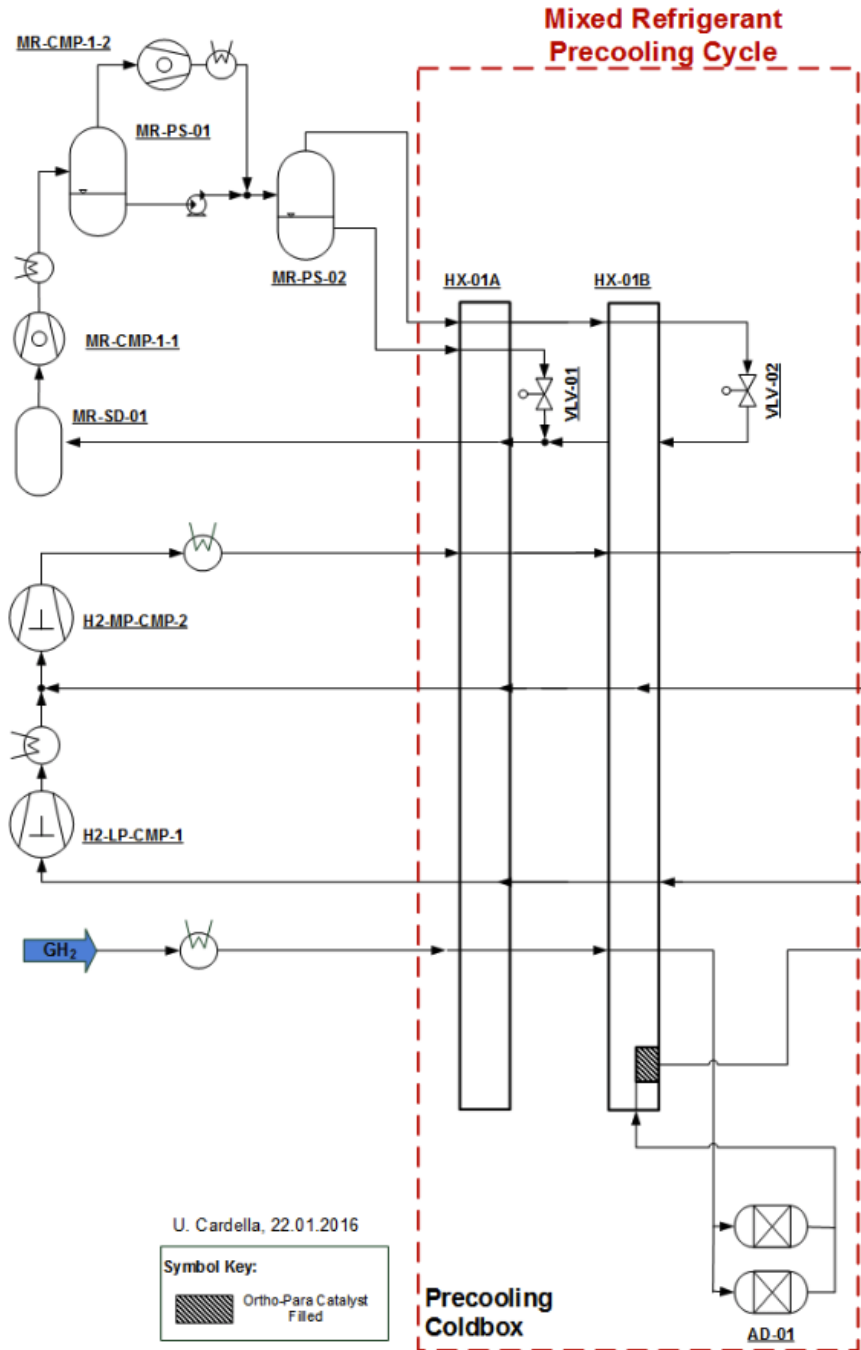


**Figure 2.18:** Concept A by Cardella et al.: MR LIMUM (two-HX-stage) precooling, by Cardella et al. [13]

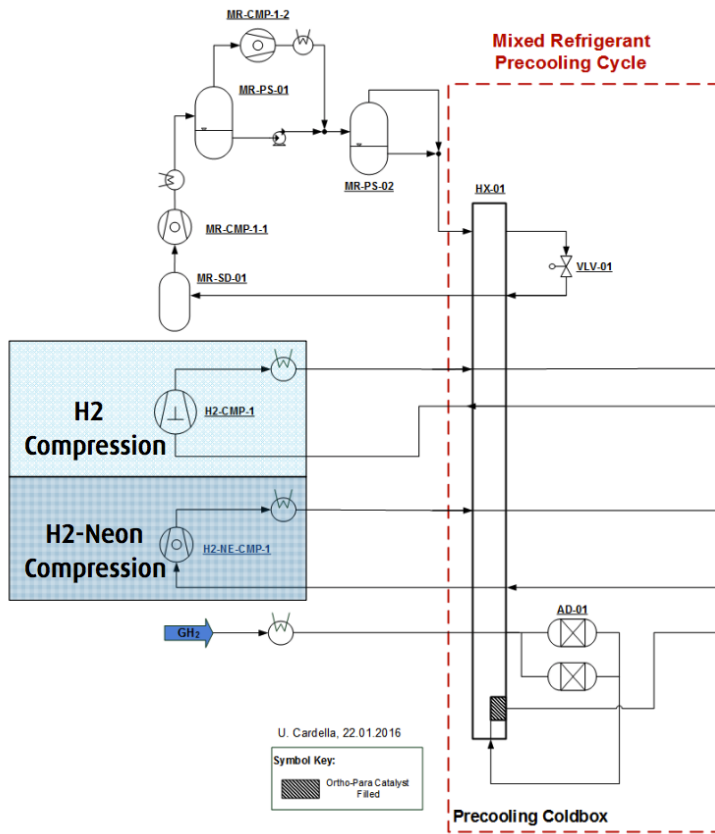


Figure 2.19: Concept B: MR single LIMUM precooling, by Cardella et al. [13]



# Chapter 3

## Case Study Process Models

### 3.1 Case study models

This chapter provide an overall introduction of the different precooling systems used for analysis in this thesis, to give an overview of the particular process designs. Initial and boundary conditions of each case will be presented more in detail in Chapter 4.

#### 3.1.1 Case 1: SMR PRICO precooling

System number one is an SMR PRICO precooling cycle. The hydrogen feed is either compressed at high pressure delivered from the compressor train or at an intermediate pressure delivered by an arbitrary production plant. Typically a PSA unit for hydrogen purification is the last step in a production process, which delivers hydrogen at a pressure of 20 bar<sup>1</sup>.

Figure 3.1 indicates that the MR compressor train comprises two stages with inter-cooling. However, the simulation model allows for integrating additional compression stages to the cycle, and will therefore be further evaluated in the analysis section to verify whether there is an energy saving potential or not. The MR composition is made of light hydrocarbons and nitrogen for simplicity

---

<sup>1</sup>This assumption is used consequently throughout the other case study models as well, and will be further discussed in the analysis part

reasons as mentioned earlier, and is adjusted to give a temperature fit inside the heat exchanger to minimize irreversibility's and duty.

The proposed cryogenic temperature working fluid, nelium, is only used as a generic stream with as a function of the hydrogen the mass flow, with a ratio of  $m_{H_2}/m_{nelium} = 1/10$ . Equivalent target temperature at the heat exchanger outlet are assumed. Ortho-para conversion is accomplished by calculation of adiabatic temperature rise at the given temperature, and is assigned to an imported equilibrium hydrogen file in HYSYS, assuming perfect conversion inside the heat exchanger.

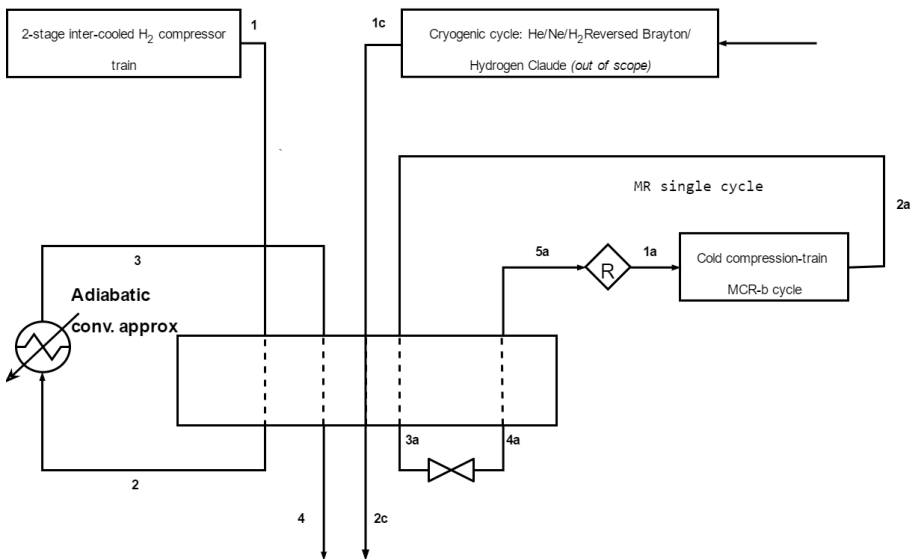
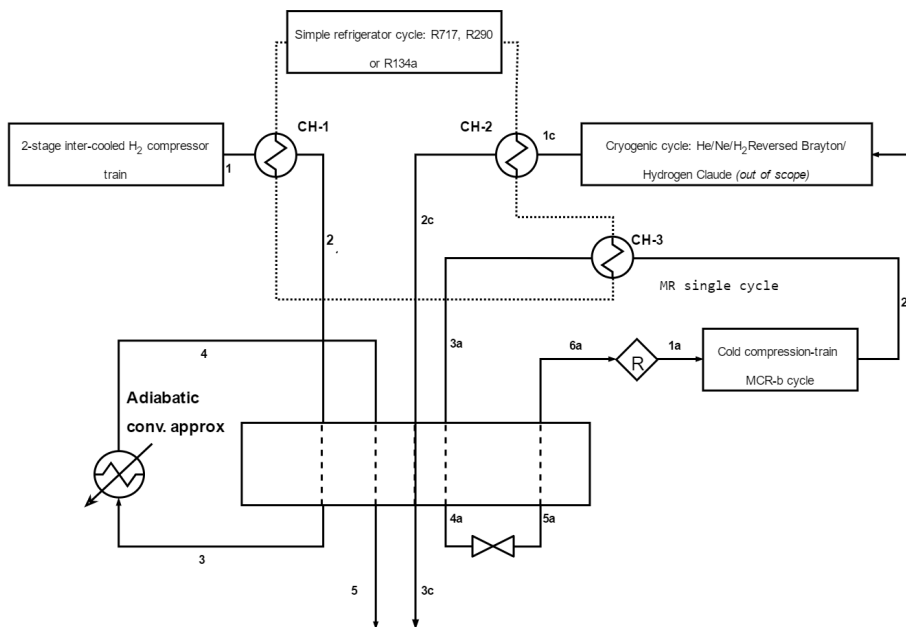


Figure 3.1: Simulation case model one: PRICO SMR

### 3.1.2 Case 2: SMR PRICO+ precooling

System number two is equivalent to system number one with the exception of the implemented chillers before the main heat exchanger. This is to reduce the duty of the heat exchanger inside the coldbox as explained in Chapter 2 and [44]. Since the inlet temperature of the hydrogen feed is reduced by around 30 K, the optimal MR composition may be different than in the first system, and could possibly reduce the required mass flow as well.



**Figure 3.2:** Simulation case model two: PRICO SMR+

As shown by the dotted lines in Figure 3.2, the chilling refrigerators can be connected in series or parallel instead of three separate units, giving a trade-off between investment costs and energy efficiency.

Ortho-para conversion is still implemented at 130 K, after the heat exchanger HX-1, giving the same adiabatic temperature rise, given by the heat of conversion explained in the next section.

### 3.1.3 Case 3: CMR precooling

System number three is an extension of the simple PRICO process, in this case a double cascade mixed refrigerant process, which from this point will be named *CMR*. The hydrogen and neon feed conditions are unchanged, with the exception of a new intermediate temperature level between HX-1 and HX-2.

The MR part of the system comprises two closed cycles with multi-stage compression and after-cooling. The two cycles are designed with respect to the hydrogen cooling temperature target at each heat exchanger outlet, which results in differ-

ent working fluid composition,  $n_i$ , mass flow,  $\dot{m}_i$  and pressure levels,  $p_i$ .

The major advantage of this modified system is assumed as follows

1. That two separate cycles can be modified with respect to the required cooling temperature. This means that each cycles can operate with different parameters to obtain the minimum energy required to cool the feed stream.
2. The boiling refrigerants can be adjusted to a smaller temperature interval, which makes it easier to generate a mixture that gives a better temperature match inside the heat exchangers.

### 3.1.4 Case 4: CMR+ precooling

System number four, the CMR+ precooling, is similar to system three, only with implementation of propane (R290) refrigerators as partial precoolers in the upper temperature region, before the feed stream enters the coldbox (HX-1), as in system number two.

As mentioned the refrigerator system can be modelled in series or parallel in the steady-state HYSYS simulation model. In the technical analysis section evaluation of energy savings will be carried out on each design, to verify which one are the most promising.

### 3.1.5 Benchmark Case 6: Conventional liquid nitrogen precooling process

Availability of nitrogen on site, is normally a prerequisite for the few hydrogen liquefaction plants in operation today, and therefore it is the only conventional method of hydrogen precooling.

A simplified process model for simulation of liquid nitrogen precooling can be obtained in Aspen HYSYS. An important criteria is that energy losses, or penalties related to generation of the liquid refrigerant must be incorporated into the energy accounting.

Data obtained from literature, [17, 15, 48] are limited, but though available. With a energy penalty of  $w_{N_2} = 0,5 - 0,4 kWh/l$  produced liquid nitrogen, it is possible to calculate the overall energy- and exergy balance for this benchmark system, on the condition that parameters related to exergy destruction in the production process, found in literature, are reliable.

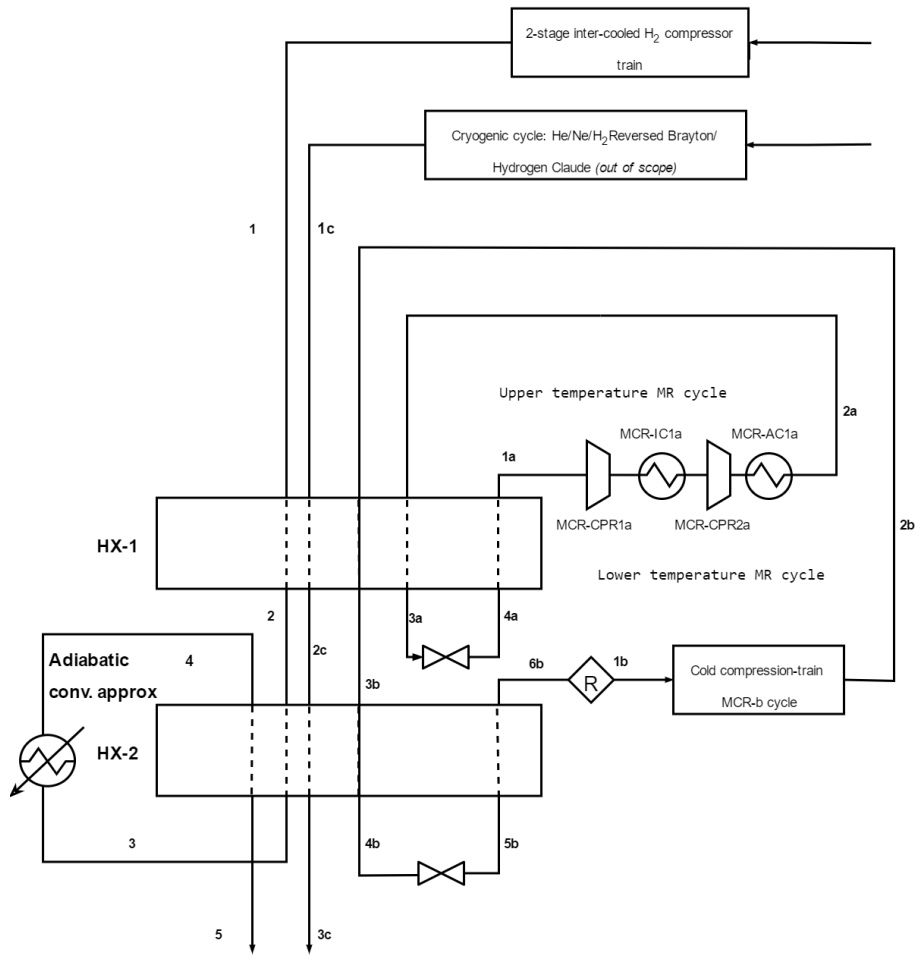
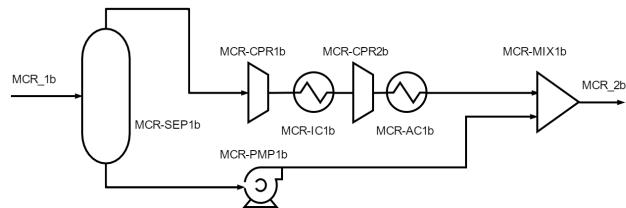


Figure 3.3: Simulation case model three: Hydrogen CMR precooling





**Figure 3.4:** Compression train of lower temperature MR cycle. The pump increase the minor fraction of liquid to the same pressure level as the compressors

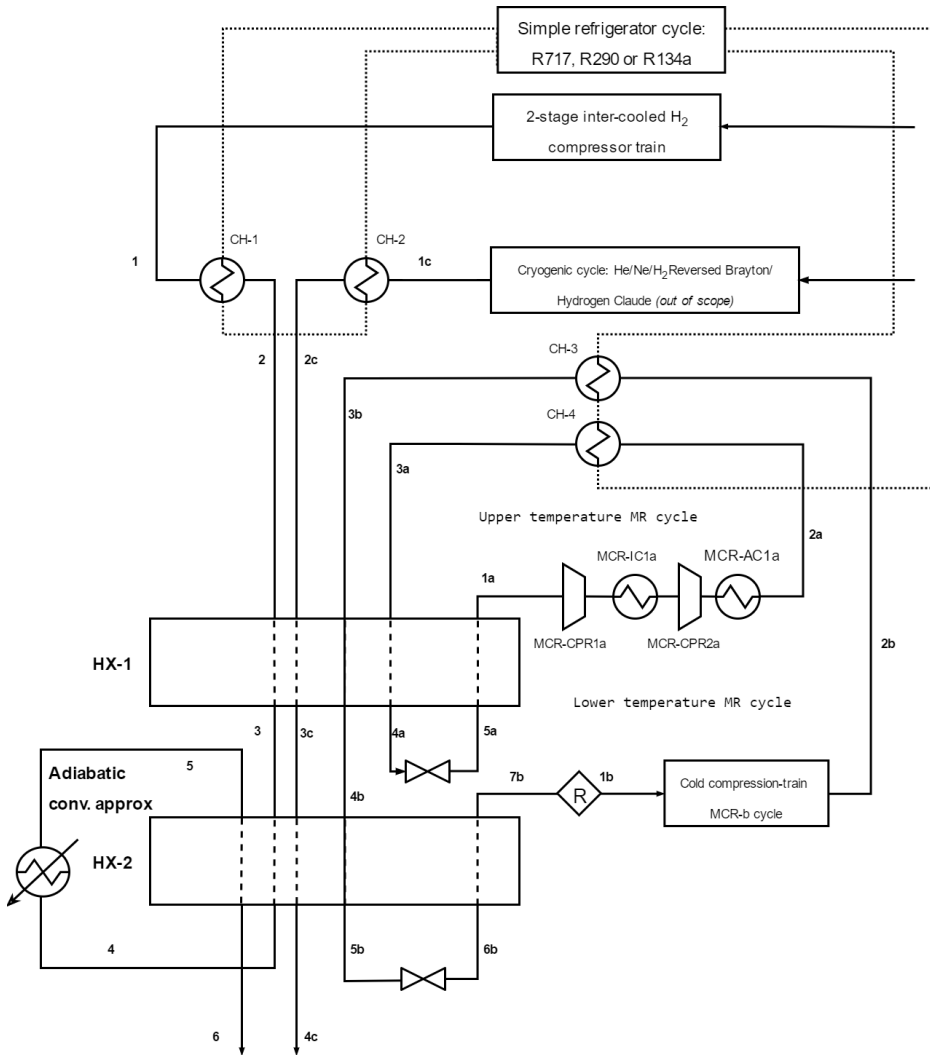


Figure 3.5: Simulation case model no. 4: Hydrogen CMR+ precooling



# Chapter 4

## Technical Methodology

This chapter will present and explain the methods used for simulating and optimization of the selected case study models used for analysis in Chapter 5. Within the scope of the thesis, the process simulation is limited to focus on the hydrogen precooling process only, down to a specified temperature and benchmarking the proposed design with an already existing technology, namely a nitrogen precooling cycle. The following hydrogen precooling designs will be evaluated in this thesis:

1. **Single mixed refrigerant PRICO process: *SMR PRICO***
2. **SMR PRICO with partial precooling refrigerator: *SMR PRICO+***
3. **Cascade mixed refrigerant process: *CMR***
4. **CMR with partial precooling refrigerator: *CMR+***
5. **Benchmark process: Liquid nitrogen precooling adapted from literature**

The partial precooling approach is based on the extensive work of the IDEALHY project, where simple refrigerators were proposed implemented in the upper temperature region, chilling the streams to temperatures between 268 K (-5 °C) to 278 K (5 °C) before entering the cryogenic cold box processes. A more detailed description is found within the case study model in Section 3.1

Approximations due to implementation of the cryogenic cycle into the precooling systems will be taken into account. Additional approximations due to simulation

of ortho- to para-hydrogen conversion is also defined within the scope of the thesis models, and will be presented in Section 4.1.2

Each of the systems is designed, simulated and further optimized based on a steady-state process scheme in the software Aspen HYSYS. The systems are based on a liquefaction capacity of 150 tpd of hydrogen with a purity of  $\approx 100\%$ .

## 4.1 Modelling the case study systems

### 4.1.0.1 Aspen HYSYS Simulation

The simulation model of each case, are built in the process simulation software Aspen HYSYS, assuming that every property is calculated in a steady-state environment.

Fluid packages from HYSYS are chosen for each material stream inside the boundary of the model. For normal-normal hydrogen at  $T_{H_2} > 130K$ , the Modified-Benedict-Weber-Rubens (MBWR) equation of state is chosen, after recommendations from supervisors that it is the most accurate method for property calculations of normal-hydrogen in the given temperature interval. Both the noble gas mixture of neon and helium and the MR mixture are calculated with the Peng-Robinson (PR) equation of state, which is known for high accuracy in gas- evaporation and condensation systems.

### 4.1.1 Design of simple refrigerators in case 2 and 4

The chillers in the upper temperature region is a simple propane refrigeration cycle and can initially be designed in available software tool such as CoolPack; Refrigeration Utilities. By assigning the required cooling capacity and target temperatures into CoolPack, a complete design can be found easily.

Calculation of the required cooling capacity of each evaporator in the system is derived from the driving forces from the main process. For hydrogen and the additional cooling medias, the required cooling capacity of the evaporator is given as

$$Q_{e,i} = \dot{m}_i \cdot (c_p(T_1)T_1 - c_p(T_2)T_2) \quad (4.1)$$

where  $c_p(T_1) = c_p(T_2)$  is assumed at the given temperature interval.

Table 4.1 and 4.2 shows the overall requisite cooling power for chilling each stream in case 2 and 4 from 300 K to 268, 273 and 278 K respectively, when propane

Chiller outlet temperature		$Q_{e,i}$				$(\dot{m}c_p)_i$	
		268 K	273 K	278 K			
Stream	Hydrogen	806.1	680.1	554.2	kW	25.19	kW/°C
	SMR-1	6755	5699	4644	kW	211,1	kW/°C
	Nelium	968.1	816.8	665.6	kW	30.25	kW/°C
<b>Total</b>		8529.2	7195.9	5863.8	kW	-	-

**Table 4.1:** Chiller cooling requirements in Case study 1 and 2: PRICO/PRICO+ precooling

Chiller outlet temperature		$Q_{e,i}$				$(\dot{m}c_p)_i$	
		268 K	273 K	278 K			
Stream	Hydrogen	806.1	680.1	554.2	kW	25.19	kW/°C
	CMR-1	3999	3374	2749	kW	125.0	kW/°C
	CMR-2	2277	1922	1566	kW	71.17	kW/°C
	Nelium	968.1	816.8	665.6	kW	30.25	kW/°C
<b>Total</b>		8050.2	6792.9	5534.8	kW	-	-

**Table 4.2:** Chiller cooling requirements in Case study 3 and 4: CMR/CMR+ precooling

(R290) is assumed as the refrigerant<sup>1</sup>. The data is further used as input to CoolPack to obtain the missing parameters. Note that the tabulated cooling duty of the SMR and CMR systems in Table 4.1 and 4.2 are rough estimates, based on simulation in an early optimization phase; hence, the estimated parameters may be changed throughout the path to an optimal SMR and CMR cycle. If changes are made, these are documented in the analysis and discussion part of the thesis.

#### 4.1.1.1 Data obtained from CoolPack

The supplementary package "Refrigeration Utilities" in CoolPack is a powerful tool to design and dimension simple refrigerator circuits. The only inputs required are the dimensioning evaporator cooling power,  $Q_e$ , condenser- and evaporator temperatures,  $T_c$ ,  $T_e$ . The temperature difference ( $\Delta T_e$ ) between primary and secondary fluid of the evaporator is assumed 5 K to keep heat transfer losses at a minimum. Based on the target chiller temperature,  $T_{out}$ , evaporator temperature

<sup>1</sup>Other natural- and low GWP refrigerants such as ammonia (R717) and CO<sub>2</sub> (R744) can also be utilized. For simplicity it is assumed that COP and power consumption is approximately the same for each refrigerant cycle

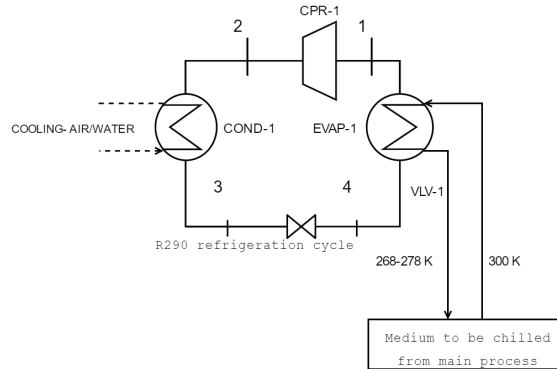


**Figure 4.1:** Single R290 refrigeration circuit, as a partial precooling process

is given as

$$T_e = T_{out} - \Delta T_e \quad (4.2)$$

Condenser temperature is assumed  $T_c = 15^\circ\text{C}$  for every chiller unit, while evaporator temperature is varying, with respect to the different chiller outlet temperature on the secondary side. Superheat,  $T_{sh}$ , and sub-cooling,  $T_{sc}$ , are assumed 2 K and 3 K respectively.

#### 4.1.1.2 Steady-state design in HYSYS

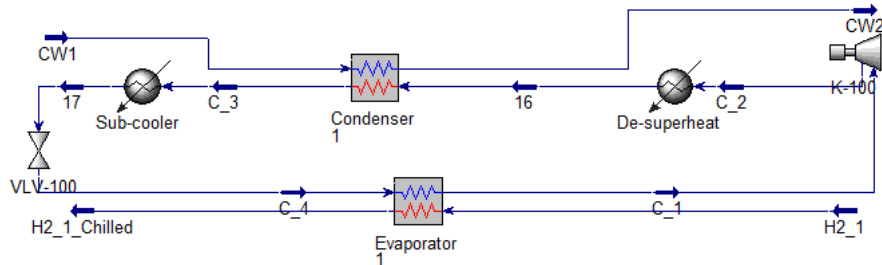


**Figure 4.2:** HYSYS Steady state model of propane (R290) refrigerator

The propane chiller design can be simulated in HYSYS, using a standard Steady-state flow scheme with the four different components that comprises a conventional refrigeration cycle.

	$T_{out}$ [K]	$T_e$ [K]	H2	Nel.	MR-PRICO	MR1-CMR	MR2-CMR
$Q_e$ [kW]	278	273	554.2	665.6	4644	2749	1566
	273	268	680.1	816.8	5699	3374	1922
	268	263	806.1	968.0	6755	3999	2277
$Q_c$ [kW]	278	273	598.325	718.594	5013.75	2967.87	1690.68
	273	268	750.3	901.12	6287.34	3722.32	2120.4
	268	263	909.8	1092.5	7623.82	4513.34	2569.86
$\dot{m}_{R290}$ [kg/s]	278	273	1.7	1.99	13.89	8.22	4.68
	273	268	2.1	2.48	17.33	10.26	5.84
	268	263	2.5	2.99	20.9	12.37	7.04
Pressure ratio [-]	278	273	1.77				
	273	268	2.07				
	268	263	2.43				
COP [-]	278	273	12.5				
	273	268	9.69				
	268	263	7.77				

**Table 4.3:** Design parameters generated by CoolPack, Refrigeration Utilities

The stages in the cycle can be summarized as follows;

- i) **C1–C2:** Propane (R290) compression to a pressure level, given by CoolPack, of 7,2 bar.
- ii) **C-2–C-3:** De-superheat to saturated vapour at the dew-point line. In HYSYS this is accomplished by assignment of the vapour quality in stream C-3 to 1.
- iii) **C-3–C-4:** Refrigerant condensation in two-phase region. Condenser temperature  $T_c = 15^\circ\text{C}$ , assuming available cooling water of  $15^\circ\text{C}$  and below, in nordic climate. Temperature  $T_{C3}$  are set to have vapour quality equal to zero, hence saturated liquid at the bubble point line.
- iv) **C-4–C-5:** Propane sub-cooling into sub-critical region. Increases the liquid yield into the evaporator, which gives better heat transfer.
- v) **C-5–C-6:** Isenthalpic throttling into two-phase region. JT-effect gives cooling.
- vi) **C-6– C-1:** Evaporation of refrigerant in two-phase region. Outlet temperature is controlled by setting vapour fraction equal to 1, hence saturated vapour.



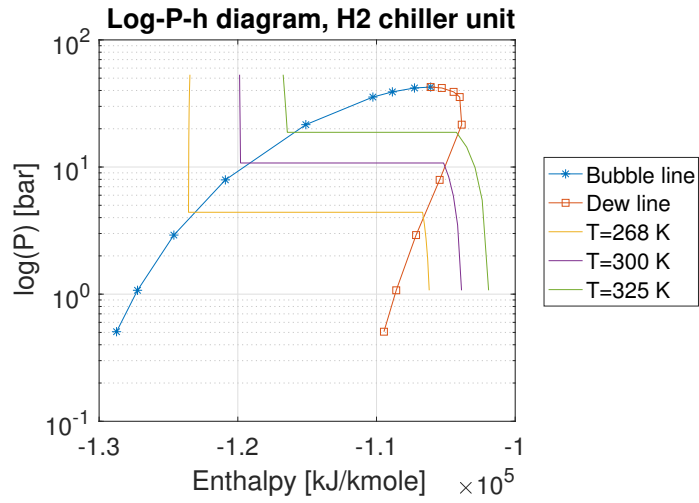


**Figure 4.3:** Pressure-enthalpy diagram for R290, with indicated isotherms

### 4.1.2 HYSYS simulation of continuous ortho-para conversion

The simulation engine Aspen HYSYS does not have any implemented tools that allows for simulation of continuous conversion within each cold-box heat exchanger. Therefore a simplified approach of realizing ortho- to para-hydrogen conversion will be analyzed and proposed as a valid solution.

The approach is based on the exothermic temperature rise that will occur at the conversion process. Assuming adiabatic conditions in the conversion process, available data from literature, of the heat of conversion,  $q_{conv}$ , at any temperature,  $T$ , can be imported directly into the HYSYS Spreadsheet tool. Figure 4.5 shows the relation between the conversion heat and the corresponding para-hydrogen content.

#### 4.1.2.1 Polynomial approach from Excel to HYSYS Spreadsheet

By polynomial regression using the build-in formula from MS Excel "LINEQ", it is possible to create a high-order polynomial based the tabulated data from Figure 4.5. The polynomial can be used in HYSYS to calculate the conversion heat,  $q_{conv}$ , and para content,  $n_{para}$ , at any temperature. Given the data from the two polynomials are found in HYSYS, it is possible to calculate the temperature rise,  $\Delta T_{conv}$  by

$$\begin{aligned} q_{conv} &= \dot{m}_{conv}(c_p)_{para} \cdot \Delta T_{conv} \\ &= ((1 - n_{para}) \cdot \dot{m}_{H_2})(c_p)_{para} \cdot \Delta T_{conv} \end{aligned} \quad (4.3)$$

where  $\dot{m}_{conv}$  is the fraction of ortho-hydrogen to be converted in the process.

#### 4.1.2.2 Implemented heater unit in HYSYS, with input imported from literature data

Since the hydrogen target temperature is fixed, a more elegant approach is to import the data values of the conversion heat, etc. directly into the spreadsheet in HYSYS, and export the conversion heat duty,  $q_{conv}$  into a heater unit. The heater automatically calculates the temperature rise of the fraction of ortho-hydrogen,  $(1 - n_{para})$ , that is converted to para-hydrogen.

When the approximated temperature rise is found, the normal hydrogen is from that point assumed perfectly converted, i.e. equilibrium is reached. A manipulated para-hydrogen stream can be imported into HYSYS via the National In-

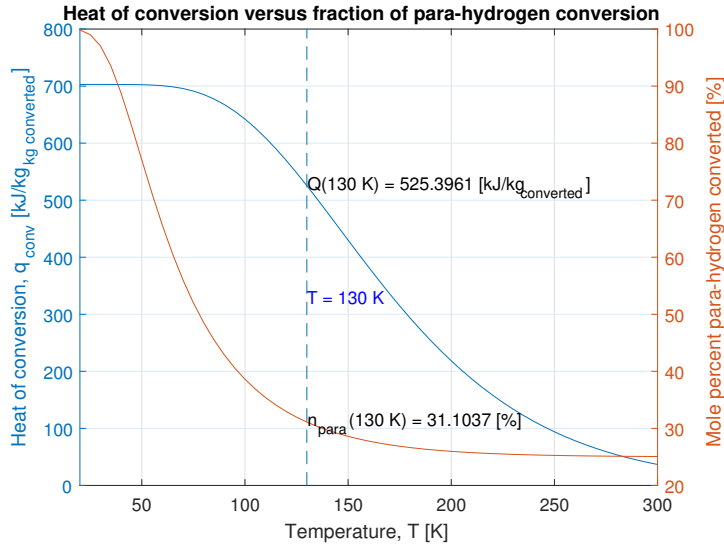


**Figure 4.4:** Caption

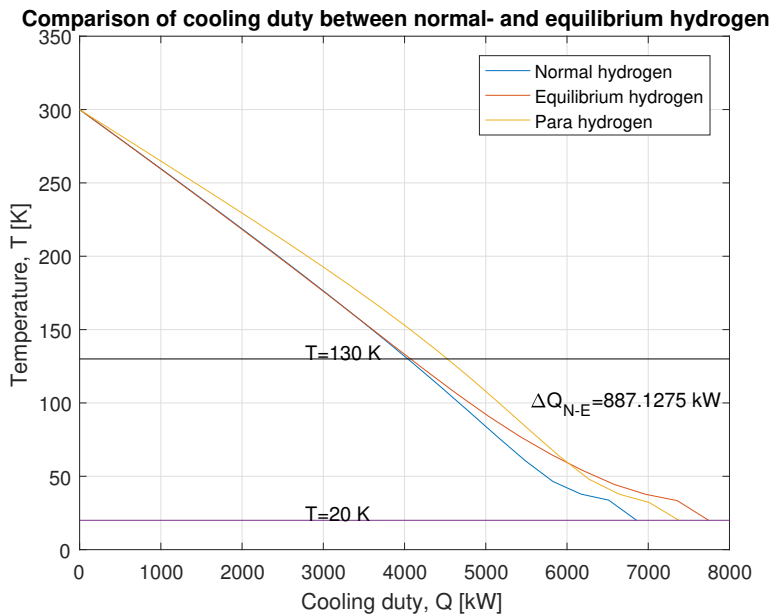
stitute of Standards (NIST) property database, RefProp, which represents the fundamental differences in properties, such as specific heat capacity between pure para- and equilibrium-hydrogen, as illustrated in Figure 2.4 in Chapter 2.

The difference in the specific heat capacities between normal- and equilibrium-hydrogen can be quantified by a simple simulation experiment in HYSYS; by cooling down each stream to liquid saturation temperature, the difference in heat duty and enthalpy of each stream can be found. The results were plotted in Figure 4.5

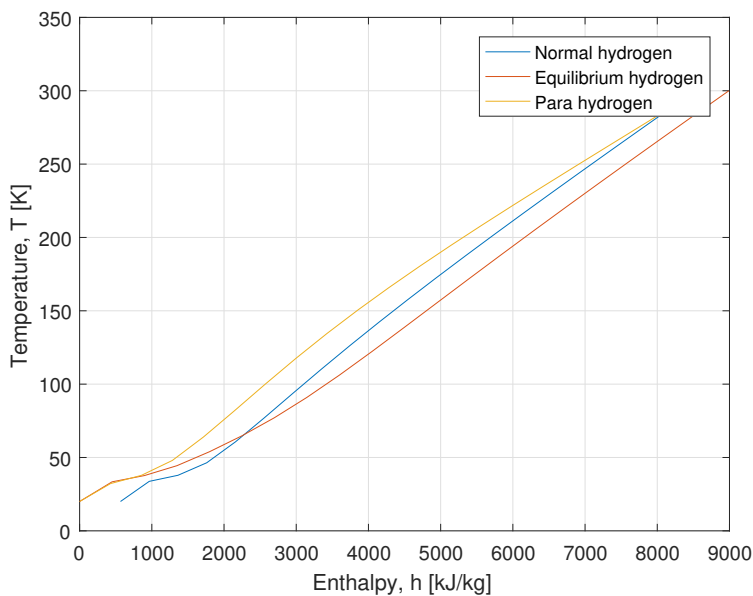
The difference in temperature increase between integrating a two polynomial functions and direct import with use of a heater, is shown in Table 4.4 below:

Approach	Temperature rise
6 <sup>th</sup> order polynomial (Excel standard)	11.08 K
9 <sup>th</sup> order polynomial (Excel LINEQ function)	10.95 K
Direct import to heater (100% accurate)	<b>13.00 K</b>

**Table 4.4:** Approximation of adiabatic temperature increase, final design parameters



(a) Cooling curves of equilibrium- and normal-hydrogen generated by heater units in HYSYS. For  $T < 130$  K the requisite liquefaction duty increases as a function of the heat of conversion.  $\Delta Q_{N-E}$  is the difference between cooling duty of equilibrium- and normal hydrogen at 20 K



(b) Enthalpy curves of equilibrium- and normal-hydrogen generated by heater units in HYSYS.

**Figure 4.5:** Test experiment to quantify the enthalpy- and cooling duty difference of the two hydrogen forms used in the HYSYS simulation environment

### 4.1.3 Baseline Design of the Case Study Models

The initial conditions of the SMR PRICO precooling systems (Case Study I and II) and the CMR Precooling systems (Case Study III and IV) are given in Table A.1 and A.2, which can be found in Appendix A. Below, a brief review of the different case studies is presented.

#### 4.1.3.1 *Mixed Refrigerant PRICO- and Cascade-cycle*

The MR stream is entering a two-stage compressor train at a pressure of 4 bar, which is assumed as a reasonable LP level, both in favor of compressor pressure-ratio and drop through throttle valves. For system III and IV, there are two separate compressor train systems, but with equivalent suction pressure. The compression is assumed isothermal, by implementing inter- and after-coolers with an intermediate temperature level of 300 K (to avoid overheating inside the compressor) between the stages. The appropriate HP level for each model is elaborated and concluded in the analysis section, due to optimization considerations. The MR stream(s) is further cooled by its own LP return stream(s), counter-flow-wise in the main heat exchanger(s), down to 130 K. The cold HP stream is throttled in the expansion valve(s), resulting in the necessary temperature drop (below 130 K) that creates the main cooling power.

The suction temperature of the MR return stream, for every Case Study Model, into the compressor train inlet, is a variable parameter. Due to the lack of degrees of freedom with the current process design, the HYSYS Multi-Channel Heat Exchanger unit is not able to specify a given outlet temperature, to maintain a preferable minimum temperature approach. Hence the outlet temperature is automatically re-calculated, each time the major variable optimization parameters, such as HP, mass flow and MR composition are changed. The optimization approach is elaborated in detail in Section 4.2.

The liquid fraction in the return stream (suction stream) is dependent on both temperature and pressure. In the MR circuit(s) in system II, III and IV, some liquid may be generated in the return stream(s), as a result of the considerable lower temperature level generated by both the R290-refrigerator, and the pre-defined outlet temperature at the cold side of the second heat exchanger in the CMR processes (III and IV). To avoid liquid in the gas compressors, the liquid fractions are separated before the compressor inlet, where it is guided through a pumping system, while gas vapour is guided through the gas compressors. At the end of the compressor train, the two streams are mixed, which then close the overall cycle.

This particular effect may be conclusive when optimizing the MR parameters in Case Study II and IV; the advantages with a higher fraction of light components is that a lower level of liquid fractions are formed in the suction stream(s), together with lower probability of freeze out in the lower temperature level. Some disadvantages are that light components may create difficulties in temperature integration in heat exchangers, due to vapour formation at lower temperature levels, than with heavier components, which will cause greater irreversibilities within the main heat exchangers.

The advantages with a higher content of heavy components is that the overall temperature level of the return (suction) streams are reduced, which may result in lower discharge temperatures at the compressor outlet, which minimize the requisite after-cooler duty, and thus the respective generation of irreversibilities. In addition, when considering the R290-chiller units, if the temperature level decreases to below the chiller target temperature, exergy- and investment savings can be applied, by simply neglecting this particular unit. For the case with higher fractions of heavy components, a disadvantage in addition to the pumping work- and investment penalty, is that the feed temperature will deviate from the refrigerant temperature at the heat exchanger inlet, which makes heat integration complicated.

The results from the high- and low liquid scenarios will be further elaborated in the Technical Results and Discussion part of the thesis in Chapter 5.

#### 4.1.3.2 Hydrogen and noble gas mixture feed

For simplicity reasons, as proposed by [9], the system boundary does not include hydrogen pre-compression in any of the models. A feed pressure of 20 bar is therefore assumed delivered from a production cite, with a flow rate of 150 tpd ( $\approx 1.74$  kg/s). The conversion of ortho to para hydrogen towards the equilibrium state is calculated based on the approach explained in Section 4.1.2, resulting in a temperature increase of 10.9 K. The normal-hydrogen stream is replaced by a new stream with the manipulated equilibrium-hydrogen equation of state and hence recycled into the heat exchanger and cooled down to 130 K.

The pressure level of the noble gas mixture (nelium) is given at 80 bar, which is a reasonable pressure level based on those found in literature. The compression train of this system remains outside the system boundary. The nelium mass flow is fixed at ten times of the hydrogen mass flow<sup>2</sup>, and cooled down to the same target temperature as the hydrogen feed.

---

<sup>2</sup>This approach was recommended by supervisor David Berstad, SINTEF Energy Research

The remaining specifications of the HYSYS model and component design parameters can be seen in Appendix A.

#### 4.1.4 Definition of system boundaries when evaluating exergy parameters

To evaluate the exergy efficiency and the specific energy consumption for the case study processes, an evident system boundary must be defined. Based on recommendations from literature concepts, hydrogen pre-compression remains outside the system boundary. Hence, the streams,  $s$ , that crosses the system boundary are: 1) the inlet- and outlet hydrogen streams;  $s1$  and  $s4$  in system I (Figure 3.1),  $s1$  and  $s5$  in system II (Figure 3.2),  $s1$  and  $s5$  in system III (Figure 3.4) and finally  $s1$  and  $s6$  in system IV; 2) the inlet- and outlet helium streams;  $s1c$  and  $s2c$ , for system I,  $s1c$  and  $s3c$  for system II,  $s1c$  and  $s3c$  for system III and  $s1c$  and  $s4c$  in system IV.

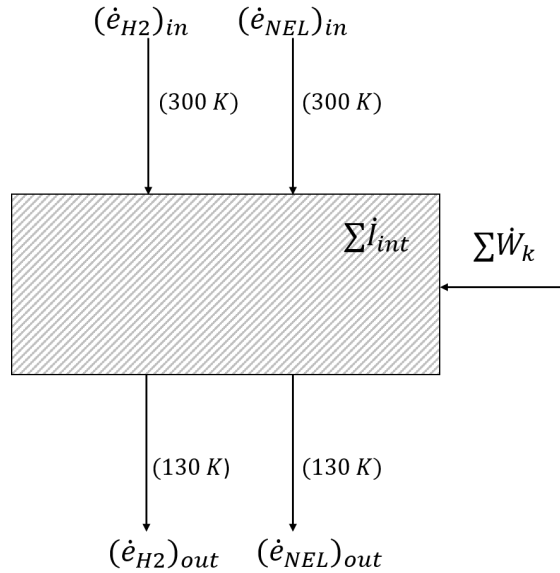


**Figure 4.6:** System boundary benchmark for each MR Precooling Case Study Model

Inspection of the system boundary model in Figure 4.6, shows that the external streams crossing the system boundary of each Case Study Model are equal.

Hence, the overall exergy balance for each Case Study becomes

$$(\Delta\dot{E}_{H2} + \Delta\dot{E}_{NEL})_b + \sum \dot{I}_{int} = \sum \dot{W} \quad (4.4)$$

where  $\Delta E_{H2} = \dot{m}(e_{out} - e_{in})_{H2}$  and  $\Delta E_{NEL} = \dot{m}(e_{out} - e_{in})_{NEL}$ , and represents the increased exergy content supplied to the feed streams by the internal system, due to the precooling process, which again is equivalent as the minimum required work to cool the streams down to the target temperature,  $W_{min} = (\dot{m} \cdot w_{min})$ .  $\sum \dot{I}_{int}$  equals the overall sum of irreversibilities generated within the system boundary, for each system I, II, III and IV. In system II and IV, the irreversibilities generated by the chillers has to be taken into account.  $\sum \dot{W}_{net}$  equals the net power consumed within the system boundary black box.

For system I and III,  $\sum W = \sum W_{c,k}$ , where  $W_{c,k}$  is the power consumption of compressor  $k$ . For system II and IV,  $\sum W = \sum W_{c,k} + \sum W_{ch,k}$ , where  $W_{ch,k}$  is the power consumption of chiller  $k$ , related to each refrigerant stream.

The final exergy efficiency of the two systems are

$$\varepsilon_x = \frac{W_{min}}{\sum \dot{W}} = \frac{(\Delta\dot{E}_{H2} + \Delta\dot{E}_{Nel})}{\sum \dot{W}} = \frac{\Delta\dot{e}_{H2} + \Delta\dot{e}_{Nel}}{w_{net}} \quad (4.5)$$

where  $w_{net} = \frac{(\sum W_k)}{\dot{m}_{H2}}$  in kWh/kg<sub>H2</sub>. The specific formulas for the component-irreversibilities were presented in Chapter 2

#### 4.1.4.1 System boundary exception: Liquid Nitrogen Precooling (LIN-PC)

The system boundary for Case Study V, using liquid nitrogen, is different from the other systems. Since the system only involves a multi-channel heat exchanger, every stream involved in the process crosses the system boundary at both inlet and outlet. The remaining exergy content in the evaporated nitrogen stream at the cold outlet, leaves the system (open cycle), and thus it is considered lost. Therefore this exergy content cannot be considered as a part of the efficiency calculation, which makes the efficiency quite low, in general. As for the specific energy consumption related to generation of liquid nitrogen,  $w_{(net,LN2)}$ , it is based on data provided from literature, where the energy consumption is associated with the penalty (kWh) of producing 1 litre of liquid nitrogen. The specific energy consumption of LIN precooling of hydrogen,  $w_{(net,LIN-PC)}$ , is therefore defined as

$$w_{(net,LIN-PC)} = \left( \frac{w_{(net,LN2)} \cdot 10^3}{\rho_{(LN2)}} \right) \cdot \left( \frac{\dot{m}_{(LIN-PC)}}{\dot{m}_{(H2)}} \right) \quad (4.6)$$



Hence, the exergetic efficiency of system V is defined as

$$\varepsilon_{(LIN-PC)} = \frac{w_{(min,LIN-PC)}}{w_{(net,LIN-PC)}} = \frac{\Delta\dot{E}_{H2} + \Delta\dot{E}_{NEL}}{\dot{W}_{(LIN-PC)}} \quad (4.7)$$

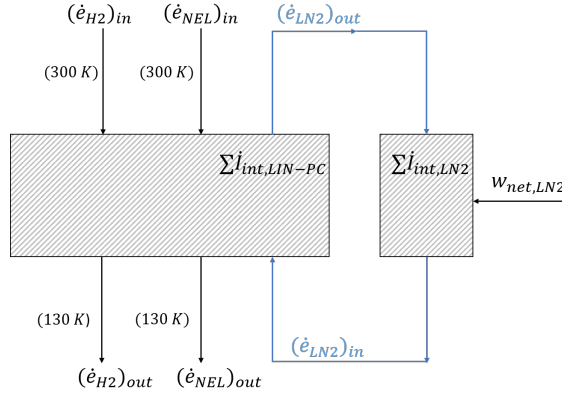


**Figure 4.7:** System boundary benchmark for LIN Precooling Case Study Model

## 4.2 Optimization Approach

In order to fulfill a good optimization of the case study models within the time limitations, it has to be as simple as possible. In a paper by Aspenlund et al. [6] an optimization model for a single LNG PRICO process was proposed, using Tabu Search (TS) and a modified simplex (NMDS) connected to HYSYS through MS Excel using the Visual Basics programming software.

It can be concluded that such an implementation is too extensive with emphasis on the thesis scope. Nevertheless, the assumptions and results can be used as a benchmark. The assumptions, which for the LNG PRICO process are comparable with the proposed hydrogen precooling cases, are the following;

If a fixed internal temperature approach ( $MITA/\Delta T_{min}$ ) is chosen in the heat exchanger(s), e.g. 2-1 K for cryogenic processes, to minimize the irreversibilities,  $I_i$ , the following requirements are conclusive

	Constraint
1	The shape and match between the hot and cold Composite Curves (CC) must be as good as possible by minimization of the area between the two.
2	The pinch point should be located in the cold end of the heat exchanger and gradually open up at higher temperatures (due to higher exergy loss at lower temperatures, as explained by Figure 2.2 in Chapter 2).
3	The reduction of irreversibilities is done by minimizing the transferred heat in the heat exchangers.
4	The restrictions in the PRICO process due to temperatures at the heat exchanger outlet must be above dew-point (gaseous phase). Otherwise liquids in compressor will cause problems. The same restriction applies to the CMR process in case study 3 and 4.

**Table 4.5:** Caption

With emphasis on these specifications, the optimization variables for every case study becomes

- a) Flow rate of mixed refrigerant,  $\dot{m}_{MR}$
- b) The composition of the mixed refrigerant,  $n_i$ . Where  $i$  is ranging from C1-C4 plus N<sub>2</sub>
- c) High- and low-pressure.

Due to the lack of degrees of freedom in the simulation environment, the unknown optimization variables mentioned above, must be manipulated to reach the desired solution. To reach the target results the following approaches will be executed for each simulation iteration case:

1. Adjustment of the pressure of the MR cycles, with a fixed and partly optimized MR composition and fixed mass flow. The target variables used for comparison of performance of the models are either with a) a fixed UA value, obtained from one of the systems, or b) a fixed heat exchanger duty obtained likewise.
2. Adjustment of the mass flow and composition of the MR cycles with fixed pressure values. Target variables used for comparison are equivalent as in the first approach explained above.

The optimization approach is summarized in Table 4.5



## Chapter 5

# Technical Results and Discussion

As the different precooling methods are presented in the previous chapter, this chapter will elaborate which of the proposed hydrogen precooling systems that possibly could be integrated as a part of a large-scale liquefaction plant in Norway. Exergy efficiency is already considered as the major key performance parameter in this context, however, other parameters will be evaluated, such as specific energy consumption of the precooling plant and irreversibilities generated within each component that comprise the overall process.

With emphasis on the optimization approach explained in Section 4.2 in Chapter 4, the results from each model will be presented as iteration steps (*i . . . (num.)*), where the variable optimization parameters are adjusted until a preferable solution is reached. In summary, it is

- 1) Optimization of MR component concentrations
- 2) Optimization of MR pressure and mass flow simultaneously
- 3) Evaluation of overall exergy balance, efficiency and irreversibility for each iteration

## 5.1 Results and discussion: SMR PRICO precooling

System one, the PRICO SMR hydrogen precooling concept, defines the basis of the entire parametric analysis, which means that each initial parameter of each Case Study model were established based on the ones found in this case.

### 5.1.1 Mixed Refrigerant Optimization Procedure

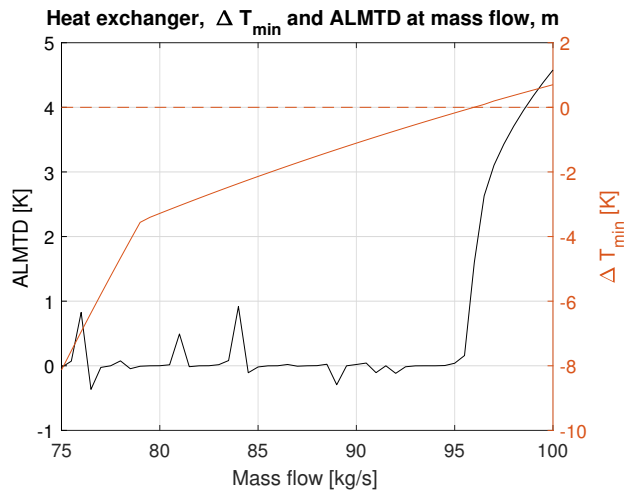
The initial MR composition that showed promising results in the PRICO system was found by a trial and error adjustment, where the high pressure level from the IDEALHY-MR-model in [44], was bench-marked and kept constant at 25 bar. A mass flow rate of 73 kg/s was found with acceptable temperature match in the heat exchanger, resulting in a specific precooling work of 2.04 kWh/kg<sub>H<sub>2</sub></sub>. The first simulation with the initial parameters above, did not include the synthetic ortho-para adiabatic conversion temperature rise at the 130 K hydrogen outlet. The parameters were adapted into the updated model, which gave a temperature cross in the heat exchanger. The molar fractions of the initial MR composition and the following iteration steps are given in Table 5.1. The corresponding composite curves (T-Q-diagram) are shown in Figure 5.14a.

Iteration		0 <sup>a</sup>	1	2	3	4	5	6
Molar fraction [mole-%]	Nitrogen	0,110	-	-	-	0,187	-	-
	Methane	0,343	-	-	-	0,264	-	-
	Ethane	0,124	-	-	-	0,203	-	-
	Propane	0,206	-	-	-	0,169	-	-
	i-Buthane	0,218	-	-	-	0,178	-	-
Mass flow [kg/s]		73	-	96	73	-	-	-
High pressure [bar]		25	-	-	46	-	45	42

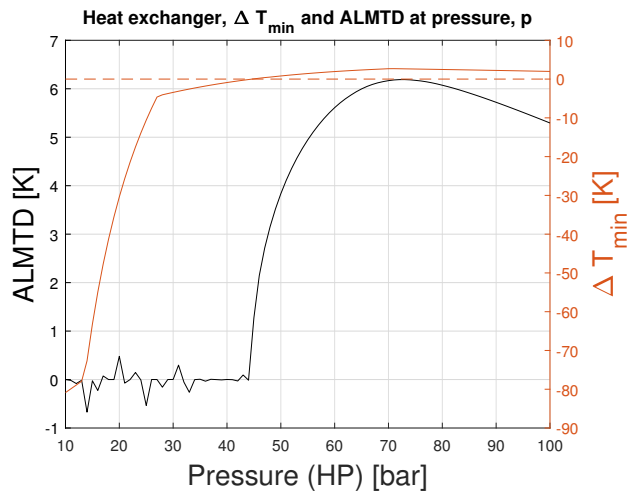
<sup>a</sup> First iteration is simulated without integration of ortho-para conversion. Therefore only the parameters are of particular interest, not the results.

**Table 5.1:** Final results of optimization parameters, Case Study I

To fix the initial temperature cross problem, search for a new optimal solution is done by the Case Study tool in Aspen HYSYS; the first simulation is searching for an optimal MR mass flow to obtain a temperature match in the heat exchanger that require  $\Delta T_{min} > 0$ , to fulfill criteria number one, from Table 4.5. The MR composition is kept constant.



(a) Case Study test run, with mass flow,  $m$ , as dependent variable with a fixed MR composition and pressure,  $p$  equal as in *i1*. The mass flow target in this case must be above the point where  $\Delta T_{min} > 0$ , to avoid temperature cross inside the heat exchanger



(b) Case Study test run, with pressure,  $p$ , as dependent variable. Fixed mass flow and MR composition. The pressure target values must satisfy the same conditions as described above.

**Figure 5.1:** Test run generated in HYSYS to quantify pressure- and mass flow values with the given heat exchanger constraints

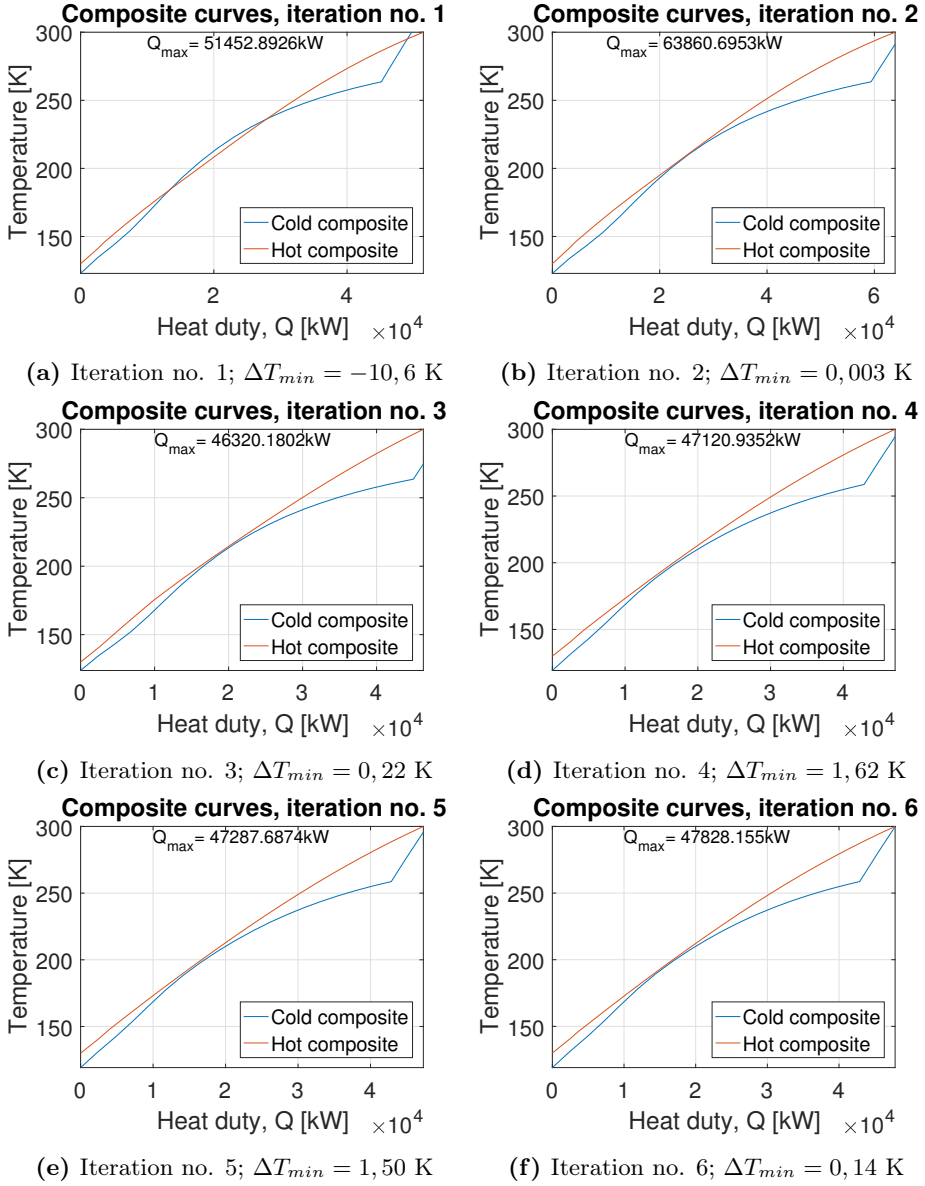


**Figure 5.2:** Optimization of the composite curves within the main heat exchanger (HX-1), Case Study I

The result from the first simulation (Figure 5.1a), indicate that a mass flow of 96 kg/s or higher fulfills the temperature approach criteria<sup>1</sup>.

Due to a final  $\Delta T_{min}$  of less than 2 K, a similar Case Study with variable pressure is conducted to determine the new high pressure level (Figure 5.1b). For  $p_{HP} > 45$  bar,  $\Delta T_{min}$  is positive. The new high pressure also allows for reduction of the total mass flow of 24 %, which reduces the compressor power with almost 3 %, see Figure 5.1.

By investigation of the composite curve from *i3* in Figure 5.2c, the high pressure results in evaporation of the refrigerant at a lower temperature, which causes a major gap at the hot end of the heat exchanger. As the concentration of light components is relatively low, the MR composition must be adjusted in favour of lighter components, such as nitrogen, to avoid major losses caused by poor temperature match.

Therefore the nitrogen content is increased with approximately 40%, at the same mass flow and pressure conditions. This results in a better temperature match, as indicated in Figure 5.2d, but both the heat exchanger duty and compressor power are increased by 1,7 and 10 % respectively.

### 5.1.2 Key Performance Indicators in the Case Study I process

In Table 5.2 and 5.3, the compressor- and heat exchanger performance parameters are summarized for each iteration. Note that even if the compressor power are much lower in *i0* – 3 than 4 – 6,  $\Delta T_{min}$  is too low. As explained in chapter 2, achievement of such a close temperature match will require considerably larger heat exchangers, which can be quantified by use of i.e. the overall heat transfer coefficient  $UA$ .

---

<sup>1</sup>This value is assigned to *i2*



Iteration	0	1	2	3	4	5	6
WLMTD <sup>a</sup> [K]	4,80	-0,53	1,60	2,15	5,56	5,30	4,22
$\Delta T_{min}^b$ [K]	0,75	-10,6	0,003	0,22	1,62	1,50	0,14
Duty, $Q$ [MW]	48,6	95,1	63,2	45,9	47,1	47,3	47,8
UA [MW/°C]	10,2	50,9	39,5	21,4	8,50	8,91	11,3
NTU [MW/°C]	409,2	2041,7	1584,4	858,4	341,0	357,4	453,3

**Table 5.2:** Heat exchanger performance indicators,  $i0-i6$ , Case Study I

a: Weighted LMTD calculated by HYSYS, with 20 temperature intervals inside the heat exchanger

b: Is formulated in HYSYS as Minimum Internal Temperature Approach (MITA)

Iteration	0	1	2	3	4	5	6
Compressor power <sup>a</sup> [MW]	12,73	13,02	16,42	16,00	17,77	17,75	17,22
Pressure ratio [-]	6,25	-	-	11,5	25	11,5	11,25
Suction temperature [K]	291	310	291,2	272,2	262	295,7	299,9
Liquid fraction <sup>b</sup> [-]	0	0	0	3,24E-02	0	0	0
After-cooler duty <sup>c</sup> [MW]	25,33	25,33	28,81	32,52	29,77	29,66	29,30
Mass flow, MR [kg/s]	73	96	73	73	73	73	73

**Table 5.3:** Performance indicators of Mixed Refrigerant compressor train, Case Study I

a: Net power,  $\dot{W}_{net}$

b: Liquid fraction at suction

c: Net after-cooler duty

In order to satisfy the rigid heat exchanger constraints mentioned above, the most promising and realistic results at this point, are found in  $i4$  and  $i5$ , resulting in an overall power consumption between 17.77 – 17.75 MW for the compressors. Figure 5.3, illustrates the difference in increased compressor power, when increasing the mass flow and pressure, with respect to the given MR composition used in  $i4-i6$ .

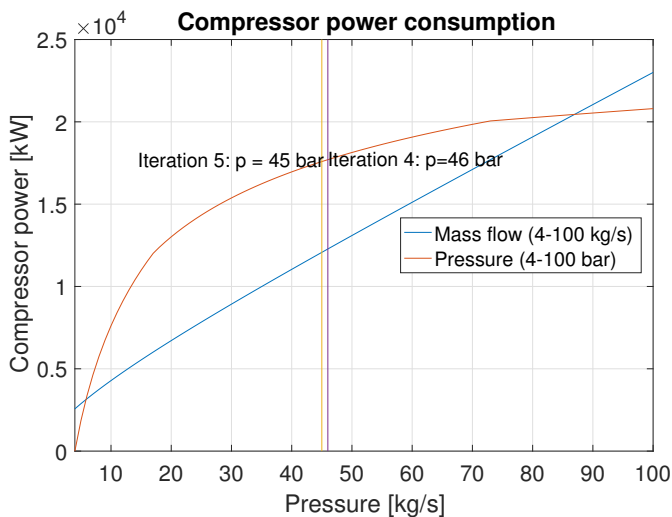


**Figure 5.3:** Compressor power impact at variable pressure and mass flow in the MR cycle with a given MR composition, Case Study I

### 5.1.3 Analysis of exergy losses and efficiency

This section will elaborate on and discuss the exergy- input and destruction throughout the entire process. In order to determine in which component changes can be made, an exergy balance for every component that comprises the overall process have been made. An overall summary of the total irreversibilities generated by each iteration step, together with the equivalent exergetic efficiency, are presented in Table 5.4.

Figure 5.4 represents the total exergy balance in and out of the system boundary, plus the irreversibilities generated inside the boundary on the left hand side (Eq. 4.4). The compressors covers the total amount of power requirement to the system. Table 5.4 shows that the total input power equals the overall exergy distribution, with minor deviation. It is noticeable that  $i1$  has considerably lower fraction of losses in the heat exchanger than  $i2$ -  $i6$ . This is due to the temperature cross, which result in lower differences between inlet and outlet flow exergy, hence lower irreversibilities.

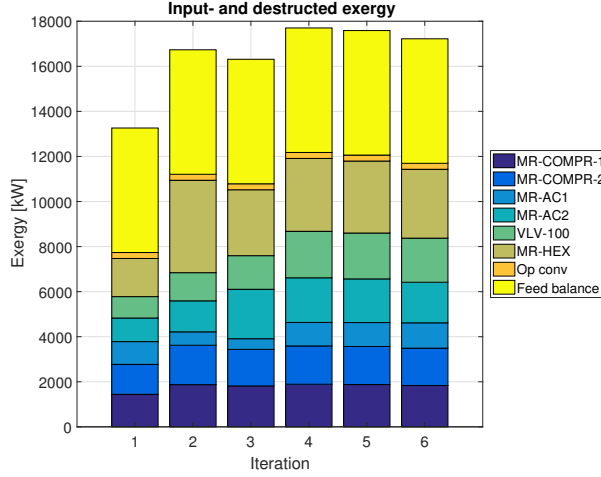


**Figure 5.4:** Overall exergy balance of Case Study I. The stacked bars indicates that the overall exergy input and destruction within the system (LHS, Eq. 4.4), equals total power input (RHS, Eq. 4.4) into the system, for each iteration

As concluded in previous section,  $i1$ -  $i3$  cannot be a feasible solution, even if the total amount of exergy losses are 7-25 % lower, as can be calculated from the resulting parameters in Table 5.4. Therefore the results from  $i4$  and  $i5$  are candidates for further analysis.

$i$	$\sum \Delta \dot{E}_{boundary} + \sum \dot{I}_{PC}$ [MW]	$\sum W_{net,PC}$ [MW]	$\varepsilon_x$ <sup>a</sup>	$w_{net,PC}$ [kWh/kg <sub>H2</sub> ]
1	13,262	13,262	41,6 <sup>b</sup>	2,122
2	16,734	16,734	33,0	2,677
3	16,313	16,313	33,9	2,610
4	<b>17,702</b>	<b>17,702</b>	<b>31,2</b>	<b>2,832</b>
5	<b>17,586</b>	<b>17,587</b>	<b>31,4</b>	<b>2,814</b>
6	17,221	17,221	32,1	2,755

a: Exergy efficiency of the precooling process. Not a complete efficiency measure of the overall liquefaction system

b: Not feasible, due to temperature cross inside heat exchanger

**Table 5.4:** Main resulting exergy parameters in the Case Study I process

### 5.1.3.1 Elaboration of exergy destruction and improvement proposals of system $i4$ and $i5$

Referring to the exergy efficiency targets from Figure 2.3 in Chapter 2, it is desirable to increase the exergy efficiency from 31,2-31,4% as for  $i4$ -  $i5$ , to above 40%.

Component	( $i4$ )		( $i5$ )	
	$\dot{I}$ [kW]	[%]	$\dot{I}$ [kW]	[%]
MR compressors	3589,96	29,48	3566,41	29,57
MR aftercoolers	3024,84	24,84	2999,16	24,87
Throttle valve	2062,07	16,93	2036,05	16,88
Main heat exchanger	3234,72	26,57	3194,27	26,49
Ortho-para conversion	264,76	2,17	264,76	2,20
Tot	12176,4	100	12060,6	100

**Table 5.5:** Exergy destruction in process components,  $i4$  and  $i5$ , Case Study I

It can be seen from Table 5.5, that the major fraction of exergy destruction are generated in the compression- and aftercooler system. Due to a lower pressure ratio in  $i5$ , the aftercooler- losses are reduced by approx. 25 kW, which reduce the overall exergy destruction, and compressor power are reduced with 116 kW, wich increase the exergetic efficiency by 0.5%.

The main heat exchanger losses are also quite extensive compared to the first three iterations, which can be seen in detail for each iterative approach in Appendix B.

Since compressor- aftercooler system parameters are dependent on the same parameters that affect the heat exchanger losses, these will not be further adjusted. Yet, it is interesting to reduce the considerably large throttle valve losses, which represents almost 17% of the total. By e.g. integrating a liquid turbo expander at the 130 K MR outlet, while assuming a feasible isentropic efficiency, the entropy generation has to be smaller, compared to the current isenthalpic throttling. As a final alternative, the effects of increasing the isentropic efficiency of both compressors and expanders will be investigated in favour of the best performing iteration solution, in order to increase exergy efficiency even further.

**Expanders with equal pressure ratio** Below, the results from expander integration are presented. As the turbo expansion gives a higher cooling capacity, hence a lower temperature level, a bigger temperature gap in the heat exchangers

results in an increase of exergy destruction of 23,5% and 24,4 % for  $i4$  and  $i5$  respectively. The major difference is still, as expected, a decrease in exergy destruction of the turbo expansion; 14,2% and 14,1% respectively for  $i4$  and  $i5$ , which gives a total reduction of 8 % and 6,2 % of the total exergy destruction within the system.

	$i4 - a$ (LP = 4,0 bar)		$i5 - a$ (LP = 4,0 bar)	
	$\dot{I}$ [kW]	[%]	$\dot{I}$ [kW]	[%]
MR compressors	3558,0	32,0	3581,26	31,70
MR aftercoolers	2845,4	25,40	2869,9	25,40
Expander	310,20	2,77	314,2	2,78
Main heat exchanger	4227,4	37,72	4277,7	37,83
Ortho-para conversion	264,60	2,36	264,60	2,36
<b>Tot</b>	11205,6	1	11307,7	1

**Table 5.6:** Results from integration of expander, LP = 4 bar, Case Study I

**Integrated expanders with  $\Delta T_{min}$ -adjusted pressure ratio** Another approach is to maintain the temperature approach from the original process scheme. This is done by increasing the low pressure level, to simply control the temperature drop of the expander. With a new LP level of 4,9 bar and 5,0 bar for  $i4$  and  $i5$  respectively, the  $\Delta T_{min}$  criteria is satisfied. Inspection of Table 5.7, reveals that the heat exchanger losses are reduced to the original results, with some minor deviations and that the total amount of invisibility's are further reduced by 1560 kW and 1760 kW, see Table 5.7 and 5.6.

	$i4 - b$ (LP = 4,75 bar)		$i5 - b$ (LP = 4,80 bar)	
	$\dot{I}$ [kW]	[%]	$\dot{I}$ [kW]	[%]
MR compressors	3306,97	33,47	3315,35	33,46
MR aftercoolers	2617,30	26,49	2633,00	26,57
Expander	282,44	2,86	284,79	2,87
Main heat exchanger	3410,29	34,51	3411,75	34,43
Ortho-para conversion	264,60	2,68	264,60	2,67
<b>Tot</b>	9881,60	100	9909,49	100

**Table 5.7:** Results from integration of expander, LP-4 = 4,75 bar and LP-5 = 4,8 bar, Case Study I

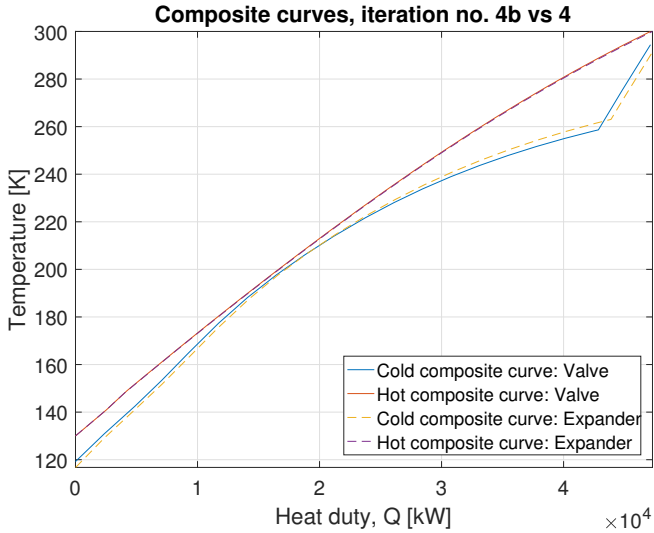
**Increased isentropic efficiency of expanders and compressors** As case  $i5 - b$  has the best performance, it is preferable to exploit the effect of higher isentropic efficiency of rotary equipment (now  $i5 - b'$ ) By increasing the isentropic efficiency of the compressors ( $\eta_c$ ) and the liquid expander ( $\eta_e$ ) from 75- to 85%, the exergy efficiency calculates to 40,77%, with a specific power consumption of 2,166 kWh/kg<sub>H2</sub>, which is an increase in efficiency of 14%, and a specific power reduction of 12,3%, compared to the iteration with lower motor efficiency.

**Final results** The final results, used for comparison with the remaining Case Study models are given in Table 5.8<sup>2</sup>. A complete exergy analysis has proven to be quite useful in order to improve process design and efficiency. For Case Study number one, the iteration approach with the best performance, with respect to the exergy efficiency is  $i5 - b$ , with integrated liquid turbo expander and adjusted low pressure level at  $p_{LP,4b} = 4,8$  bar. Exergy efficiency calculates to 35,8 %, which is 12,2% higher than for the original case  $i5$ . A total power consumption of 16,06 MW gives a specific pre-cooling work of 2,469 kWh/kg<sub>H2</sub>, which is a reduction of 12,3% compared to the original setup.

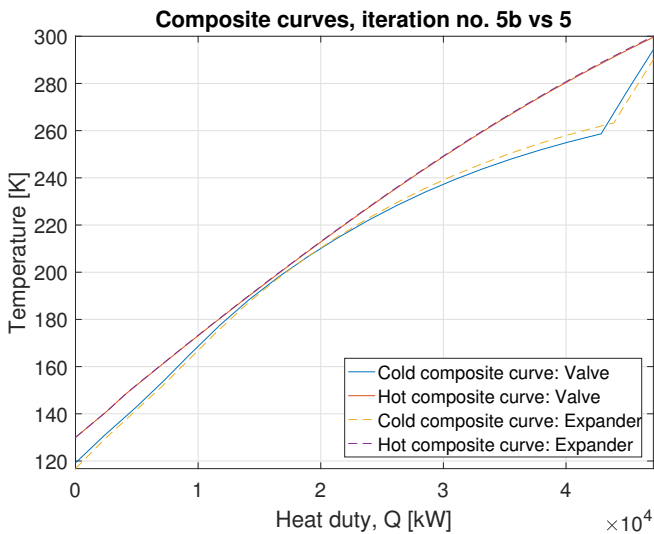
	Exergy efficiency [%]	Relative to org. design ( $\delta_k$ ) [%]	$w_{PC}$ [kWh/kg]
Case $i4 - b$	34,44	+9,410	2,564
Case $i5 - b$	35,78	+12,20	2,469
Case $i5 - b'$	40,77	+29,84	2,116

**Table 5.8:** Final exergy efficiency of Case Study I, PRICO SMR precooling, with integrated turbo liquid expanders

<sup>2</sup>Where the relative improvement factor compared to the original design is indicated by  $\delta_k$



(a) Composite curves of case  $i4$  compared to case  $i4 - b$  with expanders for improved temperature match. For  $T > 220$  K, the expander clearly lifts the cold composite closer to the hot composite. It is also possible to see that for  $190 < T < 200$  K,  $\Delta T_{min}$  is lowered to meet the desired criteria.



(b) Composite curves of case  $i5$  compared to case  $i5 - b$  with expanders for improved temperature match.

**Figure 5.5:** Comparison of composite curves with throttling valves and isentropic expanders

## 5.2 Results and discussion: SMR PRICO+ pre-cooling

To improve the exergy efficiency and further reduce the heat transfer duty inside the main heat exchanger, propane chillers are implemented in the upper temperature region, from 300 K - 268 K (-5°C). The new adjustment to the PRICO design lower the overall temperature level at the hot high pressure, and cold low pressure side of the MR cycle. As a consequence, some of the components may not fully evaporate inside the heat exchanger, hence some liquids must be removed before entering the compressor system, if a major fraction in the mixture consists of heavy components.

### 5.2.1 Mixed Refrigerant Optimization Procedure

The initial parameters of the PRICO+ system is adapted from the preferred model from the previous Case Study, without any adjustment. The content of buthane and propane represents more than 30 % of the mixture composition. As the temperature interval of the new system is decreased with a  $\Delta T = 32$  K by the chillers, still assuming that the temperature approach at the inlet and outlet of the heat exchanger must satisfy the  $\Delta T_{min}$  criteria, a minor fraction of the cold return stream is liquid.

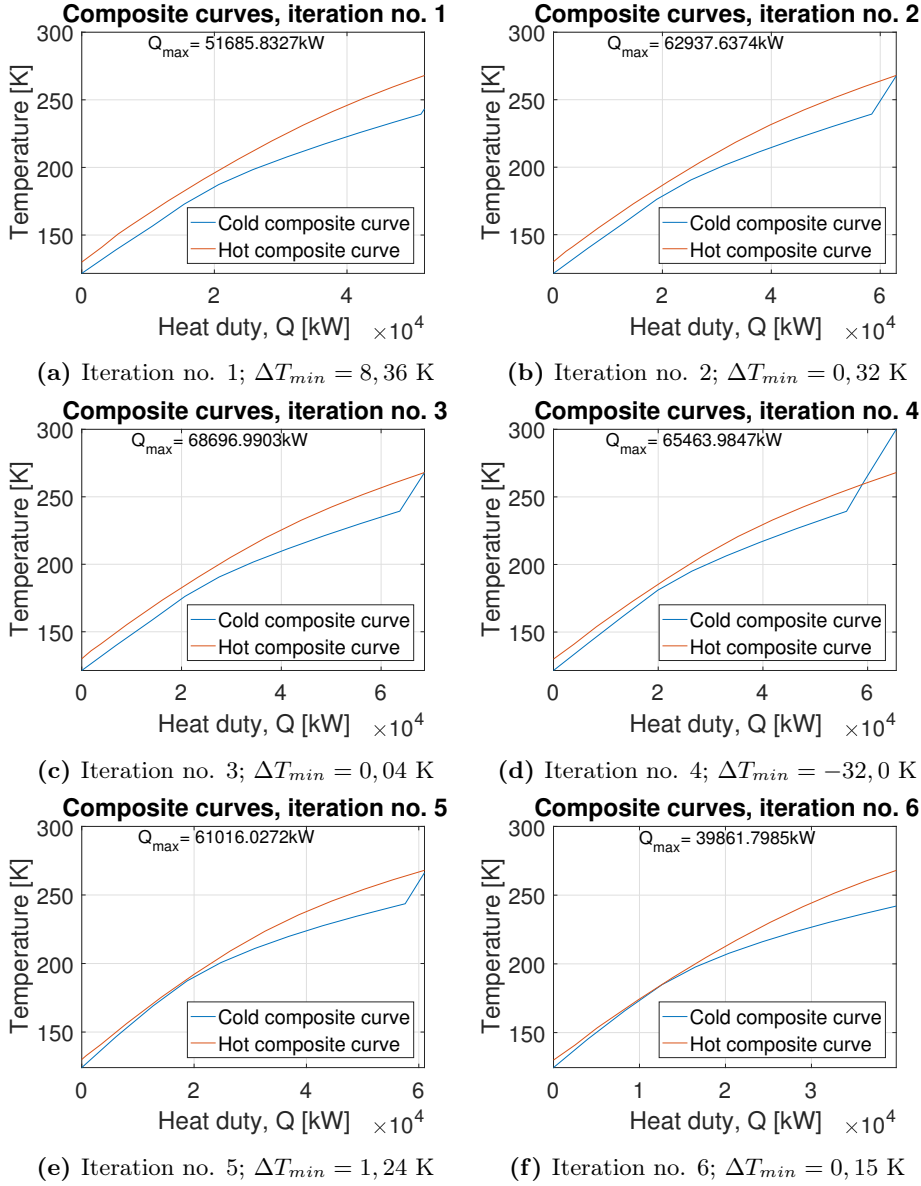
To avoid liquid formation in the compressors, a liquid fraction of  $y_{MR,suction} = 0,1355$  is separated and led through a pump to the same high pressure of 43 bar. The temperature match was not as bad as expected and with a reduced heat transfer duty  $\Delta Q = 11,8$  MW, since  $\Delta T_{min} = 1,30$  K further adjustments are required for the new system.

Table 5.9 shows that the search for an optimal temperature match for the heat exchanger is more extensive than in the previous case. There are 13 different combinations of MR- compositions, high pressure and mass flow; which can be classified as solutions based on if the liquid content of the suction stream,  $y_{MR,suction} = 0$  or ( $0 < y_{MR,suction} < 1$ ) (recall PFD's in Chapter 4). The corresponding composite curves are displayed in Figure 5.6.

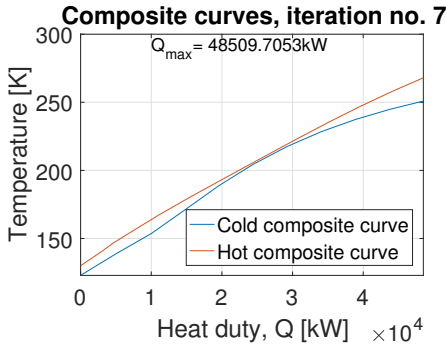
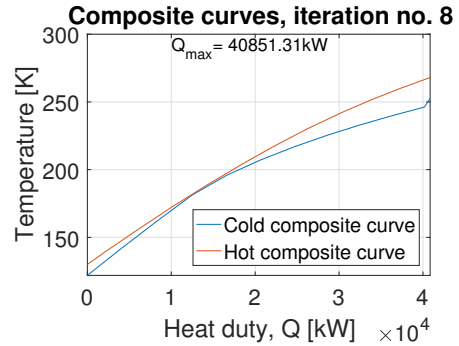
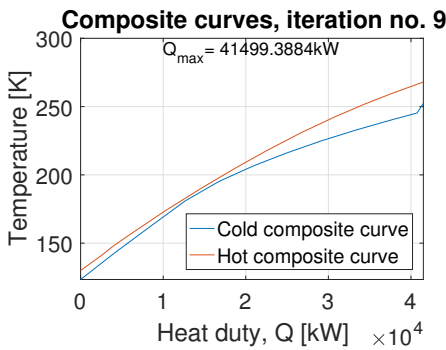
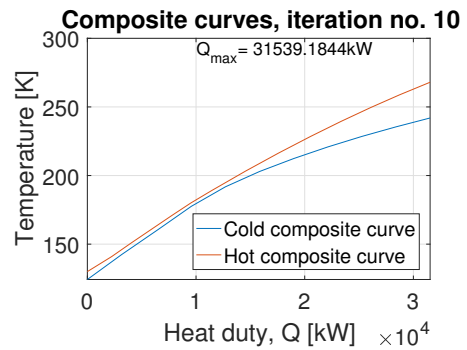
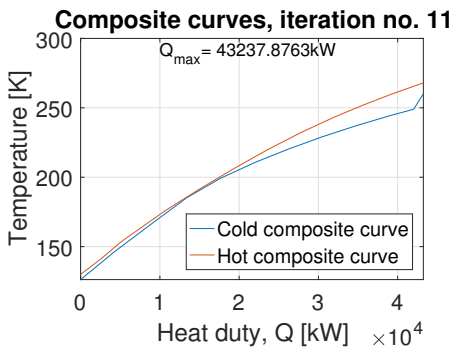
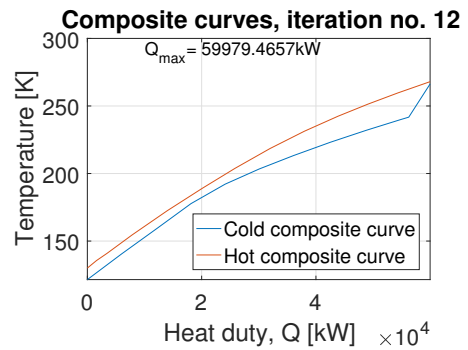


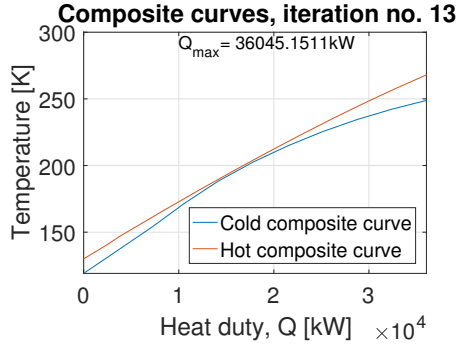
$i$	Molar fraction, $n_x$ [mole-%]					$\dot{m}$ [kg/s]	$p_{2,mr}$ [bar]
	Nitrogen	Methane	Ethane	Propane	Butane		
0	<b>0,19</b>	<b>0,26</b>	<b>0,20</b>	<b>0,17</b>	<b>0,18</b>	<b>73</b>	<b>43</b>
1	0,13	0,32	0,34	0,17	0,05	85,2	28
2	0,13	0,32	0,34	0,17	0,05	97,2	20
3	0,13	0,32	0,34	0,17	0,05	106	19
4	0,13	0,32	0,34	0,17	0,05	93,2	15
5	0,10	0,25	0,36	0,24	0,04	93,2	15
6	0,10	0,25	0,36	0,24	0,04	66,36	25
7	0,11	0,34	0,12	0,21	0,22	93,7	25
8	0,13	0,27	0,32	0,21	0,07	66,3	23
9	0,11	0,29	0,33	0,21	0,06	66,3	23
10	0,11	0,29	0,33	0,21	0,06	54,3	42,7
11	0,07	0,31	0,33	0,21	0,09	66,36	18
12	0,13	0,31	0,33	0,17	0,05	93,17	19

**Table 5.9:** Final results of optimization parameters, Case Study II



**Figure 5.6:** Optimization of cooling curves within heat exchanger HX-1

(g) Iteration no. 7;  $\Delta T_{\min} = 0,19 \text{ K}$ (h) Iteration no. 8;  $\Delta T_{\min} = 0,55 \text{ K}$ (i) Iteration no. 9;  $\Delta T_{\min} = 1,90 \text{ K}$ (j) Iteration no. 10;  $\Delta T_{\min} = 2,64 \text{ K}$ (k) Iteration no. 11;  $\Delta T_{\min} = 0,48 \text{ K}$ (l) Iteration no. 12;  $\Delta T_{\min} = 1,68 \text{ K}$

(m) Iteration no. 13;  $\Delta T_{min} = 1,30$  K**Figure 5.6:** Optimization of temperature match in MR cycle, Case Study II

In iteration  $i0$ ,  $i6$ ,  $i7$ , and  $i10$ , a high propane- and buthane content together with a high pressure results in a minor liquid fraction, causing a bigger temperature gap at the hot inlet. The composite curves for  $i0$ - $i13$  in Figure 5.6, indicates that the curve of the cold streams in the high-liquid iterations are more or less continuous, compared to the other cases, where evaporation of the MR is indicated by a break in the curve, around 250 K.

Before further elaboration can be done, it is obvious that several iteration iteration cases can be neglected; Iteration  $i4$  cannot be a valid solution, due to the big temperature cross caused by a far too low pressure, with a majority of light components.  $i2$ -  $i3$  results in an  $WMTD > 10$ , and an average temperature gap too big in the given interval. The temperature approach of  $i5$ -  $i8$  are too tight at the temperature interval in the lower end, and too open in the upper end.

The conclusion is that the best temperature matches are found in  $i9$ -  $i12$ . Even if  $\Delta T_{min,i11} = 0,48$  K, a further investigation of expander utilization can be a possible approach to make a better match. Recall the LP/HP adjustment method from Case Study I,  $i1$  may have potential for improvements by "lifting" the cold composite curve. From this point in Case Study II, the five most promising iteration solutions mentioned will be further analyzed, with respect to component KPIs and exergy losses, in the next section.

### 5.2.2 Key Performance Indicators in the Case Study Process

$i$	1	9	10	11	12	0
WLMTD [K]	13,98	5,66	5,63	2,95	10,04	3,98
$\Delta T_{min}$ [K]	8,36	1,90	2,64	0,48	1,69	1,30
Duty, $Q$ [MW]	51,7	41,5	31,5	43,2	59,98	36,04
UA [MW/°C]	3,70	7,33	5,60	14,7	5,97	9,05
Liquid fraction after exp., $x_{5b}$	0,87	0,89	0,89	0,94	0,87	0,81
Liquid fraction at suction, $x_{6b}$	0	0	0,043	0	0	0,135

**Table 5.10:** Heat exchanger performance indicators, Case Study II.

The key performance indicators in Table 5.10 validates that the heat exchanger duty are minimized when the liquid fraction of the MR outlet stream are greater than zero<sup>3</sup>. In  $i10$  and  $i13$ , the fraction of heavier components are larger, which gives a better heat transfer due to differences in heat capacities of boiling- and condensation of vapour and liquid fluids. A closer look on these effects will be elaborated in the exergy analysis.

$i$	1	9	10	11	12	0
MR compressor power [MW]	17,54	11,70	12,27	9,950	15,66	14,05
Pressure ratio [-]	7,00	5,75	10,67	4,50	4,75	10,75
Suction temperature [K]	243,5	252,4	242	260	266,3	248,8
After-cooler duty [MW]	12,90	8,640	12,81	7,140	12,60	15,40
Mass flow, MR [kg/s]	85,2	66,3	54,3	66,36	93,17	73

**Table 5.11:** Performance indicators of Mixed Refrigerant compressor train, Case Study II

In case  $i1$ , compressor input power is significantly higher than for the other iterations (high mass flow and pressure ratio). The best improvement is a reduced power consumption in  $i11$  of 7,8 MW, compared to minimum in case I. Still, a new source of power requirement is present, the three propane chillers. Power requirement of the chiller system was assumed ideal and with high COP, due to a temperature difference between the evaporator and condenser of less than 30

<sup>3</sup>The heat exchanger simulation work presented by Wilhelmsen et al. [54], proved that a two-phase flow regime enhanced the heat transfer coefficient significantly, which resulted in a reduced size of heat transfer area.

K. For case *i*11 the power requirement for the total chiller system is 2,06 MW, hence a total power reduction of 5,74 MW is accomplished.

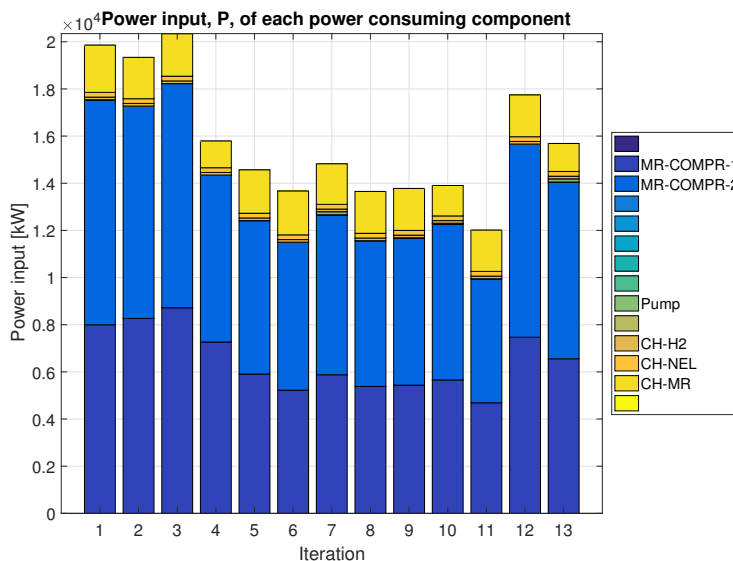


**Figure 5.7:** Power input for each iteration in case II

### 5.2.2.1 Propane chillers performance in the lowest power consuming iteration case

For the hydrogen chiller, COP calculates to 7,231, when a power consumption of 109,9 kW is required for the compressor with a mass flow of 3,425 kg/s. The cycle simulation in HYSYS did not converge with the estimated parameters obtained from CoolPack, as explained in Chapter 4. Mostly caused by poor temperature matches in the evaporator due to lack of mass flow of propane. The deviation between estimated and simulated COP and mass flow resulted in -0,5 and -0,11 respectively, which is acceptable. Deviations in the Nelium chillers were a little higher, and resulted in a COP and mass flow of 6,08 ( $\Delta = -1,68$ ) and 4,362 ( $\Delta = +1,372$ ).

As for the MR chiller, COP deviation calculates to the equivalent value of 7,23 in HYSYS, but a higher mass flow of refrigerant was needed, compared to the estimation by CoolPack. The main reason is that the initial input parameter, the MR mass flow as a function of the cooling duty target, was partly changed

throughout the optimization procedure, which cause deviations in design parameters. Nevertheless, power consumption relative to the MR compressors are low, hence deviations concerning kW does not affect the performance extensively.

Chiller	COP [-]	Cooling duty [kW]	Mass flow [kg/s]	Compressor power [kW]
Hydrogen	7,261	797,9	2,39	109,9
MR	2,669	4664	38,0	1747,3
Nelium	6,082	1220	4,36	200,6

**Table 5.12:** R290-Chiller performance, Case Study II

### 5.2.3 Analysis of exergy losses and efficiency

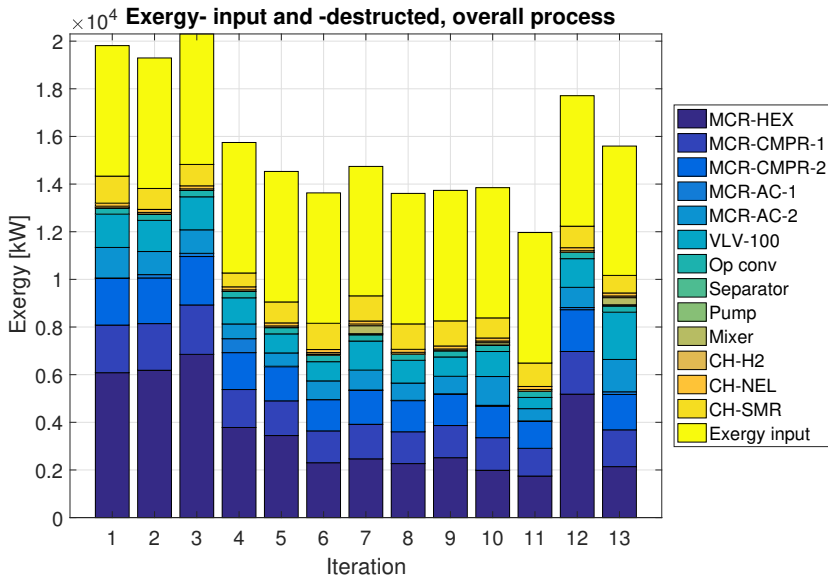


**Figure 5.8:** Exergy input plus exergy destruction within the process, Case Study II

Similar as for Case Study I, exergy balances are calculated for each process stream and component within the process. Figure 5.8 visualize the overall exergy destroyed and brought into the system. The yellow bars at the top represents the exergy balance of the streams that are crossing the system boundary. The

remaining bars represents the net exergy destruction generated inside the system boundary, and according to Eq. (4.4), the input power has to be equal to the sum of these two parameters.

Further investigation of Figure 5.8 and tabulated data in Table 5.13 reveals that the exergy destruction within case  $i1$  are between 40-30 % higher than for case  $i9$ - $i11$ . Still, a major fraction of the losses are generated within the heat exchanger, indicated by the lower bars in dark blue, which is nearly twice as high than for  $i9$ - $i11$ . Therefore, as predicted in the previous section, the total amount of invisibility's may be considerably reduced by integration of an turbo expander, as in case I.

$i$	$\sum \Delta \dot{E}_{boundary} + \sum \dot{I}_{PC}$ [MW]	$\sum W_{net,PC}$ [MW]	$\varepsilon_x$	$w_{net,PC}$ [kWh/kg <sub>H2</sub> ]
$i0$	15,70	15,60	0,346	2.504
$i1$	19,81	19,90	0,276	3.188
$i9$	13,74	13,77	0,397	2,21
$i10$	13,85	13,90	0,393	2,23
$i11$	11,96	12,01	0,456	1,928
$i12$	17,71	17,80	0,309	2,85

**Table 5.13:** Main resulting exergy parameters in the Case Study II process

With emphasis on the poor temperature match which has been proven to generate a great amount of losses, iteration case  $i1$  will be subject for improvement. Case  $i9$  and  $i11$  will also be investigated, due to the already high performance, with both minimal losses and high exergy efficiency. In order for  $i11$  to be realized, the temperature gap has to be adjusted to satisfy the  $\Delta T_{min}$  criteria.

### 5.2.3.1 Elaboration of exergy destruction and improvement proposals of system $i1$ , $i9$ and $i11$

The exergy destruction within the main heat exchanger in  $i1$  represents almost the half of the overall irreversibility's in the system, and compared to  $i9$  and  $i11$ , the percentage also exceeds the fraction of compressor losses significantly. The improvement potential is in other words quite extensive.



Component	( $i1$ )		( $i9$ )		( $i11$ )	
	$\dot{i}$ [kW]	[%]	$\dot{i}$ [kW]	[%]	$\dot{i}$ [kW]	[%]
Main heat exchanger	6083,47	42,44	2515,42	30,46	1743,84	26,87
MR compressors	3963,52	27,65	2670,56	32,34	2304,78	35,52
MR aftercoolers	1293,03	9,02	745,80	9,03	525,43	8,10
Throttle valve	1397,64	9,75	812,10	9,83	469,98	7,24
Ortho-para conversion	264,60	1,85	264,60	3,20	264,60	4,08
Separator+Mixer	-0,07	0,00	0,01	0,00	0,00	0,00
Chillers	1332,12	9,29	1249,89	15,13	1180,19	18,19
Net	14334,31	100	8258,38	100,00	6488,82	100,00

**Table 5.14:** Exergy destruction of the original process design;  $i1$ ,  $i9$  and  $i11$

It can also be seen that separators and mixer irreversibility's are more or less equal to zero, when the three cases analysed does not involve any liquid handling in the compressor system. The chiller system losses are more or less constant for each iteration, still considerably high. Further improvements are recommended for a future study using this particular approach, but is out of scope in this thesis work. Similar as in Case Study I, the throttling losses can be reduced by expander integration, which will be elaborated in the upcoming subsection.

**Expanders with equal pressure ratio** Without any pressure adjustment, the losses within heat exchanger in every iteration are as expected increased, due to the increased temperature drop as explained in the Case Study I section. Anyhow, the expansion exergy losses are reduced with 75,0, 74,9 and 75,9 % for case  $i1$ ,  $i9$  and  $i11$  respectively, which is remarkable. An important feature of lowering the cold composite curve, is that the performance of the heat exchanger will change, especially important is the  $UA$  parameter. For  $i1$ ,  $UA$  is calculated to 3,38 MW/°C which is 9,5 % lower than the original design. In practice, a lower  $UA$  means a smaller heat exchanger. For  $i9$  and  $i11$ ,  $UA$  are also reduced by 18,5 and 25,6 %.

Component (LP=4)	<i>i1a</i>		<i>i9a</i>		<i>i11a</i>	
	$\dot{I}$ [kW]	%	$\dot{I}$ [kW]	%	$\dot{I}$ [kW]	%
Main heat exchanger	6606,45	47,88	2826,45	35,82	1925,32	30,50
MR compressors	3957,71	28,68	2667,74	33,80	2303,50	36,49
MR aftercoolers	1284,22	9,31	739,30	9,37	521,76	8,26
Expander	352,25	<b>2,55</b>	204,14	<b>2,59</b>	117,63	<b>1,86</b>
Ortho-para conversion	264,60	1,92	204,14	2,59	264,60	4,19
Separator+Mixer	-0,07	0,00	0,01	0,00	0,01	0,00
Chillers	1332,12	9,65	1249,89	15,84	1180,19	18,69
Net	13797,28	100,00	7891,67	100,00	6313,00	100,00

**Table 5.15:** Exergy destruction with integrated expander, operating at equal pressure ratio

With the current modified process design,  $\Delta T_{min}$  for each solution increased from 8,36 to 10,05 for *i1*, 1,9 to 2,9 for *i9* and from 0,48 to 1,17 for *i11*. For the first iteration solution, it is preferable to reduce the temperature drop of the cold stream in order to improve the match of the composite curves, hence a lower pressure ratio is required.

Similar approach with *i9*, but in the last case solution, the temperature drop must be further increased, to increase  $\Delta T_{min}$  to above the 2 K criteria, see next section.

**Integrated expanders with  $\Delta T_{min}$ -adjusted pressure ratio** The low pressure of *i1* is increased to 8 bar, which gives a reduction in heat exchanger losses of 65,7%. The  $\Delta T_{min}$  criteria is also satisfied, with a value of 2,06. Due to the heavy component composition in *i1*, a minor fraction of the heat exchanger outlet stream enters the compression system as liquid, which results in a portion of exergy destruction related to the pump. The results for system *i1* is concluded as more than satisfying compared to the starting point in the original design, with an exergy efficiency that calculates to 41,05 %, which in comparison is nearly 1,5 times better. Still, a drawback of the efficiency improvement is the increased  $UA$  value of 68,8 % compared to case *i1 - a*, and 65,8 % increase compared to the original design. In practice this may result in a scenario with unrealistic sizing dimensions.

Component	$i1 - b$		$i9 - b$		$i11 - b$	
	$\dot{I}$ [kW]	[%]	$\dot{I}$ [kW]	[%]	$\dot{I}$ [kW]	[%]
Main heat exchanger	<b>2267,61</b>	28,61	2460,13	33,00	2368,33	34,24
MR compressors	2518,18	31,77	2554,74	34,27	2438,13	35,25
MR aftercoolers	1436,46	18,12	734,09	9,85	537,68	7,77
Expander	197,88	2,50	192,15	2,58	127,61	1,85
Ortho-para conversion	264,60	3,34	264,60	3,55	264,60	3,83
Separator+Mixer	49,74	0,63	0,01	0,00	0,00	0,00
Pump	4,66	0,06	-	-	-	-
Chillers	1186,37	14,97	1249,89	16,76	1180,19	17,06
Net	7925,49	100,00	7455,61	100,00	6916,54	100,00

**Table 5.16:** Exergy destruction with integrated expander, operating at  $\Delta T_{min}$ -adjusted pressure ratio

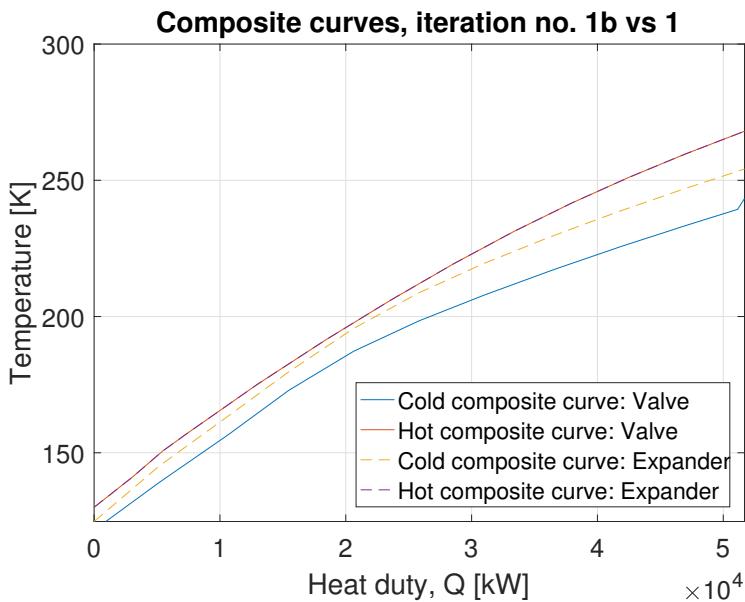
For  $i9 - b$  and  $i11 - b$  the exergy efficiency of the final pressure controlled  $\Delta T_{min}$ -adjustment calculates to 42,5 and 44,4 % respectively. Low pressure in  $i9 - b$  is increased to 4,32 bar, with a  $\Delta T_{min}=2,01$  K.  $i11 - b$  is lowered to 3,65 bar, giving a  $\Delta T_{min}=2,13$  K. For case  $i9 - b$  it is an improvement in exergy efficiency of 6,5% compared to the original design, while in case  $i11$ , it is a reduction of -2,7% compared to original design. With emphasis on heat transfer,  $UA$  calculates to 7,43 and 7,66 MW/°C for  $i9 - b$  and  $i11 - b$  respectively. For  $i9 - b$  this is a decrease of 1,4% relative to the original design, but an increase of 18,55 % compared to  $i9 - a$ . For  $i11 - b$  the difference calculates to 42,8 % decrease relative to  $i11 - a$  and almost 92 % decrease relative to the original design.

For Case Study II, system  $i11 - b$  has the overall best performance, with an exergy efficiency of above 44 %, realistic heat exchanger performance parameters and a total specific precooling work of 1,893 kWh/kg $_{H_2}$ . By increasing the isentropic efficiency of both the compressors ( $\eta_c$ ) and the expander ( $\eta_e$ ) from 75 to 85 %, the exergetic efficiency can further be increased to 49,41% with a corresponding specific power consumption of 1,787 kWh/kg $_{H_2}$ . With such a high isentropic efficiency means an overall reduction in power consumption of 7,50%, which is the main parameter for increased exergy efficiency in this case.

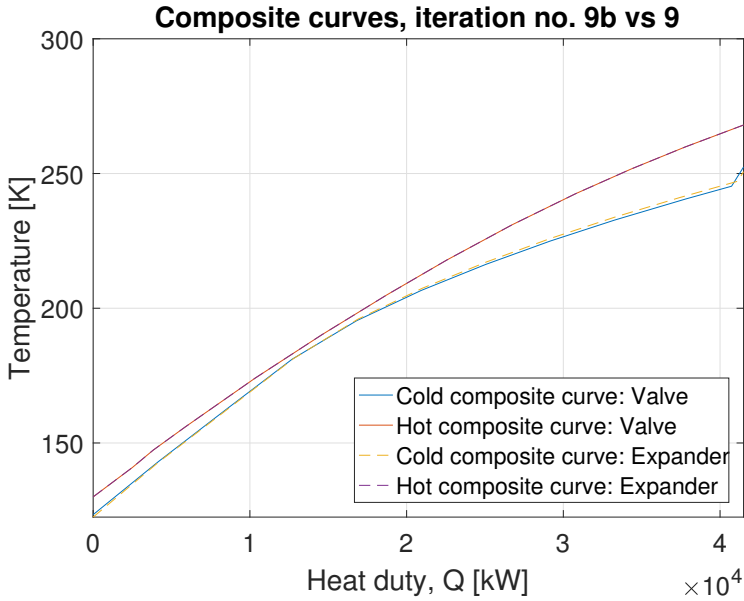
	Exergy efficiency [%]	$\delta_k$ [%]	$w_{PC}$ [kWh/kg]
Case $i1 - b$	41,05	+34,2	2,151
Case $i9 - b$	42,5	+6,5	2,076
Case $i11 - b$	44,4	-2,7	1,893
Case $i11 - b'$	49,41	+8,35	1,787

**Table 5.17:** Final exergy efficiency and power requirement of Case Study II, PRICO SMR precooling

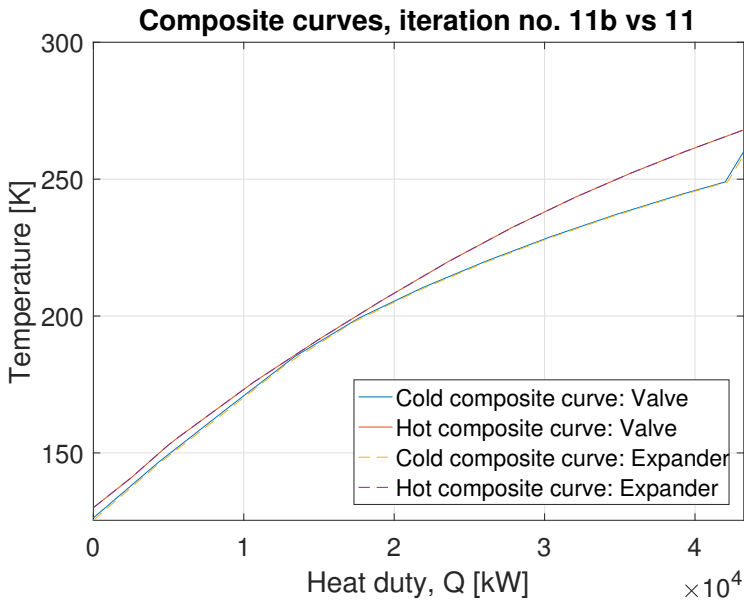
Figure 5.9 illustrates the improved heat exchanger performance initiated by the liquid expanders for the pressure ratio-adjusted approach, which as mentioned resulted in the best improvement.



(a) Composite curves comparison for case  $i1$  and  $i1 - b$ , showing that the low-pressure-adjusted expander design reduces the temperature gap between the curves significantly



(b) Composite curves comparison for case  $i9$  and  $i9 - b$ . A minor part of the cold composite is lifted at the upper temperature region



(c) Composite curves comparison for case  $i11$  and  $i11 - b$ . At 175-200 K the expander modification "opens" the tight space between the hot and cold composite, such that the  $\Delta T_{min}$  criteria is satisfied

**Figure 5.9:** Comparison of composite curves with throttling valves and isentropic expanders

## 5.3 Case 3: CMR precooling

The main argument for designing a cascade process cycle for hydrogen precooling, is to reduce the heat transfer duty and hence, the exergy destruction, by specification of a more rigid temperature interval, such as for Case Study III.

The level of complexity in design and dimensioning, are increased considerably, due to the fact that two individual cycles are both to be matched with the hydrogen and helium streams within the heat exchangers, but also with each other due to a required heat duty overlap. Because of the rigid temperature interval for each MR cycle, it was initially decided that the MR fluid in the upper temperature interval,  $a^4$  ( $210 \leq T \leq 300\text{K}$ ), should contain a major fraction of heavy components, while the MR fluid in the lower temperature interval,  $b^5$  ( $30 \leq T \leq 210 \text{ K}$ ), should contain a major fraction of light components.

Below, the overall procedure of adjustment of MR compositions are elaborated, with the summary of each iteration displayed in Table 5.18.

### 5.3.1 Mixed Refrigerant Optimization Procedure

Investigation of the composite curves for each iteration in Figure 5.10, shows that the temperature gaps in the upper end of the temperature interval are considerably more narrowed, than in the SMR PRICO case, as well as the PRICO chiller case. Before further study, some results from the iterative ( $i$ ) search for optimal solutions can be neglected;  $i3$  to  $i6$  shows the most smooth temperature match of each composite curve at the transition from HX-1 to HX-2. Still, a major fraction of the MR components evaporate at a temperature level, basically controlled by the HP level, and are too high to meet the  $\Delta T_{min}$  criteria, which gives the temperature cross with the hot composite curve. As indicated in Table 5.18, a pressure below 20 bar, with a majority of ethane in the mixture, is too low to match the hot curve. In addition, note that the net heat transfer duty (indicated inside each composite curve plot in Figure 5.10) are much higher, than for both  $i1$  to  $i2$  and  $i7$  to  $i9$ . This particular phenomena can be explained by studying the difference in liquid yield of the streams leaving the cold outlet of the heat exchanger ( $x_{1a}, x_{6b}$ ). The common thread of the "low-duty" solution proposals are the greater portion of two-phase heat transfer in the heat exchanger, especially in case  $i1$  with a net duty less than 50 MW.

---

<sup>4</sup>The PFD in Figure 3.4 indicates the prefix of MR cycle  $a$

<sup>5</sup>The PFD in Figure 3.5 indicates the prefix of MR cycle  $b$

MR cycle $a$	$i$								
	1	2	3	4	5	6	7	8	9 <sup>a</sup>
Nitrogen [mole-%]	0,00	0,00	0,00	0,00	0,00	0,00	0,00	0,00	0,00
Methane [mole-%]	0,10	0,10	0,10	0,10	0,10	0,10	0,10	0,14	0,09
Ethane [mole-%]	0,40	0,40	0,40	0,40	0,40	0,40	0,40	0,33	0,48
Propane [mole-%]	0,24	0,24	0,24	0,24	0,24	0,24	0,24	0,29	0,27
Buthane [mole-%]	0,27	0,27	0,27	0,27	0,27	0,27	0,27	0,24	0,16
$p_{2a}$ [bar]	34	34	34	16	16	16	22	29	21
Mass flow [kg/s]	40	40	30	35	32	30	30	30	35
MR cycle $b$									
Nitrogen [mole-%]	0,14	0,20	0,20	0,20	0,16	0,12	0,12	0,12	0,17
Methane [mole-%]	0,37	0,41	0,41	0,41	0,49	0,50	0,50	0,50	0,48
Ethane [mole-%]	0,31	0,34	0,34	0,34	0,33	0,33	0,33	0,33	0,31
Propane [mole-%]	0,18	0,05	0,05	0,05	0,03	0,05	0,05	0,05	0,04
Buthane [mole-%]	0,00	0,00	0,00	0,00	0,00	0,00	0,00	0,00	0,00
$p_{2b}$ [bar]	25	25	22	22	22	18	18	18	21
Mass flow [kg/s]	40	40	30	35	32	30	30	30	35

<sup>a</sup>: Low pressure,  $p_{1a/b}=4$  in iteration 1-8. For iteration 9,  $p_{1b}=7,5$  bar, and  $p_{1a}=3.5$  bar, due to modification of  $dT$  in throttle valve. The approach will be further explained later in this section

**Table 5.18:** Summary of the final result of the MR optimization procedure

	1	2	3	4	5	6	7	8	9
$x_{1a}$ [-]	0,09	0,05	0,08	0,00	0,00	0,00	0,00	0,07	0,00
$x_{6b}$ [-]	0,24	0,09	0,01	0,05	0,00	0,01	0,00	0,00	0,10
$T_{1a}$ [K] <sup>a</sup>	267,29	268,63	267,54	334,15	330,00	334,20	296,00	203,46	298,20
$T_{6b}$ [K] <sup>b</sup>	206,48	198,68	206,82	203,02	207,60	206,40	207,95	207,95	206,70
$T_{2a}$ [K] <sup>c</sup>	300,20	300,20	300,20	300,00	300,00	300,00	300,00	300,00	300,00
$T_{2b}$ [K] <sup>d</sup>	256,40	262,40	293,70	279,10	300,00	300,00	299,80	299,81	265,99

**a:** Suction temperature, cycle  $a$

**b:** Suction temperature, cycle  $b$

**c:** Discharge temperature after mixing point, cycle  $a$

**d:** Discharge temperature after mixing point, cycle  $b$

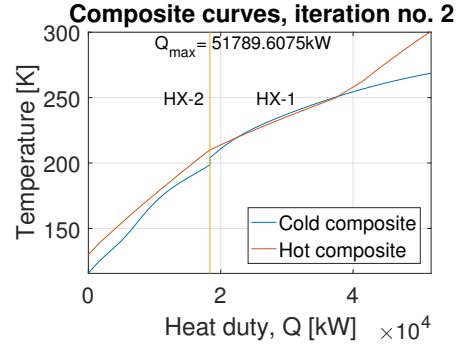
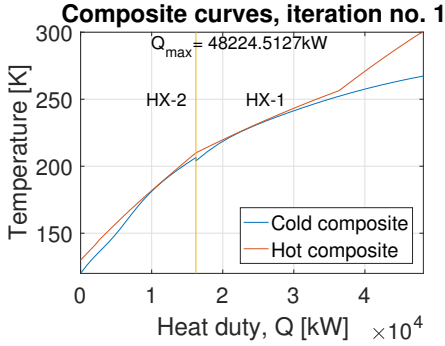
**Table 5.19:** Compressor- suction and discharge parameters of MR cycle  $a$  and  $b$

As discussed in Case Study II, the liquid fraction of the cold return stream was a serious issue to solve when the temperature level was lowered. In this Case Study, the cascade model generates an even lower temperature of the cold return stream in MR cycle  $b$  ( $198,7 \leq T \leq 207,9$  K). To consider whether to use a

separator/pump system integrated in the compressor train or not, depends on the rate of liquid in this particular return stream. In case *i1* and *i* – 09, which are designated as the two systems with best basis for improvements, the fraction are 24% and 10% respectively.

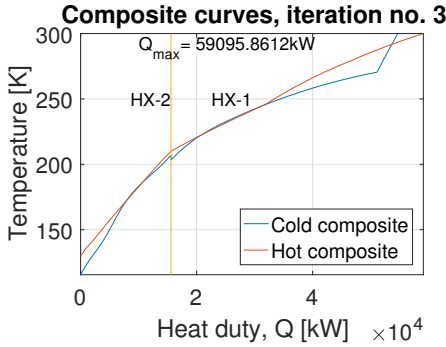
It can be seen from Table 5.18, that the MR cycle *a* composition of *i1* and *i9* are quite similar, while a greater portion of lighter components are added to MR cycle *b* in case *i9*. In theory, the liquid fraction in *i9* could be reduced even further by adding more methane and nitrogen to the mixture. This experiment was tested, and resulted in a temperature gap in HX-2, which gave considerably larger losses compared to the current design.



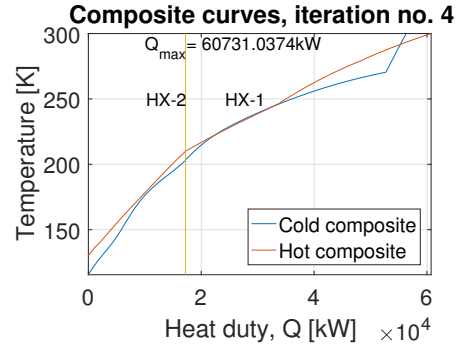


(a) Iteration no. 1;  $\Delta T_{\min, HX1} = 0,29$ ,  $\Delta T_{\min, HX2} = 0,26$

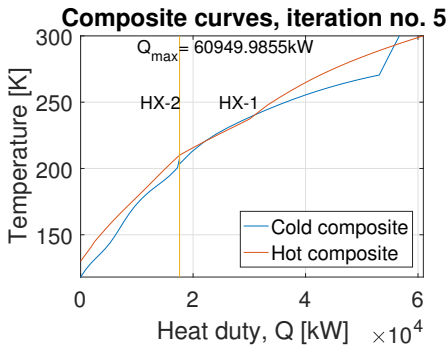
(b) Iteration no. 2;  $\Delta T_{\min, HX1} = -1,94$ ,  $\Delta T_{\min, HX2} = 5,70$



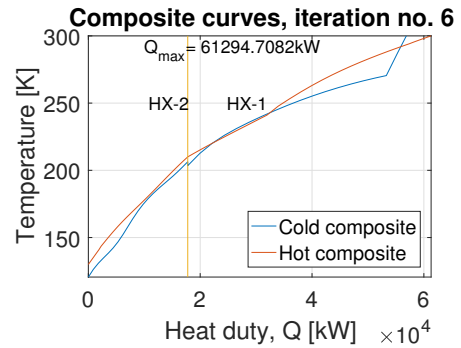
(c) Iteration no. 3;  $\Delta T_{\min, HX1} = 0,13$ ,  $\Delta T_{\min, HX2} = -0,71$



(d) Iteration no. 4;  $\Delta T_{\min, HX1} = -34,15$ ,  $\Delta T_{\min, HX2} = 1,96$



(e) Iteration no. 5;  $\Delta T_{\min, HX1} = -32,98$ ,  $\Delta T_{\min, HX2} = 2,41$



(f) Iteration no. 6;  $\Delta T_{\min, HX1} = -34,22$ ,  $\Delta T_{\min, HX2} = 1,66$

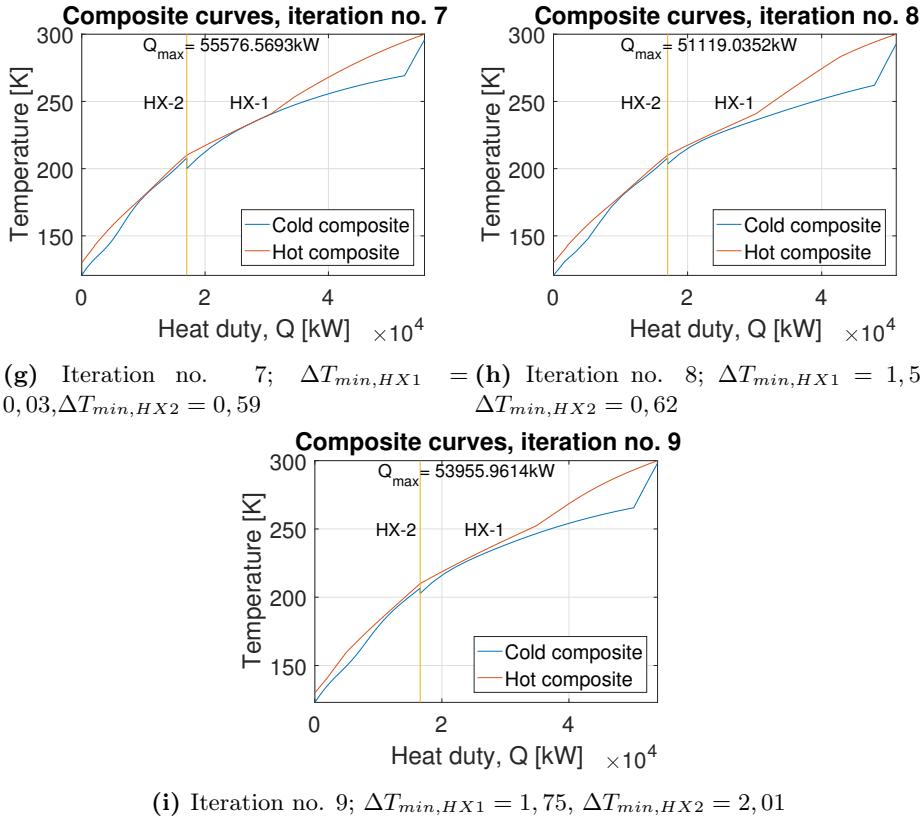


**Figure 5.10:** Optimization of temperature match in MR cycle, Case Study III

### 5.3.2 Key Performance Parameters of process components

Based on the discussions above, it can be concluded that design *i1*, *i8* and *i9* will be further analyzed, with emphasis on KPI's in process components relevant for analyzing the exergy destruction within the process.

Data from Table 5.20 shows that  $\Delta T_{min}$  for the current design in *i1* and *i8* are too small. One method of providing more cooling to the heat exchanger may be to split a minor part of the MR *b* stream before entering HX-2, throttling and create a new cold inlet to HX-1, before mixing the splitted stream with the second returning from the HX-2 outlet. This approach will be discussed and compared with throttle valve replacement with a turbo expander, as in Case Study I and

II.

$i$	1	8	9
<b>HX-1</b>			
WLMTD [K]	1,52	5,15	4,78
Duty, $Q$ [MW]	31,997	33,951	37,370
$\Delta T_{min}$ [K]	0,29	1,55	1,75
UA [MW/°C]	21,068	6,590	7,824
<b>HX-2</b>			
WLMTD	1,50	2,35	4,09
Duty, $Q$ [MW]	16,225	17,023	16,585
$\Delta T_{min}$	0,26	0,62	2,01
UA [MW/°C]	10,811	7,247	4,056
$Q_{net}$ [MW]	48,220	50,970	53,950

**Table 5.20:** Key Performance Indicators of HX-1 and HX-2, Case Study III

System  $i9$  on the other hand, shows an acceptable temperature approach in each heat exchanger. This because the low pressure value at the throttle valve outlet is modified to meet the desired  $\Delta T_{min}$  criteria.

Notice that the after-cooler duty of MR cycle  $b$  is much smaller than cycle  $a$ . Mostly because the mass flow rate is smaller, but recall the explanation of the low suction temperatures in each iteration for cycle  $b$ . Because of this effect, the discharge temperature of the first compressor is below 300 K, hence the first after-cooler can be fully neglected, since the compression process is assumed isothermal at 300 K. The average discharge temperature is much lower than for cycle  $a$ , hence an overall lower duty is accomplished.

Compressor power- and after-cooler duty requirement of the three cases are displayed in Table 5.21, while the power distribution of the compressors and pumps are displayed more in detail in Figure 5.11.

$i$	1	8	9
MR compressor power , $a$ [MW]	10,00	10,10	9,566
MR compressor power , $b$ [MW]	5,721	5,058	5,345
Pump power, cycle $b$ [kW]	64,50	0,064	31,80
After-cooler duty , $a$ [MW]	25,743	26,410	25,647
After-cooler duty , $b$ [MW]	2,180	0,817	1,367
Pressure ratio, $a$ [-]	5,90	5,40	4,96
Pressure ratio, $b$ [-]	5,00	4,24	4,64
Net compressor power [MW]	15,728	15,155	14,911
Net after-cooler duty [MW]	27,922	26,410	27,015

**Table 5.21:** Key Performance Indicators of compressors in MR cycle  $a$  and  $b$

### 5.3.3 Analysis of exergy losses and efficiency

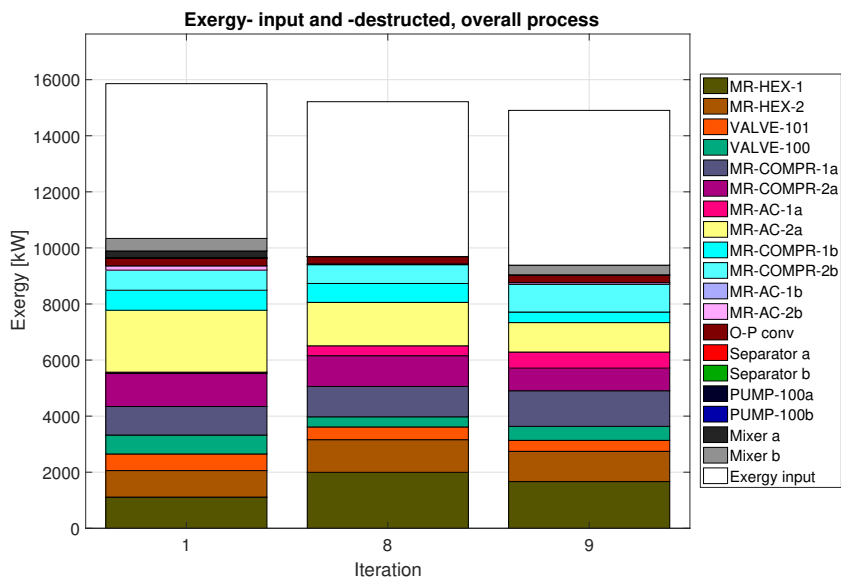


**Figure 5.12:** Exergy input plus exergy destruction within the process of the three best solution proposals in Case Study III

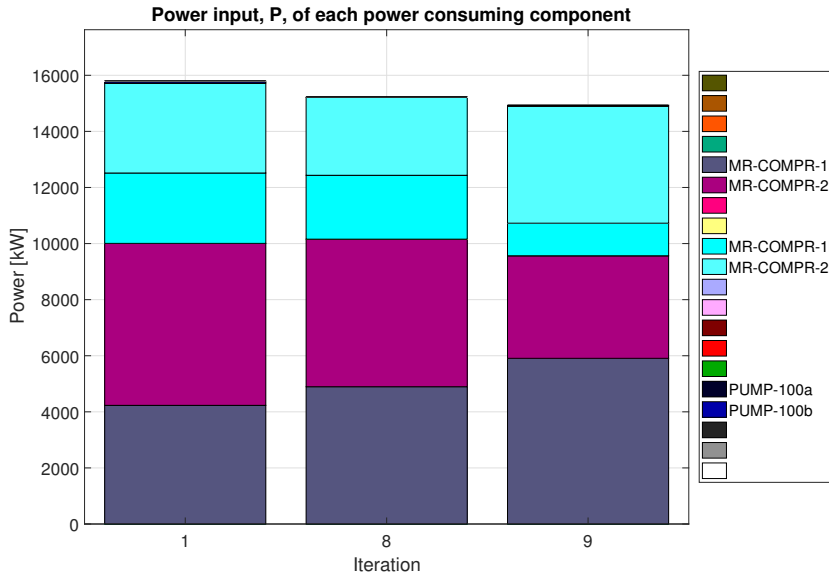


**Figure 5.11:** Net power consumption within the process of the three best solution proposals in Case Study III

Unlike in the previous case studies, Figure 5.12 shows that the total distribution of irreversibilities are more uniform, neglecting the white bars at top (which represents the exergy difference of the feed and product streams, hence the minimum required work of precooling,  $W_{min}$ ), for the three iterations. The two exceptions are the after-cooler losses in MR cycle *a* (MR-AC-2a) in *i1* and the heat exchanger losses in *i8*, which both are much higher than the "average". A quick look back at Table 5.18 and 5.19, shows for that for *i1*, the pressure ratio is much higher than for *i8* and *i9*. In addition, a greater fraction of heavy components are present in the MR-*a* mixture. Obviously the former generates a higher discharge temperature, as can be proved by basic cycle analysis with emphasis on different isentropic efficiency of compressors. The effects of increasing compressor efficiency will be discussed later in this section.

It is also noticeable that the two throttling losses has potential for improvement by replacement with expander units, as done previously, as they represent 11,4, 7,7 and 8,8 % for *i1*, *i8* and *i9* respectively, of the total exergy destruction within the process.

$i$	$\sum \Delta \dot{E}_{boundary} + \sum \dot{I}_{PC}$ [MW]	$\sum W_{net,PC}$ [MW]	$\varepsilon_x$ [%]	$w_{net,PC}$ [kWh/kg <sub>H2</sub> ]
1	15,858	15,728	35,098	2,517
8	15,214	15,214	33,801	2,435
9	14,905	14,943	36,940	2,325

**Table 5.22:** Main resulting exergy parameters in the Case Study III process

Even if the exergy efficiency's of the three basis solutions are rather high compared to the efficiencies of the basis solutions in Case Study I (without chillers), it is still preferable to increase the exergetic efficiency to above 40%, if possible. Therefore, the next subsection will go through possible modifications and also manipulations to the process design, and report on the improvement factor, which are the exergy efficiency and specific precooling work.

### 5.3.3.1 Elaboration of exergy destruction and improvement proposals of system $i1$ , $i8$ and $i9$

Table 5.23 represents the comparison benchmark for the improvement procedure, with respect to every irreversibility generated in each process components. Both heat exchanger performance and compressor work are absolute for case  $i1$ ,  $i8$  and  $i9$ , and are already tabulated in the previous section.

	(i1)		(i8)		(i9)	
	$\dot{I}$ [kW]	%	$\dot{I}$ [kW]	[%]	$\dot{I}$ [kW]	[%]
Heat exchangers	2058,43	18,54	3160,86	30,02	2744,28	27,19
MR compressors, a	2194,32	19,77	2179,82	20,71	2078,03	20,59
MR compressors, b	2194,32	19,77	2179,82	20,71	2078,03	20,59
After-coolers, a	2256,38	20,33	1901,53	18,06	1624,80	16,10
After-coolers, b	151,91	1,37	23,35	0,22	56,91	0,56
Throttle valves	1266,73	11,41	815,14	7,74	889,67	8,81
Ortho-para conversion	264,60	2,38	264,60	2,51	264,60	2,62
Separators	6,70	0,06	0,04	0,00	0,00	0,00
Mixers	679,60	6,12	2,46	0,02	342,80	3,40
Pumps	28,03	0,25	0,03	0,00	13,95	0,14
Net	11101,00	100,00	10527,64	100,00	10093,05	100,00

**Table 5.23:** Exergy destruction of the original process design;  $i1$ ,  $i8$  and  $i9$ , Case Study III

Notice the exergy destruction in the mixers are much higher in system  $i1$  and  $i9$ ; because of high liquid fractions in the cold return streams, a greater fraction of

the MR stream are guided through the pump, which generates a smaller temperature increase at discharge. Hence, the rate of exergy destruction increases with bigger temperature difference between the inlet streams to be mixed. For *i1*, this difference is 93.5 K for MR cycle *b* and 31 K for MR cycle *a*, thus 65,8 % of the mixer irreversibilities are caused by the mixer of MR cycle *b*. Referring to the difference in composition, displayed in Table 5.18, it is obvious that by modifying the MR composition in favour of lighter components, as in *i8* and *i9* results in a lower rate of exergy destruction in the mixers, due to lower temperature differences. As for the separators, the irreversibility are assumed zero, despite that 0,06% are calculated for *i1*.

Below, four different modifications proposals are discussed with emphasis on minimizing the exergy destructions further

**Integrated expanders with equal pressure ratio** Without any adjustment of the pressure ratio of the system, after replacing the throttle valves with turbo expanders, the reduced exergy destruction of system *i1*, *i8* and *i9* calculates to 15,2, 13,7 and 13,4 % <sup>6</sup> respectively. For each case, the greatest reduction of irreversibilities are in the expanders, as expected, simultaneously an increase for each case applies to the heat exchangers, due to a greater temperature drop at the expander outlet, compared to the original design. Summarized this approach results in an exergy efficiency of 36,74 , 36,57 and 37,22 % for *i1 – a*, *i8 – a* and *i9 – a*, with an improvement rate of 4,6, 8,2 and 0,8 % for each iteration respectively.

	<i>(i1a)</i>		<i>(i8a)</i>		<i>(i9a)</i>	
	Value	$\delta_k$ [%]	Value	$\delta_k$ . [%]	Value	$\delta_k$ [%]
$\dot{I}_{net}$ [kW]	9632,97	-15,2	9262,94	-13,7	8904,32	-13,4
$UA$ , (HX-1) [MW/°C]	10,63	-98,2	5,53	-19,1	6,66	-17,4
$\Delta T_{min}$ , (HX-1)	1,04	+75	2,08	+25,5	2,24	+21,9
$UA$ , (HX-2) [MW/°C]	5,06	-113,4	5,36	-35,3	3,40	-20,2
$\Delta T_{min}$ , (HX-2)	1,18	0,00	1,15	+46,1	2,62	+23,3

**Table 5.24:** Main results, expander integration with constant pressure ratio, Case Study III

For the compressors in cycle *b*, the expander design gives a minor increase in the liquid fraction on the cold return stream. This results in a reduction of the

<sup>6</sup>indicated by  $\delta_k$ , which represents the relative improvement ratio, compared to the original design

compressor irreversibilities of 35,3, 38,5 and 34,5 % for  $i1$ ,  $i8$  and  $i9$  respectively, due to a lower vapour mass flow of the suction stream.

By inspection of the results from Table 5.24, each performance parameter of the heat exchangers are changing correctly, in favour of more realistic values.  $UA$  for  $i1 - a$  are almost halved from the original design, due to a much better temperature match compared to the basis design. Still, the temperature approach,  $\Delta T_{min}$  are not satisfied according to the initial criteria. This also applies to  $i8 - a$  in HX-2, while  $i9 - a$  is satisfied, also with a reduced  $UA$  compared to the original design.

For  $i1 - a$  and  $i8 - a$ , the temperature approach must be satisfied, hence the pressure ratio of the expanders has to be adjusted, which is discussed in the section below.

**Integrated expanders with  $\Delta T_{min}$ -adjusted pressure ratio** The pressure adjustment results in, as displayed in Table 5.25, that the minimum temperature approach,  $\Delta T_{min}$  is satisfied for both  $i1 - b$  and  $i8 - b$ .  $UA$  for each iteration are hence lower in comparison with both the original case and the previous with constant pressure ratio. Especially for case  $i1 - b$ ,  $UA$  are reduced with over 200 % to a value more comparable with both case  $i8 - b$ , and also case  $i8 - a$  and  $i9 - a$ .

	(i1b)		(i8b)	
	Value	$\delta_k$ [%]	Value	$\delta_k$ [%]
$p_{1a}$	3,8		4	0,00
$p_{1b}$	3,75		3,75	
$\dot{I}_{net}$ [kW]	9970,82	-11,33	9262,94	-11,0
$UA$ , (HX-1) [MW/°C]	6,95	-202,95	5,54	-19,02
$\Delta T_{min}$ , (HX-1)	2,01	85,55	2,08	25,38
$UA$ , (HX-2) [MW/°C]	3,62	-198,77	3,71	-95,28
$\Delta T_{min}$ , (HX-2)	2,08	87,51	2,07	70,05

**Table 5.25:** Main results, expander integration with  $\Delta T_{min}$ -adjusted pressure ratio, Case Study III

The reduction in overall irreversibilities are some percent lower for this case, than the previous, mostly due to a bigger gap between the composite curves in  $i1 - b$ , to meet the  $\Delta T_{min}$  criteria, that gives higher heat exchanger losses.

The exception applies to a further adjustment of case  $i9 - a$  to a new low pressure



level from 7,5 to 7,75 bar (*i9b*) in the MR cycle *b*, to match the  $\Delta T_{min}$  more accurately. The saving potential calculates to a irreversibility reduction of 206,5 kW compared to *i9 - a*, which gives an exergy efficiency of 37,8 % which is the highest efficiency reported in Case Study III at this point.

**Reduction of after-cooler, compressor and expansion losses by increasing isentropic efficiency of rotary equipment** The isentropic efficiencies for rotary equipment, in this case compressors and turbo expanders, have throughout every baseline/original simulation been assumed  $\eta_c = \eta_e = 75\%$ . However, data from literature on similar conceptual studies has proven to obtain efficiencies for both components of 85%. Therefore, it may be convenient to explore these effects by applying a higher isentropic efficiency to the iteration case with best performance, which is *i9b* (for increased efficiency it will be named *i9b'*). The results are shown in Table 5.26

$\eta_c = \eta_e = 85\%$ ( <i>i9b'</i> )		
	Value	$\delta_{9b}$ [%] <sup>a</sup>
Net power consumption [MW]	10,94	-33,7
Net irreversibility [MW]	5471,42	-58,9
$UA$ , (HX-1) [MW/°C]	6,737	+1,14
$\Delta T_{min}$ , (HX-1) [K]	2,113	-6,01
$UA$ , (HX-2) [MW/°C]	3,481	-12,6
$\Delta T_{min}$ , (HX-2) [K]	2,211	+6,4
$\varepsilon_{i9b'}$	42,80	+11,7

*a*: Improvement factor compared to iteration case, *i9b*, with  $\Delta T_{min}$ -adjusted pressure ratio

**Table 5.26:** Net compressor power and irreversibility, for  $\eta_c = \eta_e = 85\%$ , Case Study III

By increasing motor isentropic efficiency, the exergy efficiency exceeds 40%, together with a remarkable reduction in exergy destruction within the MR process. Some deviation applies to  $UA$  and  $\Delta T_{min}$  for both heat exchangers, still within acceptable limits.

**Outlook on a manipulated process design proposal** In addition to the current design, another approach, which was outlined in the beginning of this section, may be to increase the number of degrees of freedom, by adding a stream splitter (probably in combination with a phase separator in a realistic scenario) in

between the two heat exchangers, to provide additional cooling to heat exchanger one. The intermediate cold stream of MR cycle *b* was chosen, in order to minimize the major temperature gap within HX-1. See Figure 5.13.

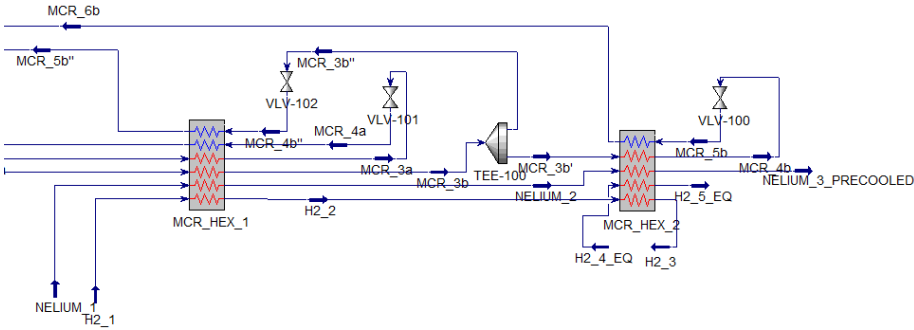


**Figure 5.13:** Draft of alternative process design to Case Study III

This approach was applied to the initial baseline design from iteration model *i8*. Because of the new design, a new composition, pressure and mass flow was needed. Due to lack of time available, further study on this model is not available in this thesis. Still, it was calculated that the net heat exchanger losses was lower than for the other iteration case design, and may therefore be a possible modification for a future work.

**Final performance review of Case Study III** The final performance summary of Case Study III is displayed in Table 5.27.

	Exergy efficiency [%]	$\delta_k$ [%] <sup>a</sup>	$w_{PC}$ [kWh/kg]
Case <i>i1</i> – <i>b</i>	35,5	+1,13	2,50
Case <i>i8</i> – <i>b</i>	36,0	+6,10	2,46
Case <i>i9</i> – <i>b</i>	37,8	-2,30	2,34
Case <i>i9</i> – <i>b'</i>	42,8	-13,7	1,75

*a*: Compared to original iteration case designs

**Table 5.27:** Final exergy efficiency and power requirement of Case Study III, Cascade Mixed Refrigerant (CMR) precooling

## 5.4 Case 4: CMR+ precooling

To further increase the exergy efficiency of the CMR process from Case Study III, propane chillers are implemented as a partial precooling process, in order to confine the heat duty interval of the composite curves. Similar as in Case Study II, the chillers are both connected to each stream crossing the system boundary and the internal MR cycles.

Because of the propane chiller units in the CMR+ process, two preliminary approaches need to be taken into account; Recall the case scenarios in the CMR models from Case Study II. The compressor train discharge temperature<sup>7</sup> of MR cycle *a* and *b* were in some cases many degrees below 300 K. In some cases, mostly in the coldest MR cycle, *b*, the discharge temperature was lower than of the chiller outlet target temperature, which in every case was assumed absolute at 268 K.

In the previous case study, only the heat exchanger temperature match between the hot inlet and cold outlet was affected by the discharge temperature decrease below 300 K. While in some iterations of the current case study, the propane chillers in MR cycle *b* may therefore be fully neglected, if the chiller inlet temperature is below 268 K. Hence, this will save both exergy destruction rates during the chiller process, but also the rate of exergy destruction within the after-coolers inside the compressor train.

Therefore, the iteration cases with a compressor outlet (discharge) temperature below the chiller target, will be prefixed with (*i* - (*num*)-\*).

### 5.4.1 Mixed Refrigerant optimization procedure

Search for a suitable mixture for the last case study was much easier than initially assumed, compared to the CMR process. At that point, the MR circuit was not fully closed in the simulation, which in every simulation resulted in a constant discharge temperature of 300 K.

As the separator-pump-mixer system is integrated into the process design, the mixtures from the "old" model are adapted into the current design, which represents iteration *i*1 and *i*12. Similar as in Case Study III, the refrigerant composition in MR cycle *a* contains a majority of heavier components, while a majority of lighter components are added to the refrigerant of MR cycle *b*.

---

<sup>7</sup>Also equal to the heat exchanger inlet temperature, and was initially assumed equal 300 K

MR cycle <i>a</i>	1 (1)	2 (12)	3	4	5	6	7	8	9	10	11
Nitrogen [mole-%]	0,000	0,000	0,000	0,000	0,000	0,000	0,000	0,000	0,000	0,000	0,000
Methane [mole-%]	0,098	0,085	0,085	0,085	0,085	0,085	0,085	0,085	0,085	0,085	0,085
Ethane [mole-%]	0,401	0,445	0,445	0,445	0,445	0,445	0,445	0,445	0,445	0,445	0,445
Propane [mole-%]	0,238	0,255	0,255	0,255	0,255	0,255	0,255	0,255	0,255	0,255	0,255
Buthane [mole-%]	0,263	0,215	0,215	0,215	0,215	0,215	0,215	0,215	0,215	0,215	0,215
$p_{2a}$	29	13	13	13	13	13	13	11	13	13	11
$\dot{m}_{mr-a}$	80	78	70	70	70	70	70	70	70	70	70
MR cycle <i>b</i>											
Nitrogen [mole-%]	0,13	0,08	0,11	0,08	0,08	0,20	0,20	0,21	0,15	0,15	0,15
Methane [mole-%]	0,39	0,34	0,49	0,41	0,41	0,38	0,38	0,40	0,45	0,45	0,44
Ethane [mole-%]	0,31	0,41	0,36	0,34	0,34	0,32	0,32	0,34	0,34	0,34	0,37
Propane [mole-%]	0,17	0,17	0,04	0,17	0,17	0,11	0,11	0,05	0,05	0,05	0,04
Buthane [mole-%]	0,00	0,00	0,00	0,00	0,00	0,00	0,00	0,00	0,00	0,00	0,00
$p_{2b}$	20	19	22	22	18	18	22	25	22	18	19
$\dot{m}_{mr-b}$	45	47	40	40	35	47	35	30	30	32	30

**Table 5.28:** Summary of the final result of the MR optimization procedure, Case Study IV

After one iteration step,  $i2$ , a suitable composition of MR cycle *a* is obtained, where steps 3-11 are minor modifications of the high pressure values. Due to an overall lower temperature intervall, generated by the chillers, a lower pressure level applies to MR cycle *a*. As a consequence, the fractions of methane are kept at a strict minimum to avoid overheating at the cold outlet, which causes temperature crosses. It can be seen in Figure 5.14, that the shape of the hot and cold composite curves in heat exchanger 1 (HX-1) are quite similar throughout the iterative optimization procedure. The gap in the upper temperature region confines, as the pressure is reduced, while the methane-content are lowered with approx. 1 mole-%

	1*	2*	3*	4*	5*	6*	7	8	9	10	11
$x_{1a}$	0,23	0,23	0,14	0,07	0,18	0,09	0,20	0,17	0,22	0,22	0,17
$x_{7b}$	0,23	0,34	0,32	0,27	0,24	0,14	0,05	0,03	0,08	0,00	0,01
$T_{1a}$ [K] <sup>a</sup>	261,01	257,00	261,10	264,00	259,30	263,20	258,40	259,90	257,40	257,50	260,00
$T_{7b}$ [K] <sup>b</sup>	205,95	203,60	196,10	205,20	209,50	203,83	203,30	205,50	205,40	206,70	204,87
$T_{3a}$ [K] <sup>c</sup>	301,14	292,70	297,10	299,90	295,20	299,50	294,30	291,00	293,10	293,30	291,10
$T_{3b}$ [K] <sup>d</sup>	251,28	246,50	264,00	252,40	262,60	249,20	280,20	289,00	287,40	291,90	296,00

**a:** Compressor suction temperature, cycle *a*

**b:** Compressor suction temperature, cycle *b*

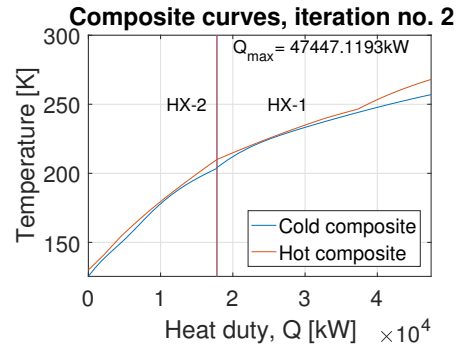
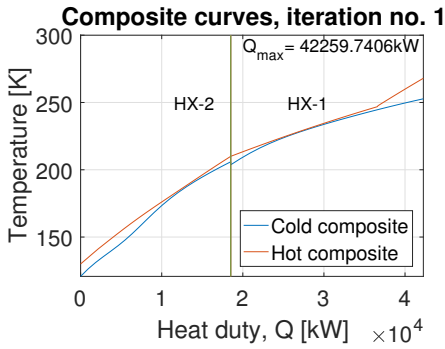
**c:** Discharge temperature after mixing point, cycle *a*

**d:** Discharge temperature after mixing point, cycle *b*

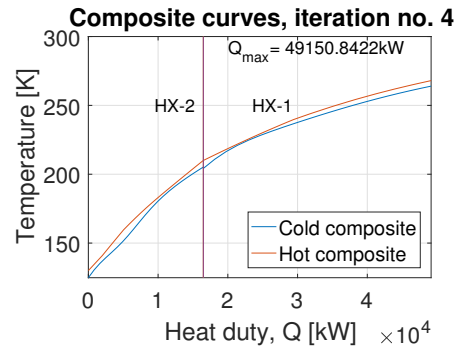
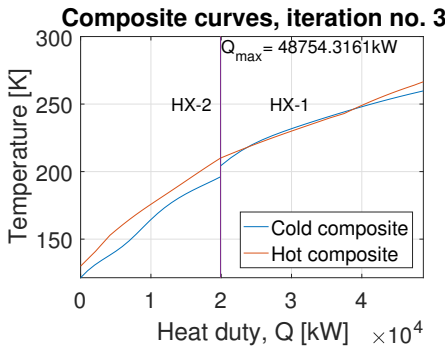
**Table 5.29:** Compressor- suction and discharge parameters of MR cycle *a* and *b*, Case Study IV

The majority of composition-, pressure- and mass flow adjustments are applied to

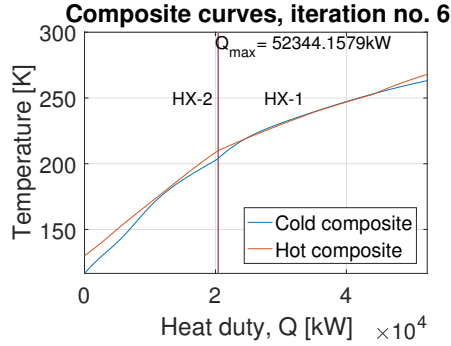
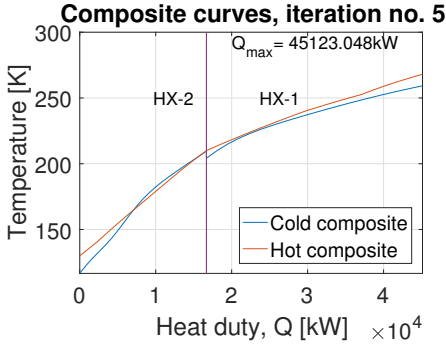
MR cycle  $b$ , because a greater fraction of liquids are present at the heat exchanger cold outlet, similar as in Case Study III. It can be seen in both Table 5.28 and 5.29, that from  $i1 - i6$ , a smaller fraction of nitrogen and methane causes much higher liquid fractions,  $x$ , in the cold return suction stream, with a majority in cycle  $b$  ( $x_{7b}$ ). As explained introductorily in this section, the chiller unit was assumed removed if the compressor discharge temperature ( $T_{3a}$ ,  $T_{3b}$ ) was below the chiller target temperature of 268 K. Since the former applies to MR cycle  $b$  in  $i1 - i6$ , the chillers in MR cycle  $b$  are neglected with emphasis on further analysis of power consumption and exergy- losses and efficiency. For simplicity reasons,  $i1 - i6$  are hereby named  $i1^* - i6^*$ .



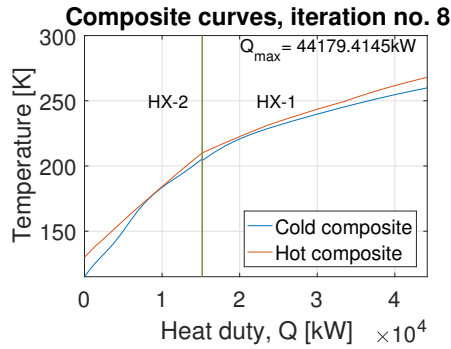
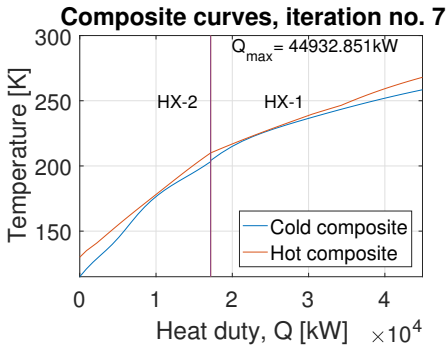
(a) Iteration no. 1;  $\Delta T_{min}(HX - 1) = 0,432K$ ,  $\Delta T_{min}(HX - 2) = 0,985K$  = (b) Iteration no. 2;  $\Delta T_{min}(HX - 1) = 0,664K$ ,  $\Delta T_{min}(HX - 2) = 1,342K$



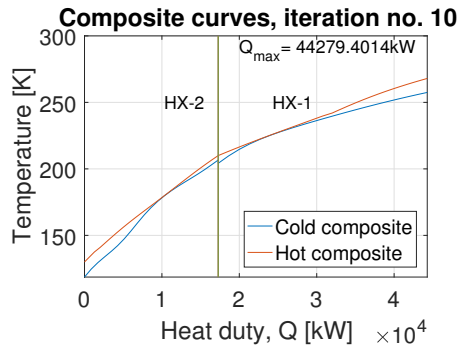
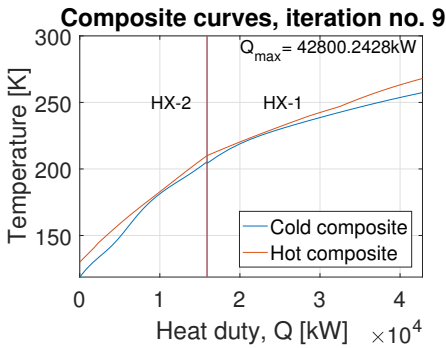
(c) Iteration no. 3;  $\Delta T_{min}(HX - 1) = -1,795K$ ,  $\Delta T_{min}(HX - 2) = 8,560K$  = (d) Iteration no. 4;  $\Delta T_{min}(HX - 1) = 0,820K$ ,  $\Delta T_{min}(HX - 2) = 2,006K$



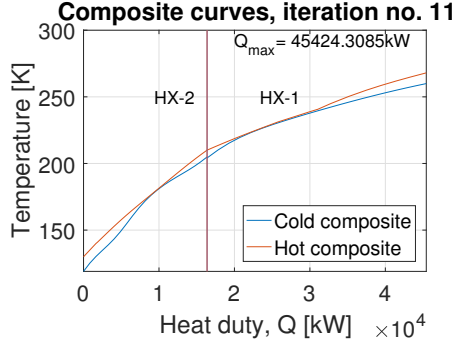
(e) Iteration no. 5;  $\Delta T_{min}(HX - 1) = 1,259K$ ,  $\Delta T_{min}(HX - 2) = -2,891K$  = (f) Iteration no. 6;  $\Delta T_{min}(HX - 1) = -1,133K$ ,  $\Delta T_{min}(HX - 2) = 1,361K$



(g) Iteration no. 7;  $\Delta T_{min}(HX - 1) = 0,515$ ,  $\Delta T_{min}(HX - 2) = -1,326$  = (h) Iteration no. 8;  $\Delta T_{min}(HX - 1) = 1,785$ ,  $\Delta T_{min}(HX - 2) = 0,278$



(i) Iteration no. 9;  $\Delta T_{min}(HX - 1) = 1,120$ ,  $\Delta T_{min}(HX - 2) = 1,553$  = (j) Iteration no. 10;  $\Delta T_{min}(HX - 1) = 0,106$ ,  $\Delta T_{min}(HX - 2) = 0,132$



(k) Iteration no. 11;  $\Delta T_{min}(HX - 1) = 0,294$ ,  $\Delta T_{min}(HX - 2) = 0,319$

**Figure 5.14:** Optimization of temperature match in MR cycle *a* and *b*, with composite curves as benchmark, Case Study IV

Closer investigation of the composite curves from *i1* – *i11* in Figure 5.14, reveals that some cases may be difficult to improve without further adjustment of the refrigerant mixture. E.g. in case *i3\**, *i6\** and *i7\** a temperature cross are present in HX-1, while in HX-2 for case *i5\**. It can be concluded that these cases are neglected for further study.

For the high-liquid cases indicated by \*, the temperature match and CC shape are better in both HX-2 and HX-1 compared to the low-liquid cases. The best iteration cases will in addition be selected with regard to both minimum heat transfer duty and most acceptable  $\Delta T_{min}$  approach. For the low-liquid cases *i7* – *i11*, *i9* is the most obvious candidate, satisfying both criteria, together with a satisfactory shape of hot and cold composite curve. For the high-liquid cases, iteration *i4\** generates a good temperature match (still too low  $\Delta T_{min}$  for HX-1), but with a high heat transfer duty. Together with *i1\** they will be compared to case *i9* and *i8*, in a further analysis with respect to both key performance indicators, exergy- losses and efficiency and improvement proposals.

## 5.4.2 Key Performance Parameters of process components

For every iteration, the minimum temperature approach is not satisfied according to the initial criteria of 2 K; hence, an improvement has to be initiated either with single pressure adjustment or a combination with expander integration, as discussed for the previous case studies. With respect to the heat transfer duty in each heat exchanger, this system has an overall reduced duty, compared to the

CMR without propane chiller, as initially expected.

Figure 5.15 shows the rate of change of the  $UA$  and duty,  $Q$  in the two heat exchangers for each iteration. The iteration cases where  $UA = 0$ , means that HYSYS is not able to calculate the value, due to the nonphysical phenomena of temperature cross within one or both heat exchangers. In theory this means that  $UA$  actually tends to infinity, relative to the other cases, as the temperature approach is to tight, or in this case, intersecting. The figure also indicates that with a higher heat transfer duty,  $UA$  decreases simultaneously. As  $UA$  is dependent on the WMTD value, this value also decreases with a greater fraction of heat transferred, as explained in Chapter 2.

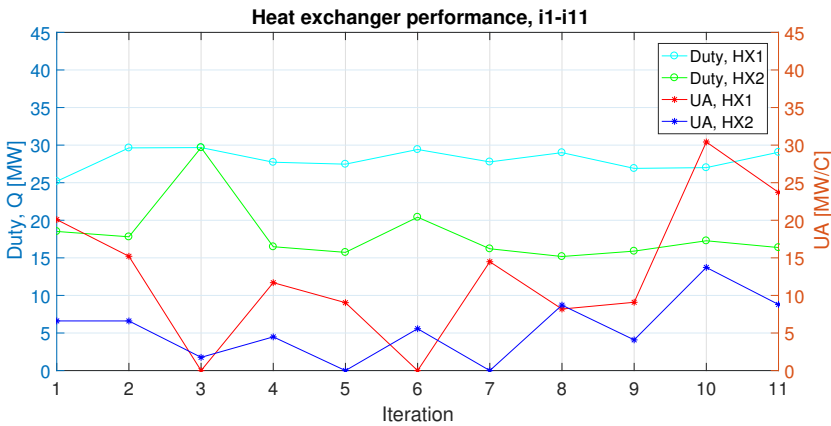


**Figure 5.15:** Heat transfer duty,  $Q$  and  $UA$  for each iteration solution, Case Study IV

Due to both high pressure and mass flow in  $i1^*$ , the compressor power consumption in MR cycle  $a$  is nearly 44 % higher than  $i4^*$ ,  $i8$  and  $i9$ . It was proven in the HYSYS case study setup in the SMR PRICO discussion, that the increase in power consumption are steeper as a function of mass flow rather than the high pressure. Therefore the mass flow of each MR cycle, especially  $a$ , was minimized as much as possible during the optimization procedure. Except from the power consumption in the compressors, the difference in after-cooler duty in MR cycle  $a$  between  $i1^*$  and the three other simulations are remarkable. The after-cooler works only as a tool to realize isothermal heat rejection in the compressors, hence the difference is temperature dependent. The discharge temperature after the second compressor<sup>8</sup> for  $i1^*$  is 370,3 K, while for the remaining simulations, the discharge temperature lies between  $314,4 \leq T_d \leq 322,9$  K. In comparison

<sup>8</sup>Due to cold compression in compressor one, no after-cooling are needed here



$i$	1*	4*	8	9
HX-1				
WMTD [K]	1,25	2,37	3,54	2,96
$\Delta T_{min}$ [K]	0,43	0,82	1,78	1,12
Duty, $Q$ [MW]	25,18	27,72	29,00	26,91
$UA$ [MW/C]	20,09	11,70	8,19	9,09
HX-2				
WMTD [K]	2,80	3,67	1,74	3,89
$\Delta T_{min}$ [K]	0,99	2,01	0,28	1,55
Duty, $Q$ [MW]	18,515	16,48	15,18	15,90
$UA$ [MW/C]	6,608	4,49	8,71	4,09

**Table 5.30:** Key Performance Indicators of HX-1 and HX-2, Case Study IV

this big temperature difference will generate considerable more amounts of irreversibilities, as will be discussed in the next section.

The compressor performance is given in Table 5.31, with an isentropic efficiency  $\eta_c = 75\%$ . Compared to the absolute minimum compressor work that was calculated in Case Study III, compressor power is reduced by 10,3%. Yet, a power consumption penalty of the propane chillers must be considered,

$i$	1*	4*	8	9
MR compressor power, $a$ [MW]	7,746	4,914	4,370	4,770
MR compressor power, $b$ [MW]	5,572	5,006	5,924	5,523
Pump power, cycle $a$ [kW]	207,60	38,52	25,25	42,39
Pump power, cycle $b$ [kW]	55,28	63,20	5,63	5,63
After-cooler duty, $a$ [MW]	12,40	2,341	1,520	2,19
After-cooler duty, $b$ [MW]	1,31	1,407	2,18	1,56
Net compressor power [MW]	13,32	9,920	9,664	10,29
Net after-cooler duty [MW]	20,46	5,120	3,70	3,75

**Table 5.31:** Key Performance Indicators of compressors in MR cycle  $a$  and  $b$ , Case Study IV

#### 5.4.2.1 Propane chillers in the lowest power consuming iteration case

The R290 chiller COP for each background process stream calculates to 7,232, with the pre-assumed condenser- and evaporator temperature level of 15 and -15 °C respectively.

Background stream	COP [-]	Cooling duty [kW]	Mass flow (R290)[kg/s]	Compressor power [kW]
Hydrogen	7,232	794,64	2,39	109,880
MR <i>a</i>	7,232	16100,1	48,41	2226,25
Nelium	7,232	1450,74	4,36	200,601

**Table 5.32:** R290 chiller performance in  $i4^*$ , Case Study IV

The deviation in COP between estimated<sup>9</sup> and HYSYS simulated parameters for the hydrogen- and nelium chiller are 7,3 % lower. As for the MR chiller system, the initial estimation was based on the current designated mass flow and temperature levels on an earlier simulation, which makes the comparison inconsistent. A total power penalty resulting in 2,54 MW is applied to system  $i4^*$ . Even if the difference in chiller inlet temperature (discharge) between  $i1^*$  and  $i4^*$  in MR cycle *a* is 1,24 K, it is not reasonable to assume that the requisite power for system  $i1^*$  is the same. For  $i1^*$ , the pressure is much higher, which gives an increased liquid fraction of nearly 70% compared to  $i4^*$ , thus the heat transfer is more efficient, which results in a required power of 1340 kW for the MR *a* stream.

Background stream	COP [-]	Cooling duty [kW]	Mass flow (R290) [kg/s]	Compressor work [kW]
MR <i>a</i>	7,232	15258,8	45,88	2109,92
MR <i>b</i>	7,232	1192,0	3,60	164,830

**Table 5.33:** R290 chiller performance in  $i8$ , Case Study IV

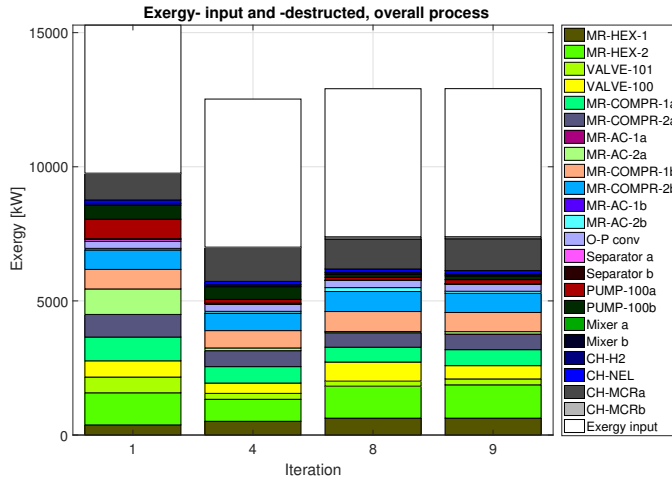
Notice that for  $i8$  and  $i9$  the discharge temperature are many degrees above 268 K. The power consumption calculated by HYSYS is 5,2 % lower for MR cycle *a* compared to  $i1^*$  and  $i4^*$ . An additional power requirement of 164,83 kW are required for the MR *b* chiller. In both cases, COP calculates to 7,23 with equal pressure level, condenser- and evaporator temperature. Due to different design parameters in system  $i8$  and  $i9$ , a deviation in power requirement of 5 and 9 kW for MR cycle *a* and *b* respectively, is calculated.

In summary, the chiller power penalty for system  $i1^*$  and  $i4^*$  are 1650,5 and 2536 kW respectively; while for system  $i8$  and  $i9$ , neglecting the minor deviations as mentioned, the chiller power penalty is therefore 2585 kW.

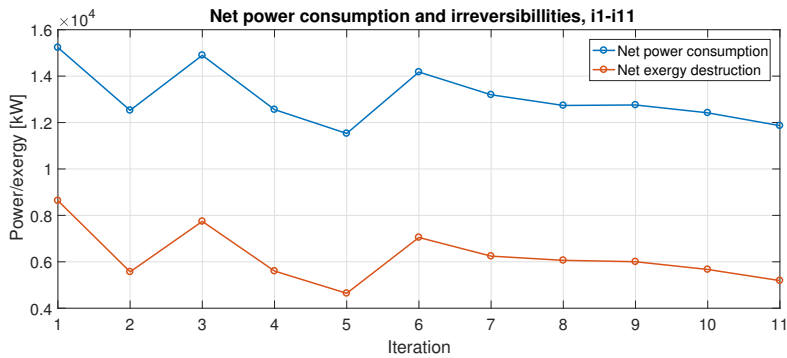
---

<sup>9</sup>CoolPack Refrigeration Utilities parameter

### 5.4.3 Analysis of exergy losses and efficiency



(a) Exergy input plus exergy destruction within the process of the four best iteration solutions in Case Study IV



(b) Net- power and exergy destruction for every iteration simulation of Case Study IV. It can be seen that the irreversibilities and power input are strongly correlated.

**Figure 5.16:** Net- power consumption and irreversibilities with its respective distribution component-wise

For Case Study IV, three out of four simulations calculates to an exergy efficiency above 40% with its original design structure.

$i$	$\sum \Delta \dot{E}_{boundary} + \sum \dot{I}_{PC}$ [MW]	$\sum W_{net,PC}$ [MW]	$\varepsilon_x$ [%]	$w_{net,PC}$ [kWh/kg <sub>H2</sub> ]
1*	15281,77	15281,08	36,12	2,45
4*	12524,14	12540,06	44,02	2,01
8	12909,55	12903,37	42,78	2,07
9	12912,54	12915,85	42,74	2,07

**Table 5.34:** Main results from best iteration solutions original design in Case Study IV

In addition to the pronounced difference in power requirement between  $i1^*$  against  $i4^*$ ,  $i8$  and  $i9$ , the exergy destruction rate tends to move in the same direction, as for the other iterations as well, as shown by Figure 5.16. Neglecting the white bars at the top of Figure 5.16a, each distribution of irreversibilities are shown for the four current iterations. Even if new components are added to system IV, compared to previous system III, the distribution of losses are in average much smaller. By further inspection, the chillers in MR cycle  $a$  represents a majority of the exergy destructed, due to a much greater flow rate, than for the other chiller systems. This parameter cannot be changed, because the internal propane refrigeration cycle is, in the exergy analysis perspective, a black box where a stream enter and leaves with a change of parameter, in this case the temperature, and the requisite power<sup>10</sup> penalty is applied to the overall balance.

Both Table 5.34 and Figure 5.16 shows that almost every key performance parameters of  $i8$  and  $i9$  are equal, with some minor deviations.  $i8$  has the greatest efficiency, simultaneously as the throttling losses of the valve in MR cycle  $b$  (VALVE-101) are a little higher. It can thus be concluded that there is no point to analyze each of the two iterations, with almost identical results, hence  $i8$  will be investigated together with  $i1^*$  and  $i4^*$ , to quantify the effects and results of expander integration.

#### 5.4.3.1 Elaboration of exergy destruction and improvement proposals of system $i1^*$ , $i4^*$ , and $i8$

The component-wise exergy loss displayed in Figure 5.16a are quantified in Table 5.35, proving that the greatest improvement potential is present for simulation  $i1^*$ , with almost 63% of the power consumption represents the exergy destructed in the system. For each iteration, the throttling losses are rather high, as well as for the mixer irreversibilities. For  $i1^*$ , the differences in both temperature and liquid fraction between the mixer streams are high; 44 K temperature difference between vapour/liquid and (44/35) kg/s vapour/liquid mass flow distribution for

<sup>10</sup>R290 compressor power

MR cycle  $a$ , while 93 K temperature difference and (30/14) kg/s vapour/liquid mass flow distribution for MR cycle  $b$ .

Component	$(i1^*)$		$(i4^*)$		$(i8)$	
	$\dot{I}$ [kW]	%	$\dot{I}$ [kW]	%	$\dot{I}$ [kW]	%
Heat exchangers	1574,20	16,58	1331,87	19,76	1821,87	25,57
Compressors, a	1728,59	18,20	1208,82	17,94	1094,01	15,35
Compressors, b	1457,47	15,35	1294,90	19,21	1490,39	20,92
Throttle valves	1192,54	12,56	605,39	8,98	899,04	12,62
AC a	950,07	10,00	99,65	1,48	44,88	0,63
AC b	55,16	0,58	69,70	1,03	145,73	2,05
Pumps, a	71,52	0,75	13,06	0,19	8,50	0,12
Pumps, b	24,09	0,25	27,68	0,41	2,46	0,03
Mixers	1249,36	13,16	616,97	9,15	222,99	3,13
Separators	0,00	0,00	0,00	0,00	0,00	0,00
Chillers	1194,01	12,57	1471,34	21,83	1394,90	19,58
Net	9497,01	100,00	6739,38	100,00	7124,79	100,00

**Table 5.35:** Distribution of irreversibilities in best iteration solutions, Case Study IV

To further increase the exergy efficiency, three proposals similar as in Case Study III are presented. A new process design scheme is not elaborated for this system, due to the already high performance compared to system III. It will in addition be interesting to reduce the high rate of exergy destruction for the compressor train, especially with emphasis on system  $i1^*$ . The different improvement proposals are presented below.

**Integrated expander with constant pressure ratio** Without any adjustment of the pressure ratio when replacing each throttle valve with expanders, the reduction of exergy destruction compared to the original design calculates to 4,92, 0,87 and 1,07 % for  $i1^*$ ,  $i4^*$  and  $i8$ , respectively (indicated by  $\delta_k$ , in Table 5.36). As expected, the expansion losses are reduced most significantly for the three cases; for  $i1^*$ , only 3,3% (instead of 12,5%) of the total. For  $i4^*$  and  $i8$ , 2,7% and 3,2%, instead of 9,0% and 12,6%, which is an acceptable improvement.

In iteration  $i1^*$  and  $i4^*$ , the throttle valve replacement result in a minor decrease of exergy destruction in both MR cycle compressors. The major reduction rate is applied in MR cycle  $a$ , where a greater portion of liquid ( $x_{1a}$ , Table 5.29) enters

the separator-pump-compressor system, which gives a lower vapour mass flow in the compressors.

For the main heat exchangers (HX-1 and HX-2), the rate of exergy destruction is as expected increased, due to a greater temperature drop over the expanders and to obtain the necessary  $\Delta T_{min}$  criteria. Yet, it can be seen in Table 5.36 that the criteria is not completely fulfilled for each iteration, with a temperature approach below 2 K. Simultaneously as the minimum temperature approach reaches an acceptable value, the  $UA$  parameter decreases rapidly towards a lower value, which means a reduction in the physical dimensions of the heat exchangers.

	$(i1^*a)$		$(i4^*a)$		$(i8a)$	
	Value	$\delta_k$ [%]	Value	$\delta_k$ [%]	Value	$\delta_k$ [%]
$\dot{I}_{net}$ [kW]	9029,33	-4,92	6680,34	-0,87	7048,27	-1,07
UA, (HX-1) [MW/C]	11,640	-53,8	9,970	-17,0	7,768	-5,40
$\Delta T_{min}$ (HX-1)	2,15		1,13		1,98	
UA, (HX-2) [MW/C]	4,712	-28,7	3,831	-17,0	3,608	-58,60
$\Delta T_{min}$ (HX-2)	1,72		2,52		1,55	

**Table 5.36:** Main results, expander integration with constant pressure ratio, Case Study IV

The overall exergy efficiency of the first improvement proposal calculates to 38,0, 45,3 and 43,9 % for  $i1^*$ ,  $i4^*$  and  $i8$  respectively, which represents an improvement rate of 5,2, 2,9 and 2,6 % compared to the original design. As the heat exchanger specifications are not yet fulfilled, the pressure adjustment will solve the  $\Delta T_{min}$  criteria; which is explained below.

**Integrated expander with  $\Delta T_{min}$ -adjusted pressure ratio** The pressure adjustment approach, similar as performed in the previous case studies, shows that the  $\Delta T_{min}$  of each iteration solution calculates to above 2 K. As explained in the previous section,  $UA$  changes in the correct direction when the temperature match becomes more realistic, which for every case (with the exception of (HX-2) in  $i4^*b$  compared to  $i4^*a$ ), is lower than both the original design, and the constant pressure ratio design.  $UA$  for  $i4^*b$  is higher than for  $i4^*a$  because the temperature approach is 2,52 K, and it is preferable to "lift" the cold composite curve closer to 2 K, to minimize the heat exchanger losses. The exergy destruction difference in HX-2 caused by this minor adjustment, resulted in a decrease of 87 kW.

In summary, pressure ratio adjustment results in a lower reduction of losses than the previous approach, but with more realistic heat exchanger parameters. Cal-

culated exergy efficiency of each iteration are 37,0% for  $i1*b$ , 45,0% for  $i4*b$  and 43,4% for  $i8b$ , which means an improvement compared to the original iteration cases.

	$(i1*b)$		$(i4*b)$		$(i8b)$	
	Value	$\delta_k$ [%]	Value	$\delta_k$ [%]	Value	$\delta_k$ [%]
$p_{1a}$ [bar]	3,8	-5,0	3,82	-4,7	3,98	-0,5
$p_{1b}$ [bar]	3,9	-2,5	4,15	+3,6	3,85	-3,9
$\dot{I}_{net}$ [kW]	9393,53	-1,08	6760,16	+0,31	7160,75	+0,50
$UA$ (HX-1) [MW/C]	7346,41	-63,4	6923,48	-40,8	7530,50	-8,05
$\Delta T_{min}$ (HX-1)	2,04		2,02		2,07	
$UA$ (HX-2) [MW/C]	4191,89	-36,5	4357,02	-2,96	3025,13	-65,2
$\Delta T_{min}$ (HX-2)	2,08		2,05		2,09	

**Table 5.37:** Main results, expander integration with  $\Delta T_{min}$ -adjusted pressure ratio, Case Study IV

**Further reduction of losses by increasing isentropic efficiency of rotary equipment** With iteration  $i4*b$  as the simulation with best results, it is preferable to investigate the rate of change when increasing the isentropic efficiency of the expanders ( $\eta_e$ ) and compressors ( $\eta_c$ ) from 75- to 85%, in order to reduce irreversibilities even further, and hopefully obtain a maximum efficiency. The results from this particular sub-iteration are named, similar as in Case Study III,  $i4*b'$ , where  $\delta_{4*b}$  is the improvement ratio compared to previous case,  $i4*b$ .

$$\eta_c = \eta_e = 85 \text{ (} i4 * b' \text{)}$$

	Value	$\delta_{4*b}$ [%]
Net power consumption [kW]	10998,50	-10,53
Net irreversibility [kW]	5460,06	-19,23
$UA$ (HX-1) [MW/°C]	6923,48	
$\Delta T_{min}$ (HX-1) [K]	2,02	
$UA$ (HX-2) [MW/°C]	4356,74	
$\Delta T_{min}$ (HX-2) [K]	2,04	
$\varepsilon_{i4*b'}$ [%]	50,36	+11,0

**Table 5.38:** Net compressor power and irreversibility, for  $\eta_c = \eta_e = 85\%$ .  $i4*b'$

A further reduction in exergy destruction of almost 20% is achieved, for the case with isentropic efficiency increase. Exergy efficiency exceeds 50%, which is

more than satisfying. Assuming that the rate of change in compressor work with respect to the variable isentropic efficiency applies similarly to every iteration case, it can be concluded that  $i4*b'$  has the overall best performance in not only Case Study IV, but for the whole case study analysis as well. Below, the final performance of the particular iterations analyzed are summarized.

	Exergy efficiency, $\varepsilon_x$ [%]	$\delta_k$ [%]	$w_{PC}$ [kWh/kg $_{H_2}$ ]
Case $i1*b$	37,0	+2,43	2,340
Case $i4*b$	45,0	+2,26	1,974
Case $i4*b'$	50,4	+14,4	1,766
Case $i8b$	43,4	+1,45	2,040

**Table 5.39:** Final exergy efficiency and spec. power requirement of Case Study IV, Cascade Mixed Refrigerant+ (CMR+) precooling



## 5.5 Benchmark comparison: Liquid Nitrogen Pre-cooling (LIN-PC)

Simulation of liquid nitrogen precooling is achieved with an adjuster unit in Aspen HYSYS, changing the mass flow,  $\dot{m}_{LN_2}$ , of the saturated liquid refrigerant at 77,24 K, until  $\Delta T_{min, LN_2HX}$  of 2 K in the heat exchanger is obtained.

The T-Q-diagram with the composite curves, both for conventional 80 K pre-cooling target and current 130 K target, are shown in Figure 5.17; indicating that a minimum temperature approach in the cold end of the heat exchanger is impossible with the current precooling target temperature at 130 K. The mass flow calculates to,  $\dot{m}_{LN_2} = 28,39$  kg/s, by the adjuster unit, to obtain the 2 K approach at the hot end.

**Composite curves (T-Q-Diagram), liquid nitrogen precooling (Benchmark Case)**

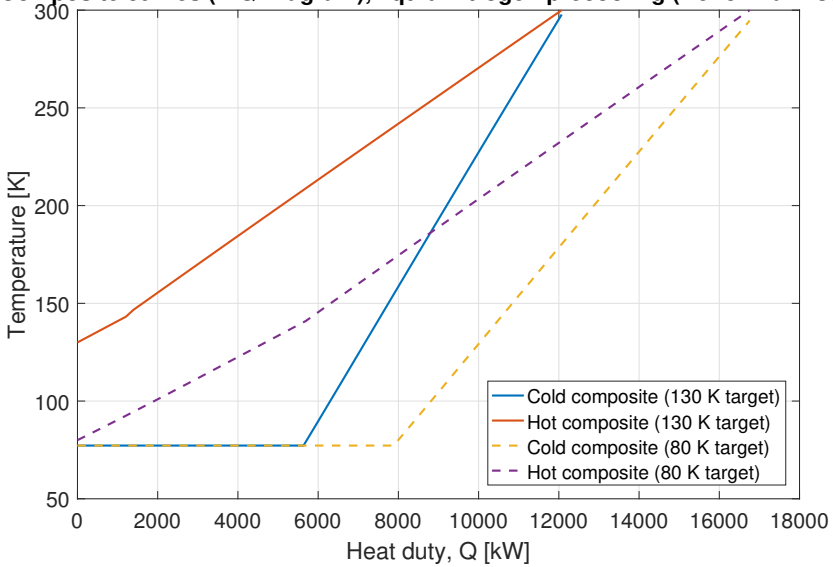


**Figure 5.17:** Composite curves (T-Q-Diagram) of liquid nitrogen precooling heat exchanger

For simplicity, the liquid nitrogen production plant is not included within the scope of this case study, hence no direct power consumption are generated in the simulation model. In order to perform an approximated exergy analysis equivalent as in the previous case study models, an energy penalty related to produc-

tion of LIN,  $w_{LN_2}$ , based on data found in literature, is imported as the external source of power consuming component of the simulation model. With  $w_{LN_2} = 0.4$  kWh/ $l_{LN_2} = 1787,7$  kJ/kg $_{LN_2}$ , given that the density of LIN,  $\rho_{LN_2} = 805,5$  kg/m<sup>3</sup>, every irreversibility related to the LIN production are included in this parameter. The specific hydrogen precooling work,  $w_{LIN-PC}$ , then becomes  $w_{LIN-PC} = (\dot{m}_{LIN-PC} \cdot w_{LN_2}) / \dot{m}_{H_2} = (1787,7 \text{ kJ/kg} \cdot 28,39 \text{ kg/s}) / (1,73 \text{ kg/s} \cdot 3600) = 8,149$  kWh/kg $_{H_2}$ .

### 5.5.1 Evaluating exergy- destruction and efficiency of Case Study V

With a mass flow,  $\dot{m}_{LN_2} = 28,39$  kg/s, at 1 bar and 77,24 K of the refrigerant, the total amount of irreversibilities, including heat exchanger losses and ortho-para conversion losses, calculates to 15,89 MW, which is over 60% greater than the losses generated in the most exergy-destruction-intensive iteration from the MR precooling case study concepts. The power penalty is calculated to  $\dot{W}_{net} = 1787,7 \text{ kJ/kg}_{LN_2} \cdot 28,39 \text{ kg/s} = 50,75$  MW, which accounts for the generation of the required amount of liquid refrigerant.

For the total exergy balance with respect to the system boundary as explained in Chapter 4, the left hand side<sup>11</sup> of the exergy balance equation calculates to 42,810 MW, while right hand side<sup>12</sup> equals 50,75 MW power input, as mentioned above. Hence, a difference rate of 7,94 MW remains as the error between simulated losses (including the rate of change in exergy content of each stream crossing the system boundary plus the internal irreversibilitites, see Table 5.40) and estimated power consumption for a LIN-production plant.

Exergy parameter	Value
Net power requirement, $\sum \dot{W}_{LN_2}$ [MW]	50,751
Net internal irreversibilities, $\sum \dot{I}$ [MW]	15,885
Exergy difference, boundary: $\sum \Delta E_{boundary}$ [MW]	26,925
Exergy efficiency, $\varepsilon_{LIN}$ [%]	10,88
Specific energy consumption, $w_{net}$ [kWh/kg $_{H_2}$ ]	8,149

**Table 5.40:** Final exergy balance of the LIN-Precooling Case Study V.

<sup>11</sup>Difference in exergy content of streams entering and leaving the system boundary,  $\sum \Delta E_{boundary}$ , plus generated irreversibilities inside the system boundary,  $\sum \dot{I}$

<sup>12</sup>Net power input,  $\sum \dot{W}$

### 5.5.2 Final comparison

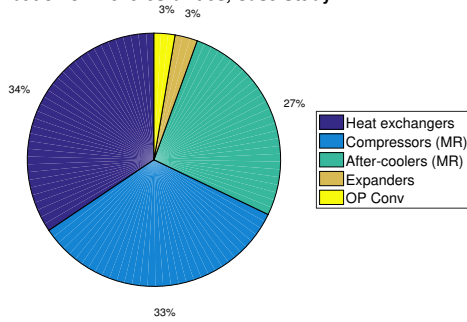
It can be concluded that the best simulation results (iteration) from each MR case study model has shown great potential in favour of minimizing the exergy losses within the components, simultaneously as the exergy efficiency has been attempted maximized. The distribution of irreversibilities for each of the best performing iterations in each case study are shown in Figure 5.18.

As a final discussion in this thesis, the conventional LIN-PC process is benchmarked with the final, optimized MR Case Study Models, with respect to exergy losses- and efficiency.

- For the PRICO SMR precooling model, the best simulation,  $i5 - b$  has a total power requirement of 15,37 MW, where the net exergy destruction accounts for 64,47 % of the total power input.
  - Compared to the LIN-PC process, the heat exchanger losses alone are above 5% higher than the overall power consumption in the SMR PRICO process, where this particular simulation represents the highest power-consuming process of the four case study models. Total power consumption of the LIN-process are more than 35 MW higher than the SMR PRICO precooling process. The difference in specific energy consumption between the two, calculates to  $(8,149 - 2,469) = 5,68$  kWh/kg<sub>H2</sub>, which represents a reduction of 69,7%.
- For the PRICO SMR+ precooling model, the best simulation,  $i11 - b$  has a total power consumption of 12,43 MW, where the net exergy destruction accounts for 55,6% of the total power input.
  - In comparison with the LIN-PC process, the net amount of irreversibilities for the SMR+ process are 56,5% lower. The difference in specific energy consumption between the two processes, calculates to  $(8,149 - 1,893) = 6,256$  kWh/kg<sub>H2</sub>, which represents a reduction of 76,8%.
- For the CMR precooling model, the best simulation,  $i9 - b$  has a total power consumption of 12,7 MW, where the net exergy destruction accounts for 56,5% of the total power input.
  - In comparison with the LIN-PC system, the net amount of irreversibilities for the CMR process are 54,8% lower, with a difference in specific energy consumption of  $(8,149 - 2,34) = 5,81$  kWh/kg<sub>H2</sub>. This represents a reduction of 71,3%.
- For the CMR+ precooling model, the best simulation,  $i4^* - b$  has a total

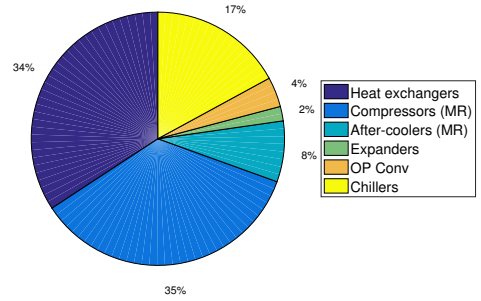
5.5. BENCHMARK COMPARISON: LIQUID NITROGEN PRECOOLING (LIN-PC)125

Distribution of irreversibilities, Case Study I



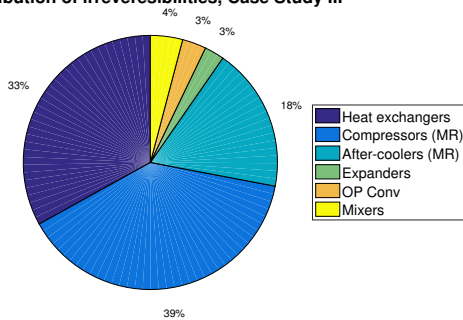
(a) Case Study I,  $i_{5-b}$

Distribution of irreversibilities, Case Study II



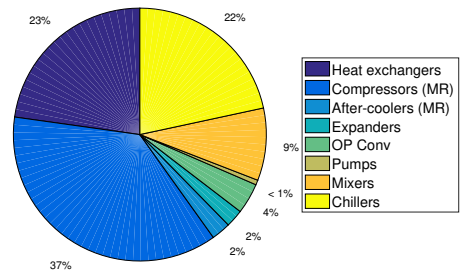
(b) Case Study II,  $i_{11-b}$

Distribution of irreversibilities, Case Study III



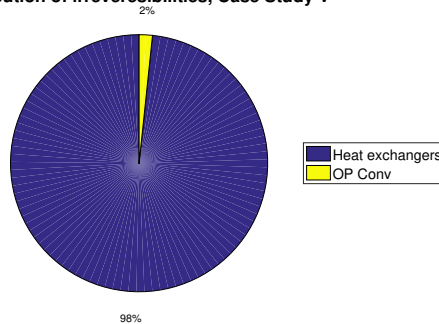
(c) Case Study III,  $i_{9-b}$

Distribution of irreversibilities, Case Study IV



(d) Case Study IV,  $i_{4-b}$

Distribution of irreversibilities, Case Study V



(e) Case Study V, Liquid Nitrogen Precooling.

Figure 5.18: Component-wise distribution of exergy destruction, best performance iteration

power consumption of 12,29 MW, where the net exergy destruction within the process accounts for 54,9%, of the total power input.

- In comparison with the benchmark process, the net amount of irreversibilities for the CMR+ process are 57,4% lower. The difference in specific energy consumption between the two processes, calculates to  $(8,149 - 1,974) = 6,175$  kWh/kg<sub>H2</sub>, which represents a reduction of 75,8%.

The main resulting exergy efficiency,  $\varepsilon_x$ , and specific energy consumption,  $w_{net}$  are displayed in Figure 5.19 and 5.20.

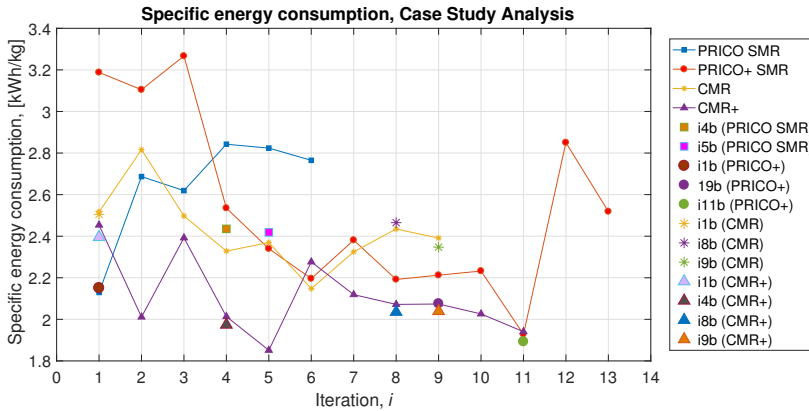


Figure 5.19: Specific energy consumption,  $w_{net}$ , Case Study I-IV

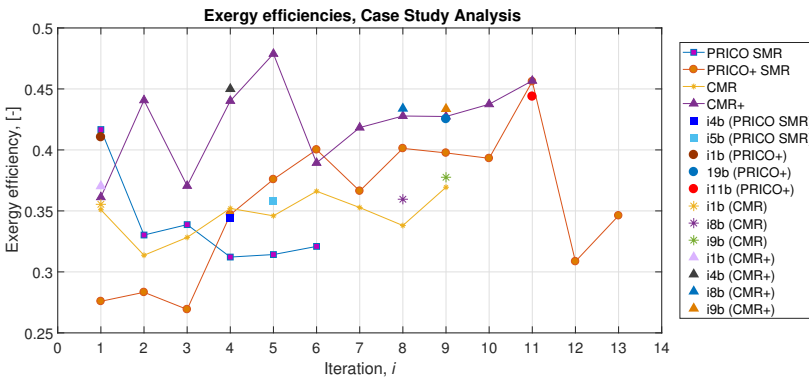


Figure 5.20: Exergy efficiency,  $\varepsilon_x$ , Case Study I-IV

# Chapter 6

## Conclusion

Development of the next-generation hydrogen liquefaction plant, target in the direction of Mixed Refrigerant Precooling integration. With emphasis on exergy efficiency and specific energy consumption related to the hydrogen precooling process, the findings evaluated from the process- simulation and optimization proposed in this thesis has shown promising results. Both compared to the state-of-the-art technology existing today and conceptual hydrogen precooling proposals discovered from literature.

In literature, conceptions related to acceptable energy and exergy efficiencies, heat integration and optimization in heat exchangers, rotary equipment efficiencies and comparison benchmarks, experience a certain level of disagreement. That is often related to the level of feasibility of reaching certain efficiencies in an overall hydrogen liquefier, simultaneously when unrealistic configurations of heat exchanger design is applied. Still, concepts in recent proposals tends to reach an optimal target in favour of specific energy consumption and exergy efficiency, with an absolute minimum reported to 5,9 kWh/kg<sub>H<sub>2</sub></sub>, and exergy efficiencies reaching 50%. Even if an acceptable efficiency is reached in future proposals at a feasible technological readiness level, research with emphasis on investment costs and operating cost of a large-scale system must be further accelerated, as quite few of the concepts evaluated in this thesis deals with these subjects in particular.

The main results from the Case Study Analysis has shown potential for further integration with a complete hydrogen liquefaction process. Initially, each of the Case Study models utilized an approximated simulation of adiabatic ortho-para conversion at the outlet of the precooling process, by import of equilibrium hydrogen data from NIST RefProp Databank via Aspen HYSYS. Each Case Study

Model was proven to satisfy the rate of change in enthalpy- and entropy values, compared to normal hydrogen properties. For each simulation model, the adiabatic conversion approach resulted in a temperature increase of 10.5-13 K at a hydrogen temperature of 130 K.

With utilization of simple Refrigerators or Chillers to reach higher efficiencies, R290 (propane) was assumed as a suitable working fluid. For each separate Chiller unit connected to the designated streams to be cooled, COP was calculated to above 7, when assuming a temperature difference in Chiller- condenser and -evaporator of 25 K. The power consumption of the Chiller-compressors were basically only mass-flow dependent, due to preassigned parameters for both pressure and temperature levels in primary and secondary circuit. Hence, power consumption was highest for the most mass-flow-intensive stream, which for every Case Study are the Mixed Refrigerant stream(s).

Each Case Study model were simulated several times, as three primary parameters were re-modified in the search of an optimal solution, together with evaluation of the respective exergy destruction generated. Liquid expanders were integrated as replacement for the throttling valves, after realizing that the throttling losses had great potential for reduction. The highest exergy efficiency achievable together with realistic process KPI's was calculated to above 45%, in Case Study IV, Cascade Mixed Refrigerant+ precooling with the integrated R290-Chillers and integration of liquid expanders. The specific energy consumption of the particular simulation was calculated to 1,974 kWh/kh<sub>H2</sub>, which in comparison with the conventional Liquid Nitrogen Benchmark process was 75,8% lower. The Case Study Models with the utilization of Chillers, also showed a much higher level of energy efficiency together with a lower rate of net exergy destruction within the process components, and are therefore recommended integrated in further study and simulations of both isolated precooling systems, or complete liquefaction processes.

For each of the Case Study models, isentropic efficiency was increased from the initially assumed value of 75% to 85%, as a final attempt to reach a maximum exergy efficiency level. After re-modification of the isentropic efficiency, the best performing CMR+ simulation resulted in an exergy efficiency above 50% and a respective specific energy consumption of 1,766 kWh/kg<sub>H2</sub>, which is a reduction of 78,3% compared to the LIN-PC process, and 14,4% compared to the low-efficiency CMR+ simulation.

# Chapter 7

## Proposal for further work

Energy efficient hydrogen liquefaction systems exist to a very limited extent in the worldwide industry today. As for a future large-scale scenario, exergy efficiencies has to be remarkably improved if the latent energy content of hydrogen can be fully utilized. As 17-18% of the total exergy content from ambient conditions down to liquid saturation at 20,3 K, is related to the precooling process, efficient precooling system are a prerequisite to complete the value chain.

The simulation, optimization and re-modification work of the Case Study Models in this thesis provide four high efficient and approximately complete Hydrogen Mixed Refrigerant Precooling-modules, ready for integration within a full baseline liquefaction simulation system. As the overall system is incomplete, proposals for further work within the process design are presented below

### 7.1 Further work proposals within process design and simulation

- **Further investigation on noble gas mixtures:** Noble gases, such as helium and neon may be further investigated as efficient working fluid refrigerants with emphasis on: the heat transfer behaviour within the complex structures of cryogenic heat exchangers, i.e. brazed plate-fin heat exchangers with a high degree of compactness; compressor- and liquid expander performance due to the particularly low molecular weights of such gases. An increase of the upper pressure limit has proven to be prefer-



able, if such a light gas mixture is to be integrated as refrigerant. Research within the field of mixing hydrogen and neon as an alternative refrigerant has already begun, and may prove higher efficiency due to heat transfer performance.

- **Completion of the liquefaction cycle with cost-estimation parameters:** Similar approach as done by the authors Cardella et al. in [13], which estimates both CAPEX and OPEX for the entire liquefaction system. Integration of the precooling processes as proposed in this thesis into an efficient cryogenic liquefaction process is recommended initiated at some point, where the cryogenic working fluid is already integrated.
- **Further elaboration and optimization of the Chiller-units:** As the R290-Chillers were implemented separately as a simplification related to the simulation model, other approaches may be evaluated; such as simulation of one centralized unit, with an improved level of heat integration.

# Bibliography

- [1] European commission. [http://ec.europa.eu/clima/policies/international/negotiations/paris\\_en](http://ec.europa.eu/clima/policies/international/negotiations/paris_en). Accessed: 2016-12-21.
- [2] On beyond oil\*: Petter nekså and hydrogen. <https://www.sintef.no/en/events/on-beyond-oil/petter-neksa/>. Accessed: 2016-12-20.
- [3] L. AG. Lng technology. in Brochure from Linde, 2010.
- [4] ASKO. Askø satser på hydrogenteknologi. 04 2016.
- [5] A. Aspelund and T. Gundersen. A liquefied energy chain for transport and utilization of natural gas for power production with {CO<sub>2</sub>} capture and storage – part 2: The offshore and the onshore processes. *Applied Energy*, 86(6):793 – 804, 2009.
- [6] A. Aspelund, T. Gundersen, J. Myklebust, M. Nowak, and A. Tomasgard. An optimization-simulation model for a simple {LNG} process. *Computers & Chemical Engineering*, 34(10):1606 – 1617, 2010.
- [7] M. Ball and M. Wietschel. *The hydrogen economy: opportunities and challenges*. Cambridge University Press, 2009.
- [8] D. Berstad, M. Börsch, L. Decker, A. Elliott, C. Haberstroh, J. Louis, B. Lowesmith, N. Mortimer, P. Neksa, H. Quack, et al. Ideally-integrated design for demonstration of efficient liquefaction of hydrogen, 2015.
- [9] D. O. Berstad, J. H. Stang, and P. Neksa. Comparison criteria for large-scale hydrogen liquefaction processes. *international journal of hydrogen energy*, 34(3):1560–1568, 2009.
- [10] D. O. Berstad, J. H. Stang, and P. Neksa. Large-scale hydrogen liquefier utilising mixed-refrigerant pre-cooling. *International Journal of Hydrogen Energy*, 35(10):4512 – 4523, 2010. Novel Hydrogen Production Technologies and Applications Novel Hydrogen Production Technologies and Applications.

- [11] Bloomberg. Shell and toyota partner on california fueling stations for hydrogen cars. 02 2017.
- [12] M. Bracha, G. Lorenz, A. Patzelt, and M. Wanner. Large-scale hydrogen liquefaction in germany. *International Journal of Hydrogen Energy*, 19(1):53 – 59, 1994.
- [13] U. Cardella, L. Decker, and H. Klein. Economically viable large-scale hydrogen liquefaction. 2016.
- [14] U. Cardella, L. Decker, and H. Klein. Roadmap to economically viable hydrogen liquefaction. *International Journal of Hydrogen Energy*, 2017.
- [15] R. Cornelissen and G. Hirs. Exergy analysis of cryogenic air separation. *Energy Conversion and Management*, 39(16–18):1821 – 1826, 1998.
- [16] E24. Ny nel-kontrakt kan være starten på fransk milliardeventyr. 06 2017.
- [17] J. Essler, C. Haberstroh, H. Quack, H. T. Walnum, D. Berstad, P. Nekså, J. Stang, M. Börsch, F. Holdener, L. Decker, and P. Treite. Report on technology overview and barriers to energy- and cost-efficient large scale hydrogen liquefaction. In *Integrated design for demonstration of efficient liquefaction of hydrogen (IDEALHY)*, 2012.
- [18] A. Fredheim, E. Solbraa, J. Pettersen, and O. Bollad. *Compendium: Natural Gas Tecnology*. Norges tekniske- naturvitenskapelige universitet, NTNU, 2014.
- [19] Gemini. Norge kan ha ti tusen tunge hydrogen-kjøretøy i 2030. 06 2016.
- [20] B. Green. Shell opens its first uk hydrogen car refuelling station. 02 2017.
- [21] HyFIVE. Hyfive project - hydrogen for innovative vehicles.
- [22] I. G. U. (IGU). Natural gas facts figures, new approach proposal, 2015.
- [23] F. P. Incropera, A. S. Lavine, T. L. Bergman, and D. P. DeWitt. *Principles of heat and mass transfer*. Wiley, 2013.
- [24] G. J. Kramer, J. Huijsmans, and D. Austgen. Clean and green hydrogen. *World Hydrogen Energy Conference 16, Lyon France*, 2006.
- [25] S. Krasae-in, J. H. Stang, and P. Neksa. Development of large-scale hydrogen liquefaction processes from 1898 to 2009. *International journal of hydrogen energy*, 35(10):4524–4533, 2010.
- [26] R. Lan, J. T. Irvine, and S. Tao. Ammonia and related chemicals as potential indirect hydrogen storage materials. *International Journal of Hydrogen*

- Energy*, 37(2):1482 – 1494, 2012. 10th International Conference on Clean Energy 2010.
- [27] A. Larsen, F. Simon, and C. Swenson. The rate of evaporation of liquid hydrogen due to the ortho-para hydrogen conversion. *Review of Scientific Instruments*, 19(4):266–269, 1948.
- [28] J. W. Leachman, R. T. Jacobsen, S. G. Penoncello, and E. W. Lemmon. Fundamental equations of state for parahydrogen, normal hydrogen, and ortho-hydrogen. *Journal of Physical and Chemical Reference Data*, 38(3):721–748, 2009.
- [29] A. H. manual. Heat exchangers, hysys simulation environment.
- [30] D. Marmolejo-Correa and T. Gundersen. A comparison of exergy efficiency definitions with focus on low temperature processes. *Energy*, 44(1):477 – 489, 2012. Integration and Energy System Engineering, European Symposium on Computer-Aided Process Engineering 2011.
- [31] H. Matsuda and M. Nagami. Study of large hydrogen liquefaction process. kanagawa, japan: Nippon sanso corp. we-net: Summary of annual reports, 1998.
- [32] R. McCarty. A modified benedict-webb-rubin equation of state for methane using recent experimental data. *Cryogenics*, 14(5):276 – 280, 1974.
- [33] J. P. Meagher. Modeling of hydrogen liquefiers with kinetic conversion of ortho to para hydrogen in plate-fin heat exchangers. Master's thesis, Faculty of the Graduate School of the University at Buffalo, State University of New York, Department of Chemical and Biological Engineering, 2008.
- [34] M. Moran and H. Shapiro. *Fundamentals of Engineering Thermodynamics: Appendices - Tables in SI Units and in English Units*. Wiley, 2010.
- [35] E. "Mr Jacques Pieraerts | Vice President, Communication and E. Affairs". "h2 : The path to a sustainable society", toyota motor europe. <http://www.whec2016.com/index.php/programme/plenary-sessions/plenary-sessions-summary>. Accessed: 2016-12-20.
- [36] K. Ohlig, S. Bischoff, and L. K. AG. Dynamic gas bearing turbine technology in hydrogen plants. *Advances in Cryogenic Engineering*, 57:814–819, 2012.
- [37] K. Ohlig, L. Decker, J. Weisend II, S. Breon, J. Demko, M. DiPirro, J. Fesmire, P. Kittel, A. Klebaner, J. Marquardt, et al. The latest developments and outlook for hydrogen liquefaction technology. In *AIP Conference Proceedings*, volume 1573, pages 1311–1317. AIP, 2014.

- [38] U. N. F. C. on Climate Change. Global response to climate change keeps door open to 2 degree c temperature limit. 10 2015.
- [39] J. M. Øverli. Strømningsmaskiner. *Termiske maskiner, Bind, 3*, 1992.
- [40] S. Pérez and R. Díez. Opportunities of monetising natural gas reserves using small to medium scale lng technologies. In *IGU 24th world gas conference, REPSOL, Argentina*, 2009.
- [41] H. Quack. Conceptual design of a high efficiency large capacity hydrogen liquefier. In *ADVANCES IN CRYOGENIC ENGINEERING: Proceedings of the Cryogenic Engineering Conference-CEC*, volume 613, pages 255–263. AIP Publishing, 2002.
- [42] H. Quack, J. Essler, C. Haberstroh, H. Walnum, D. Berstad, M. Drescher, and P. Neksa. Search for the best processes to liquefy hydrogen in very large plants. In *The 12th CRYOGENICS 2012, IIR International Conference*, 2012.
- [43] H. Quack, I. Seemann, M. Klaus, C. Haberstroh, D. Berstad, H. Walnum, P. Neksa, L. Decker, J. Weisend II, S. Breon, et al. Selection of components for the ideally preferred cycle for the large scale liquefaction of hydrogen. In *AIP Conference Proceedings*, volume 1573, pages 237–244. AIP, 2014.
- [44] H. Quack, H. T. Walnum, D. Berstad, P. Neksa, A. Elliott, and L. Decker. Schedule for demonstration plant including options for location. In *Integrated design for demonstration of efficient liquefaction of hydrogen (IDEALHY)*, 2013.
- [45] E. The Norwegian Research Council. Liquefied hydrogen production from surplus wind/hydro power and fossil sources in norway (popular science presentation). 2016.
- [46] T. Ukeblad. Tungtransportens tesla blir til tungtransportens toyota mirai. 08 2016.
- [47] G. Valenti and E. Macchi. Proposal of an innovative, high-efficiency, large-scale hydrogen liquefier. *International Journal of Hydrogen Energy*, 33(12):3116 – 3121, 2008. 2nd World Congress of Young Scientists on Hydrogen Energy Systems.
- [48] L. van der Ham and S. Kjelstrup. Exergy analysis of two cryogenic air separation processes. *Energy*, 35(12):4731 – 4739, 2010. The 3rd International Conference on Sustainable Energy and Environmental Protection, {SEEP} 2009.

- [49] G. Venkatarathnam and K. D. Timmerhaus. *Cryogenic mixed refrigerant processes*. Springer, 2008.
- [50] H. T. Walnum, D. Berstad, M. Drescher, P. Neksa, H. Quack, C. Haberstroh, and J. Essler. Principles for the liquefaction of hydrogen with emphasis on precooling processes. 12th Cryogenics - IIR Conference - Dresden, 2012.
- [51] K. Wark. *Advanced thermodynamics for engineers*. McGraw-Hill New York, 1995.
- [52] J. Wolf. Lh2 makes you mobile. Linde Technology, 2003.
- [53] V. Åtland and D. Jakobsen. Concepts for large-scale hydrogen production. Master's thesis, Norwegian University of Science and Technology (NTNU), 2016.
- [54] Øivind Wilhelmsen, G. Skaugen, D. Berstad, A. Aasen, and P. Neksa. Understanding the physical phenomena that occur inside heat exchangers for liquefaction of hydrogen. 2017.







# Appendix A

## Technical design parameters

### A.1 Case Study I and II

Parameter	Value	Unit
<b>Hydrogen feed:</b>		
Feed pressure:	20	Bar
Feed temperature:	300	K
Mass flow:	1.736	kg/s
Precooling temperature:	130	K
Ortho-para concentration (inlet)	75-25	mol-%
Para concentration (at 130 K)	$\approx 99.9\%$	mol-%
<b>Mixed refrigerant:</b>		
Suction temperature (system one)	$>T(DP)+5$	K
Suction temperature (system two)	$<T(DP)$	K
HX inlet temperature:	300	K
Multi-compression (system one)	2	-
Multi-compression (system two)	2 + pump	-
HX outlet temperature:	130	K
Low pressure:	4	Bar
Isentropic efficiency, compressor, $\eta_c$	75	[%]
Isentropic efficiency, expander, $\eta_e$	75	[%]
<b>Nelium feed:</b>		
Feed pressure:	80	Bar
Mass flow:	17.36	kg/s
Neon fraction:	0.25	-

**Table A.1:** Initial parameters applied to Case Study I and II

## A.2 Case Study III and IV

Parameter	Value	Unit
<b>Hydrogen feed:</b>		
Feed pressure:	20	Bar
Feed temperature:	300	K
Mass flow:	1.736	kg/s
Intermediate temperature	210	K
Precooling temperature:	130	K
<b>Mixed refrigerant cycle a:</b>		
Suction temperature	$>T(DP)+5$	K
HX inlet temperature:	300	K
Multi-compression	2	-
HX outlet temperature:	210	K
Low pressure:	4	Bar
Isentropic efficiency, compressor, $\eta_c$	75	[%]
Isentropic efficiency, expander, $\eta_e$	75	[%]
<b>Mixed refrigerant cycle b:</b>		
Suction temperature	$>T(DP)+5$	K
HX inlet temperature:	210	K
Multi-compression	2	-
HX outlet temperature:	130	K
Low pressure:	4	Bar
Isentropic efficiency, compressor, $\eta_c$	75	[%]
Isentropic efficiency, expander, $\eta_e$	75	[%]
<b>Neon feed:</b>		
Feed pressure:	80	Bar
Mass flow:	17.36	kg/s
Neon fraction:	0.25	-

**Table A.2:** Initial parameters applied to Case Study III and IV



## Appendix B

# Exergy analysis and equations of Case Study I, SMR PRICO

Below, the expression for the total irreversibility of each component within the PRICO SMR process are listed, to exemplify how each parameter from the remaining Case Study models were obtained. Total rate of irreversibilities within the system is given as

$$\dot{I}_{tot} = \sum_i^n \dot{I}_i \quad (\text{B.1})$$

where  $n$  is the total number of components,  $i$  in the system

### B.1 SMR PRICO

**Heat exchanger (HX-1):**

$$\begin{aligned} \dot{I}_{HX-1} = & \dot{m}_{H2_1} ((e_{H2-1} + e_{H2-3-EQ}) - (e_{H2_2} + e_{H2-4-EQ})) \\ & + \dot{m}_{NEL-1} (e_{NEL-1} - e_{NEL-2}) + \dot{m}_{MCR-1} (e_{MCR-2} \\ & - e_{MCR-3}) + \dot{m}_{MCR-1} (e_{MCR-4} - e_{MCR-5}) \end{aligned} \quad (\text{B.2})$$

**Compressors (CPR1 and CPR2):**

$$\begin{aligned} \dot{I}_{CPR-net} &= \dot{m}_{MCR-1}((e_{MCR-1} - e_{MCR-2-i}) \\ &\quad + \dot{m}_{MCR-1}((e_{MCR-2-ii} - e_{MCR-2-iii}) + \dot{W}_{CPR-tot} \quad (\text{B.3}) \\ \dot{W}_{CPR-net} &= \dot{W}_{CPR-1} + \dot{W}_{CPR-1} \end{aligned}$$

**Valve (VLV-100):**

$$\dot{I}_{VLV} = \dot{m}_{MCR-1}(e_{MCR-4} - e_{MCR-5}) \quad (\text{B.4})$$

**Aftercoolers (MCR-AC-1 and MCR-AC-2):**

$$\dot{I}_{AC-tot} = \dot{m}_{MCR-1}((e_{MCR-2-i} - e_{MCR-2-ii}) + (e_{MCR-2-iii} - e_{MCR-3})) \quad (\text{B.5})$$

**Overall exergy balance:** The overall exergy balance of the system is given by the exergy difference of the material- and energy streams that crosses the system boundary, which gives the remaining irreversibility generated in the system, which are

$$\Delta \dot{E}_{H_2} + \Delta \dot{E}_{He/Ne} + \sum_i \dot{I}_i = \sum \dot{W}_{net} \quad (\text{B.6})$$



Iteration	1		2	
Process component	$\dot{i}$ [kW]	Power [kW]	$\dot{i}$ [kW]	Power [kW]
MR_COMPR_1	1443,66	7006,90	1872,85	8507,86
MR_COMPR_2	1328,81	6254,98	1747,50	8225,73
MR_AC1	1010,41		596,42	
MR_AC2	1045,95		1375,50	
VLV-100	950,60		1250,10	
MR_HEX	1691,70		4100,50	
Op conv	264,76		264,76	
Feed balance	5526,00		5526,00	
<b>Net</b>	<b>13261,89</b>	<b>13261,90</b>	<b>16733,60</b>	<b>16733,60</b>
Iteration	3		4	
MCR_COMPR_1	1815,56	8226,27	1890,27	9175,07
MCR_COMPR_2	1621,89	8086,41	1699,69	8527,20
MCR_AC1	473,40		1043,03	
MCR_AC2	2193,92		1981,81	
VLV-100	1492,16		2062,07	
MCR_HEX	2924,96		3234,72	
Op conv	264,76		264,76	
Feed balance	5526,00		5526,00	
<b>Net</b>	<b>16312,64</b>	<b>16312,69</b>	<b>17702,34</b>	
Iteration	5		6	
MCR_COMPR_1	1890,27	9175,07	1876,88	9128,46
MCR_COMPR_2	1699,69	8527,21	1689,53	8458,12
MCR_AC1	1043,03		1061,71	
MCR_AC2	1981,80		1937,45	
VLV-100	2062,07		2036,05	
MCR_HEX	3234,72		3194,27	
Op conv	264,76		264,76	
Feed balance	5526,0		5525,99	
<b>Net</b>	<b>17702,34</b>	<b>17702,3</b>	<b>17586,65</b>	<b>17586,6</b>
Iteration	5		6	
MCR_COMPR_1	1834,42	8981,36		
MCR_COMPR_2	1656,91	8239,49		
MCR_AC1	1125,03			
MCR_AC2	1800,28			
VLV-100	1957,93			
MCR_HEX	3055,62			
Op conv	264,76			
Feed balance	5526,00			
<b>Net</b>	<b>17220,96</b>	<b>17220,85</b>		

Table B.1: Calculated irreversibilities for Case Study I, SMR PRICO

## Appendix C

# Case Study Process Flow Diagrams, HYSYS







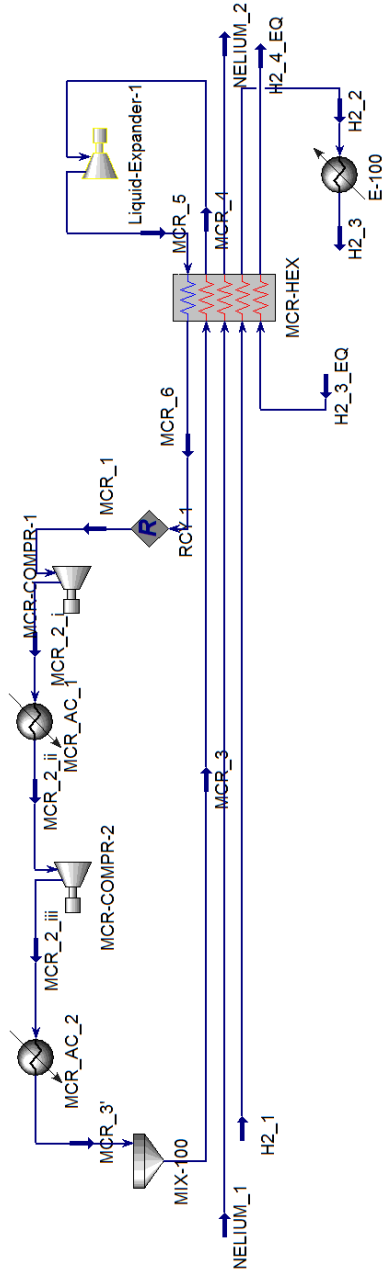


Figure C.2: SMR PRICO model, with isentropic expansion



## C.2 Case Study II: SMR PRICO+

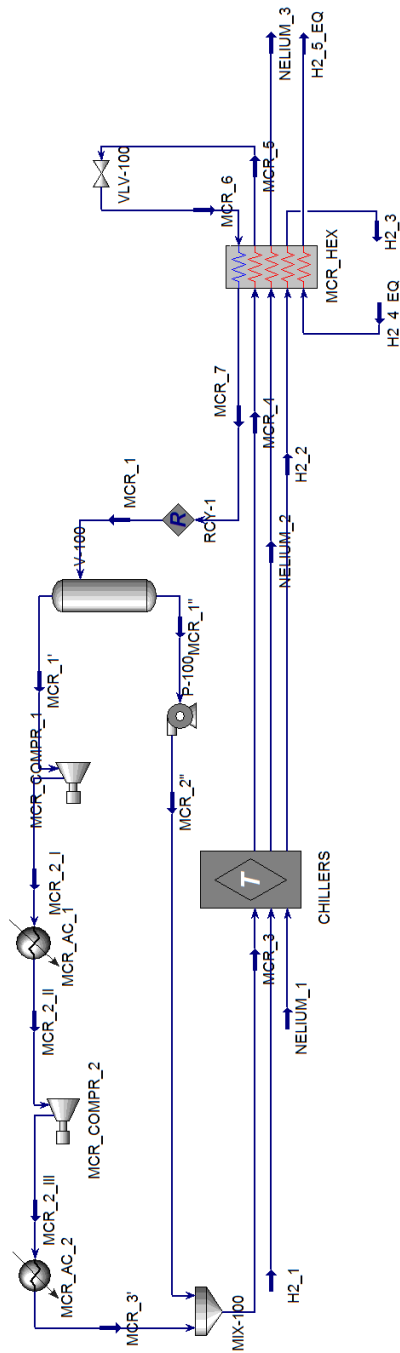


Figure C.3: SMR PRICO+ model, with isenthalpic throttling





### C.3 CMR

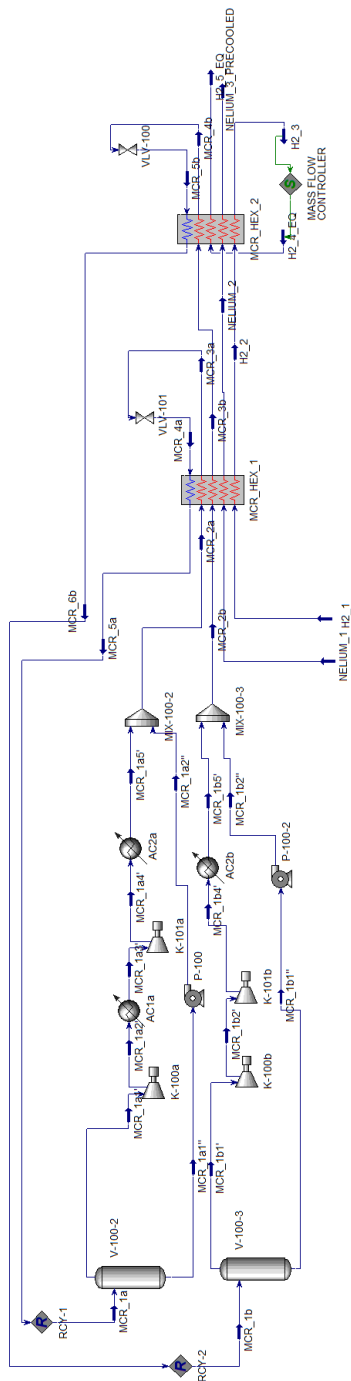


Figure C.5: CMR precooling model, with isenthalpic expansion



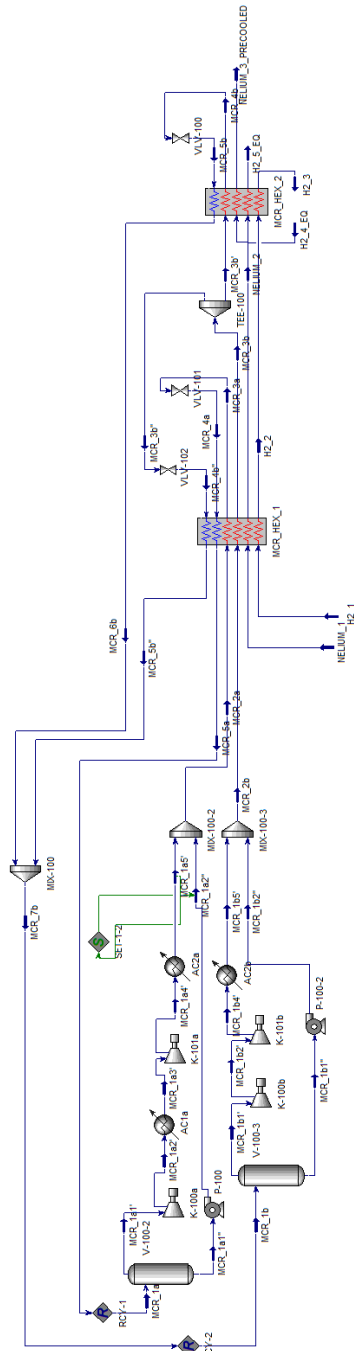


Figure C.6: Alternative CMR precooling model design, with isenthalpic expansion



### C.4 LIN-PC

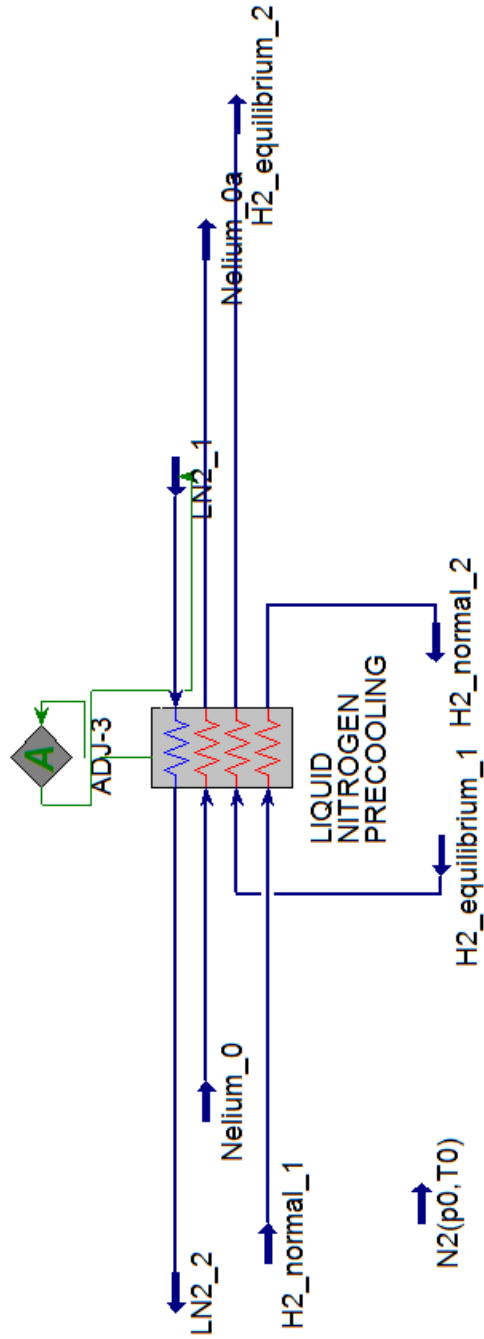


Figure C.7: Simple model of Liquid Nitrogen Precooling